Ondo

Aalto University School of Engineering

Department of Mechanical Engineering

Marine Technology

MEC-E2004 – Ship Dynamics

Polar research, supply, and passenger vessel Ondo

Final report

Submitted 02.06.2021

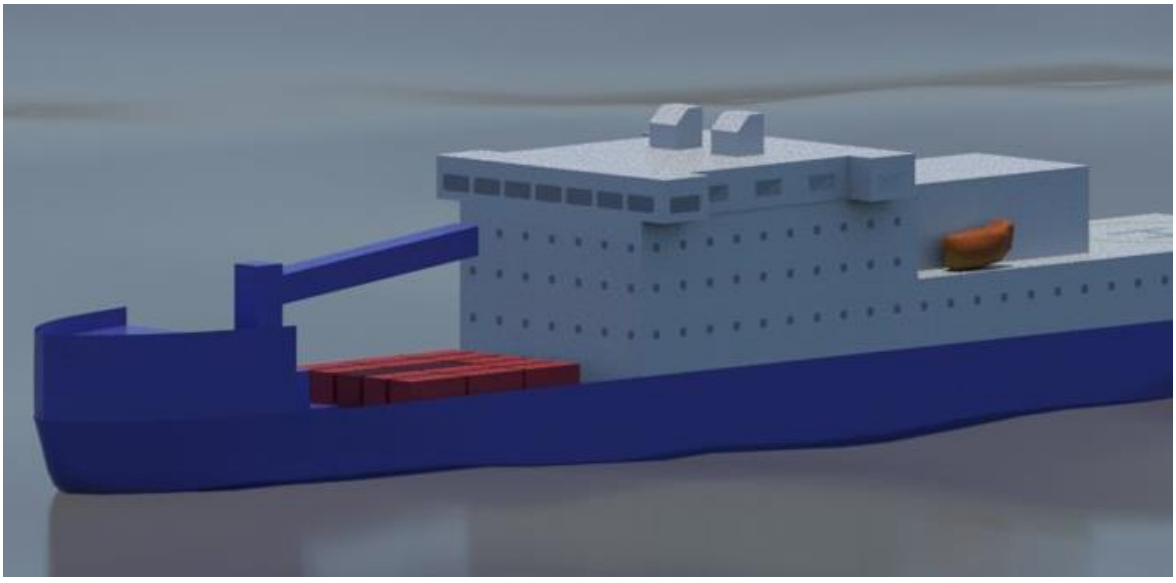

Team:

Ali Hazrati Niyari
Ilja Makarov
Tomás Sanches

Contents

1 Operational profile

Polar research, supply, and passenger vessel Ondo main operational information is known from vessel type prefix. Polar means that ship operates in North or South Pole regions, Arctic, and Southern Oceans. Main features of these regions are that the ship can run year-round into ice fields on its way to the destination. Not only Polar region operations define ship design. To get from Helsinki's Länsisatama port (home port), through the Baltic Sea to the Arctic or Antarctic regions the ship must navigate in the Atlantic Ocean. In the Atlantic the ship will encounter rough ocean waves and sometimes even storms. The North Sea or the Bay of Biscay which lay on the route of the ship are regions with harsh weather conditions and storms. Good open water characteristics are required and thus, Ondo's seaworthiness is as important as its icebreaking capability in order to provide safety and comfort for crew, permissible loads on structures, and cargo position hold.

Research in Ondo ship type means that there is made scientific work on board. Researchers live and work on board. Different measurements of environment, experiments must be done. Ondo must fulfill requirements for scientific work from ship dynamics point of view. Ship voyage is called expedition. Arctic expedition in Northern Hemisphere's summer takes around 60 days. Antarctic expedition which takes place during Northern Hemisphere's winter takes around 120 days. Expedition period choice is influenced by favorable ice conditions during summer.

Supply in ship type means that Ondo is also a cargo ship. Cargo on board is intended to work as supply for remote stations in Polar regions where researchers work and live. Ship Dynamics' impact on cargo must be studied in depth because cargo is very valuable for remote stations. In addition, also remote stations' crew change can be made using Ondo.

In Figure 1 are shown some example navigation routes for Ondo. When the vessel gets nearer to the Poles, it faces harder ice conditions. On the other hand, it can be seen that the ship navigates also a lot in open water, for instance, when moving in the Atlantic Ocean.

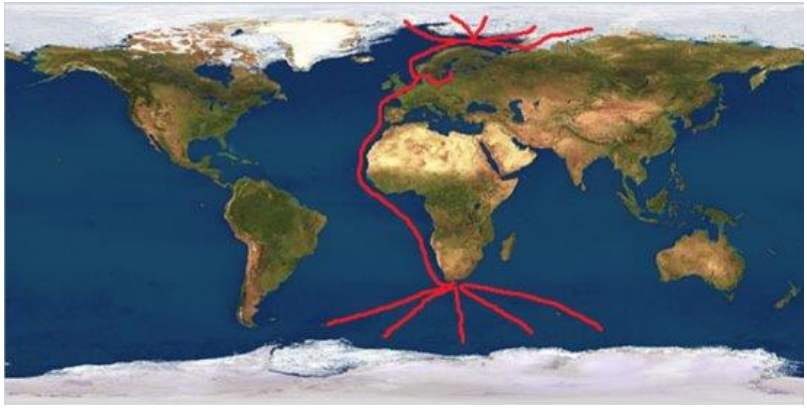

Figure 1. Possible navigation routes for Ondo.

For the purpose of this course, a typical voyage is considered. Figure 2 shows a typical route of Ondo up to the Russian Arctic and Figure 3 shows the variation in speed throughout that journey by considering winter conditions.

Figure 2. Route Helsinki - Russian Arctic.

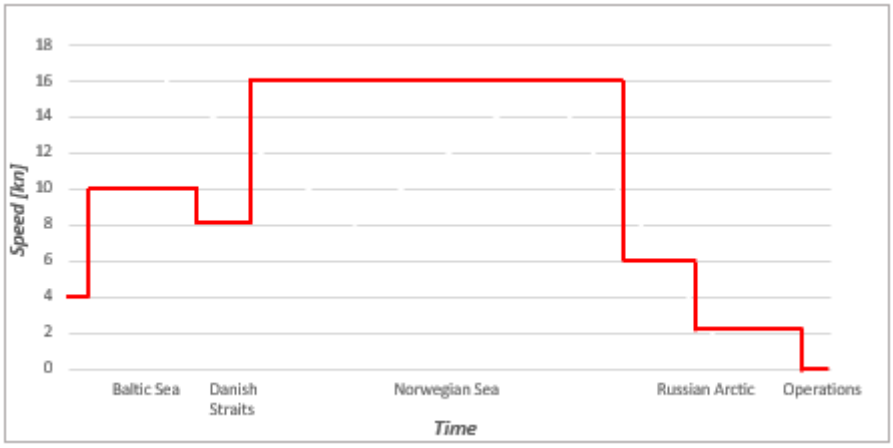

Figure 3. Speed variation in route Helsinki - Russian Arctic.

As mentioned previously, this example operational profile consists of a trip from Helsinki Länsisatama terminal (Ondo's home base) to the Russian Arctic. The speed variation in Figure 3 is related to winter conditions where ice is present in several regions. While navigating in the port, channels and archipelago of Helsinki, the average speed is set at 4 knots. This speed increases when in the 'open Baltic Sea' to 10 knots but does not reach its maximum due to ice coverage. In the Baltic Sea the level ice thickness is assumed 50 cm. Then, the Danish Straits are used to move from the Baltic Sea to the North Sea. Although there is no ice cover in the Straits, the average speed is reduced to 8 knots due to regulatory constraints. Once in the

Norwegian Sea the design speed of Ondo (16 knots) is reached as open-water conditions take place. When approaching the destination in the Russian Arctic, the average speed starts to reduce due to an increase in the level ice thickness in Barents and Kara Seas. The two last speed steps shown in Figure 3 are due to 80 cm and 1.2 m -thick level ice, respectively. Finally, speed reduces to 0 knots as Ondo is in operations using its Dynamic Positioning System, for example.

2 Ship dynamics requirements

Ship dynamics' requirements must be such that ensure good seaworthiness and seakeeping. Motions of the ship must not be harmful for crew, passengers, or cargo. People work and live on board for long periods of time and thus, excessive motions can cause stress, seasickness, falls and injuries. On the other hand, when looking at the influence undesirable ship motions might have on cargo is that these may lead to losses in cargo due to its failure/breaking. All previously mentioned are not admitted for a ship with good design form ship dynamics perspective.

Motions have impact not only on people but also on ship structures. Ship must be designed that the highest loads (for this particular ship type/class) caused by ship motions will not cause damage or structural failure.

Since the ship being considered is partially a supply type vessel there is cargo on board. Most of the cargo will be carried in standardised sized containers. Ship's excessive motions can cause containers to shift their position, if they are not well attached to the fixing structures, which is not admitted on this type of Polar supply vessel because remote stations depend highly on this cargo and cargo movements might lead to unsafe situations.

Ship resistance increases in waves. To maintain the same speed more fuel must be consumed and this increases usually exponentially. This leads to more operational costs which in good design must be minimised as much as possible, but operations quality level should not drop.

Last but not least, during icebreaking process ship motions must be such that provide a continuous icebreaking process.

3 Manoeuvring devices

A Polar research and supply vessel's common propulsive system consists of two propellers in the aft and one bow thruster. Sometimes a thruster can be installed in the aft for better manoeuvring.

Ondo's design aims at implementing a propulsion system consisting of two Azipods on the aft and one bow thruster to improve manoeuvrability. This solution is supposed to provide good manoeuvring characteristics in both open water and difficult ice conditions.

The ship has one transverse thruster at the bow. The advantage of this is the good turning characteristics at low speeds in harbour operations, for example. The benefit of the transverse thruster greatly reduces when the ship has some forward speed. Thus, Ondo is outfitted with two Azipod units at the stern in order to give good manoeuvrability options when moving with significant forward speed. The combination here presented has shown to be very effective in previously designed ships and this has been seen in full-scale observations.

Ondo is aimed at carrying out research. In several situations such as when launching and using autonomous underwater systems (e.g. ROVs), it is important to be able to hold the ship in the same position. This is done using a dynamic positioning (DP) system.

A conceptual dimensioning of the propulsion system is illustrated in Figure 5. Ondo is equipped with two ABB Azipod ICE units, with 4.5 MW each.

	Azipod ICE
A [m]	5.2–6.2
B [m]	2.4–3.0
C [m]	2.8–2.9
ØD [m]	2.5–3.5
E [m]	0.7–1
F [m]	2
G [m]	2.7–3
H [m]	N / A
J [m]	N / A
K [m]	N / A
L [m]	N / A
Tilt [deg]	0

Figure 4. Dimensions for ABB Azipod ICE.

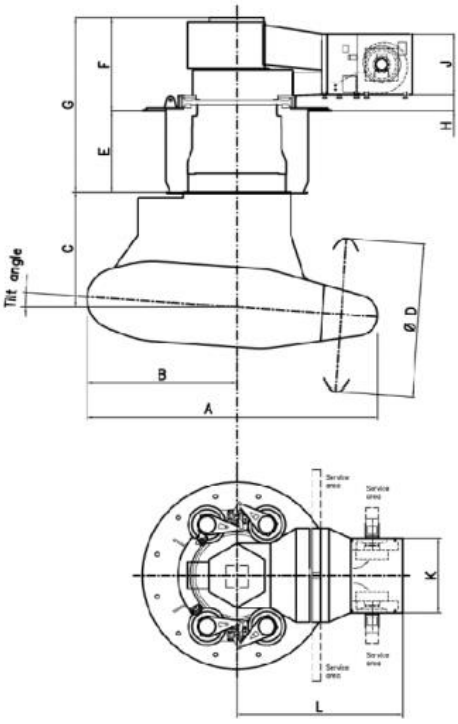

Figure 5. Sketch of dimensions for ABB Azipod Ice.

From Figure 4, we can conclude that the diameter (D) of the Azipod ICE to be used (4.5 MW each, with a maximum Azipod ICE delivering 7 MW) is around 3.3 metres, the length (A) is 5.8 metres and the height (C+E) of the Azipod out of the hull is 3.6 metres.

At the bow region there is one bow thruster, as mentioned previously. This is of Wärtsilä CT/FT 125 H type. This type of transverse thruster can deliver during manoeuvring 516 kW and in dynamic positioning operations 501 kW. Its dimensions are as shown next in Figure 6 and Figure 7:

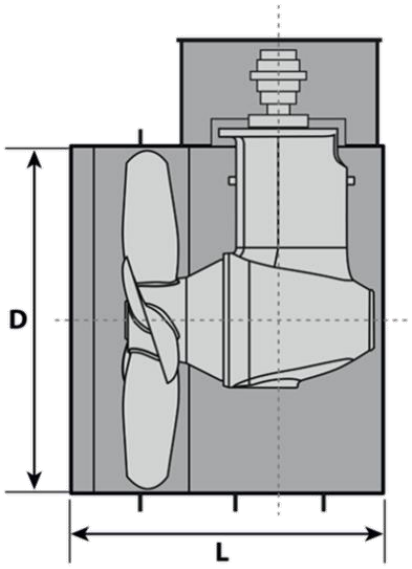

Figure 6. Sketch of dimenions for Wärtsilä transverse thruster.

Thruster type	Electrical Frequency	Input Speed	Maximum Power [1]		Propeller Diameter (D)	Length (L)	Weight [2]
			Manoeuvring	Dynamic Positioning			
	(Hz)	(rpm)	AUX (kW)	DP (kW)	(mm)	(mm)	(kg)
CT/FT 125 H	50	1480	516	501	1250	1550	2820

Figure 7. Wärtsilä transverse thrusters - range and dimensions.

In Figure 8 and Figure 9, the sketches of the beforementioned manoeuvring devices are shown on the NAPA-input got from the Ship Design Portfolio (SDP) course.

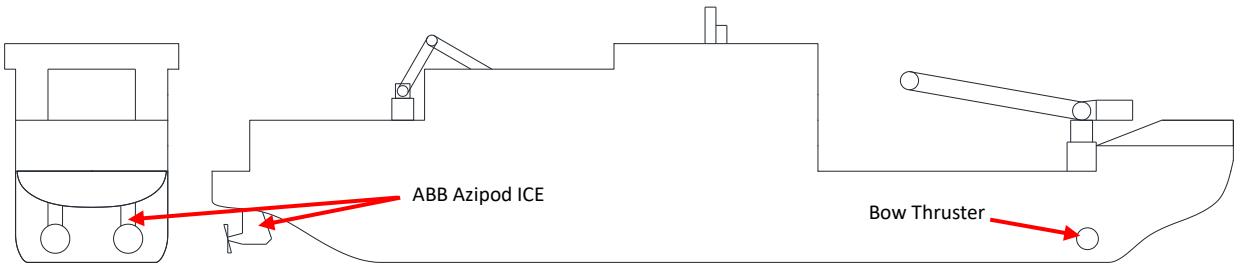

Figure 8. Sketch of manoeuvring devices on NAPA-input (1).

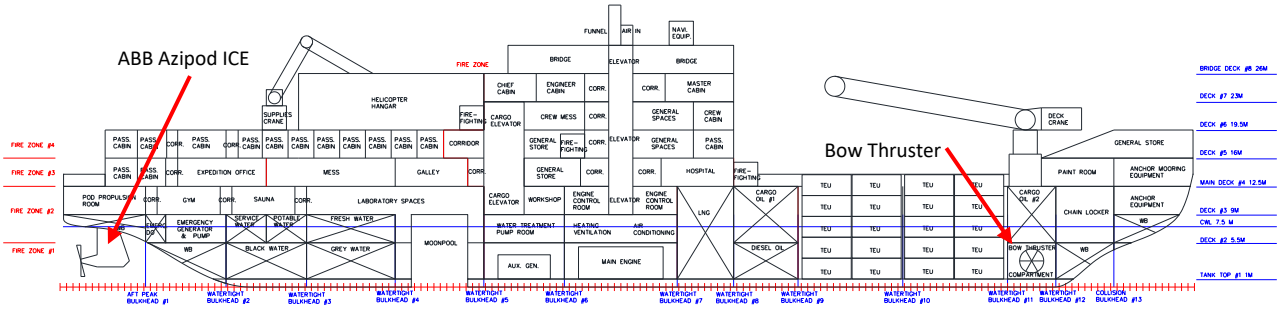

Figure 9. Sketch of manoeuvring devices on NAPA-input (2).

In addition, other possible devices to consider in terms of ship dynamics are bilge keels and stabilizer fins (both looked at their feasibility through articles read as part of this project work) and passive and active anti-roll tanks. Passive anti-roll tanks are considered in the design stage of Ondo and their location can be seen in Figure 10:

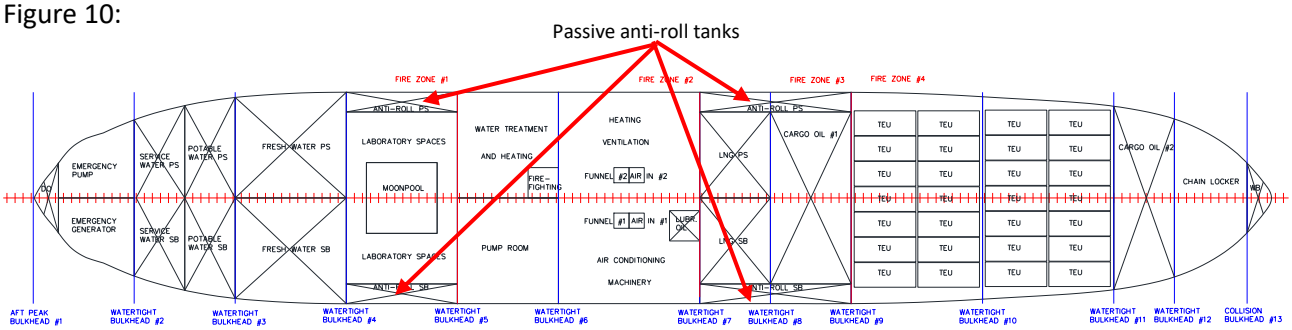

Figure 10. Location of the anti-roll tanks on the GA of Ondo.

4 Main features of hull form affecting ship dynamics

The hull form has a big effect on ship dynamics. For instance, the hull form should be such that it enables homogenous inflow to propellers so that it is possible to take the advantage of the highest efficiency possible of the propellers and also to avoid excessive stresses and vibrations. How to optimise in the best way the hull form is fairly looked at in the article discussed in Section 19.1.1. The bow form of the vessel influences seakeeping characteristics. After several iterations in the hull form of Ondo, starting with the hull form obtained during the Principles of Naval Architecture course to the different iterations made while defining the new hull form using NAPA, we came up with a bow form which is not optimised to either ice breaking nor open water navigation. In other words, we looked at finding a compromise between both of these so that we could get reasonable advantages from both of these and minimise up to some point their negative influences. An optimised bow for icebreaking has excellent properties to break ice but lacks good operation characteristics in open seas. For instance, this type of bow brings high roll motions, wave resistance, and slamming which are extremely harmful to the type of vessel being defined. On the other hand, a bow optimised to open water leads to very high ice breaking resistance, which in our case is not allowed. Taking into consideration the operational profile defined previously, it is concluded that a compromise between both of this is ideal to our design. In addition, regarding the stern, we also have present a transom. Its behaviour in waves might affect both positively or negatively the resistance of the ship. For instance, if the transom gets submerged up to some point it will increase considerably the resistance due to flow separation.

The form of the ship's hull is estimated by means of various form coefficients. The value of block coefficient is one for a ship with the rectangular cross-section. Hence, for a typical ship's hull form, it would be less than one. The higher the block coefficient, the fuller is the hull form (e.g. oil tankers, bulk carriers). Finer hull-forms have lower block coefficients (e.g. container ships, warships). For instance, ship with greater block coefficient coupled with a wider beam leads to smaller rolling motions. In addition, pure loss of stability might be related to designs with lower block coefficients where changes in the draft of the ship (due to waves) lead to significant changes in the waterplane area. However, in the case of Ondo the Froude number is lower than 0.24 and consequently, there should not be issues related to pure loss of stability (Ship Buoyancy and Stability course lecture notes). Another situation that needs to be accounted for is the vulnerability to parametric roll which cannot be assessed easily at this point.

In addition to the few aspects mentioned here, there are many other aspects of a ship's hull that play a major role in the performance of the ship at sea. Calculation of bare hull resistance is an important step in determining the energy efficiency of the hull. Another vital aspect of the ship's hull is its watertight integrity. To ensure this, we must ensure the intact and damaged stability of the ship. Vibration and dynamic response

of the ship's hull is a factor that determines not only the performance of the ship but also its longevity at sea. Out of all the different vibrations on a ship, vibration of a ship's hull girder is of major concern.

5 Water depths and seasonal variations of wave conditions

5.1 Water depths

As seen in Section 1 of this report, Ondo's ship route being considered starts in Helsinki and runs through Baltic, North, Norwegian and Barents Seas to the Arctic regions for research and supply missions. The Baltic Sea is relatively shallow with average water depth of 55 m. Maximal depth is 459 m. Ondo Baltic Sea route lays in water depths of around 50-75 m in Gulf of Finland and Danish Straits region, and in depth of 75 up to 150 m in Gotland Island region - Figure 11.

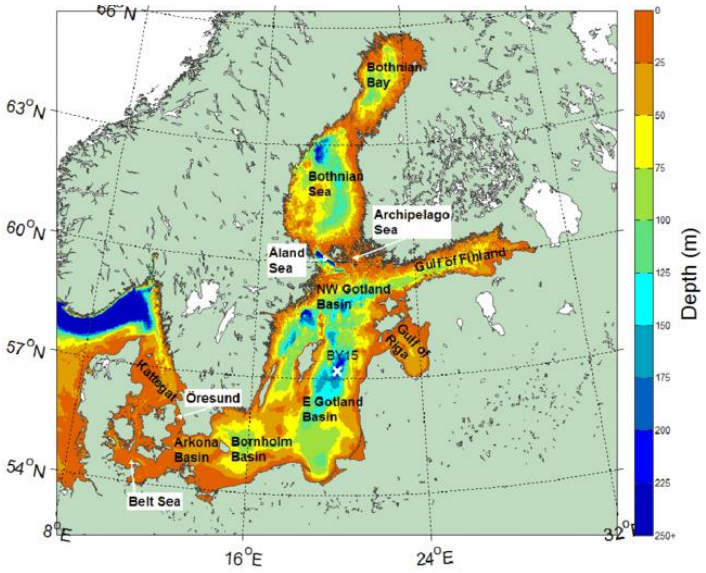

Figure 11. Baltic Sea water depths.

North Sea's average depth is around 95 m. Maximal water depth is 700 m. Ondo North Sea part of the route lays in water depths around 200 m - Figure 12.

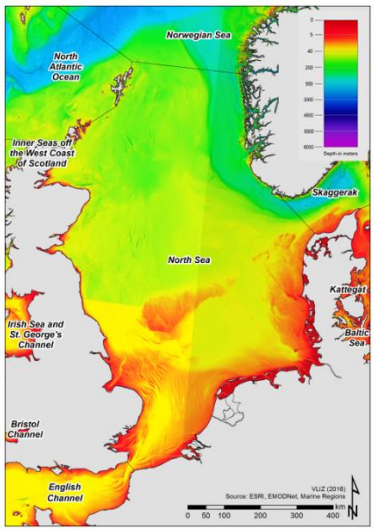

Figure 12. North Sea water depths.

Norwegian Sea average water depth is 2000 m. Maximal water depth is 3970 m. Ondo will go through regions of sea which are located on continental shelf where depths is around 300 m - Figure 13.

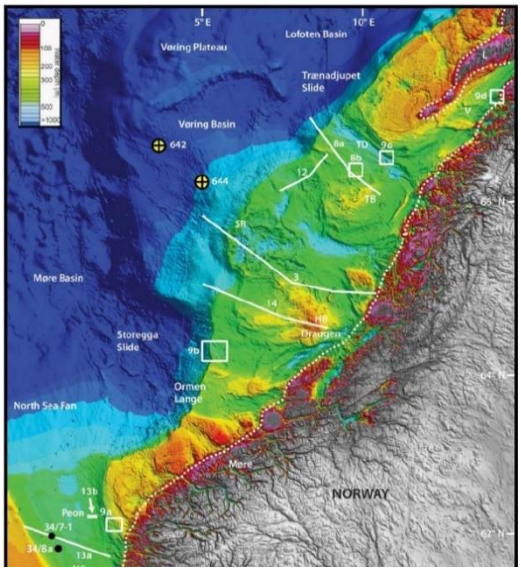

Figure 13. Norwegian Sea water depths.

Barents Sea average water depths is 230 m. Maximal depth is 600 m. In the Barents Sea Ondo will go to the north-east regions where water depth is up to 500 m - Figure 14. In these regions intensity of ice conditions starts to increase.

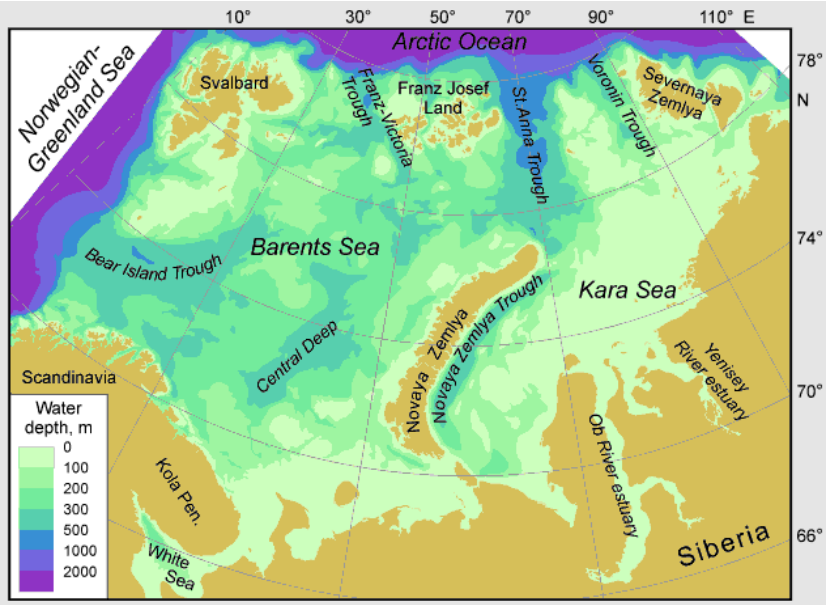

Figure 14. Barents Sea water depths.

5.2 Seasonal variations of wave conditions

Northern Europe's part of the route across Baltic, North and Norwegian Seas in autumn/winter periods has more severe wave conditions. This is because of European windstorms which come from North Atlantic and are most frequent between October and March.

In Baltic Sea in period of windstorms strongest winds from west/southwest cause waves with heights of 5-6 m and length of 50-70 m. On the other hand, North Sea in period of windstorms has waves with heigh of 8-10 m in the north. Last but not least, in the Norwegian Sea storms significant wave height can be up to 17 m.

The results which have been summed up above can be found in Figure 15 and Figure 16. The worst and more demanding wave conditions are seen to happen in January where the Baltic, North and Norwegian Seas have the highest significant wave height. On the other hand, the significant wave period (approximated to the mean peak period) is found to increase when Ondo moves, during a voyage, from the Baltic Sea to the North Sea and finally gets to the Norwegian Sea to continue up north, for instance, to the Barents Sea. Important to note is that for the scope of this course on Ship Dynamics, data got from *Metoceanview* was used instead of the more accurate and reliable data included in the atlas of Global Wave Statistics developed by the British Maritime Technology, due to us not having access to it for copyright reasons.

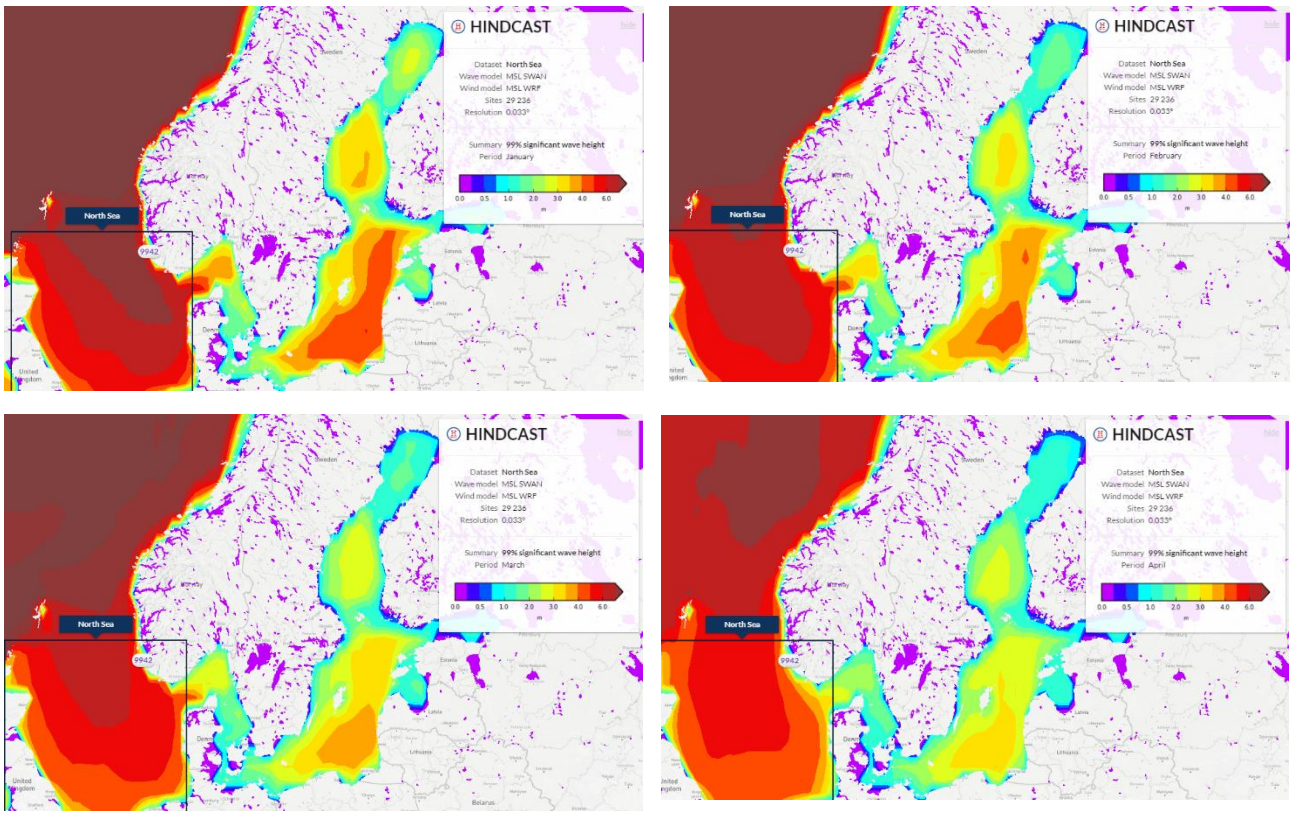

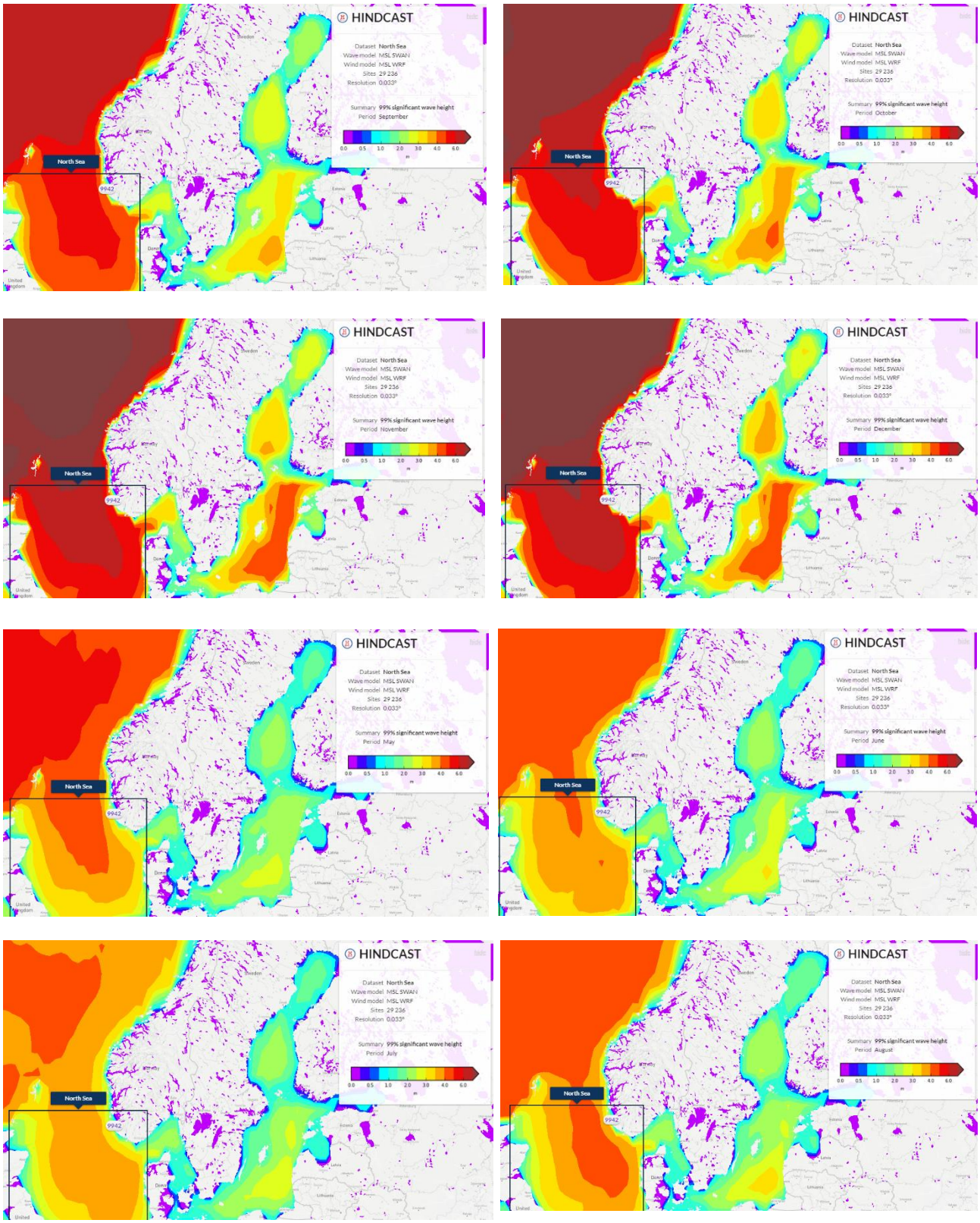

Figure 15. Significant wave height variation throughout the year (January to December).

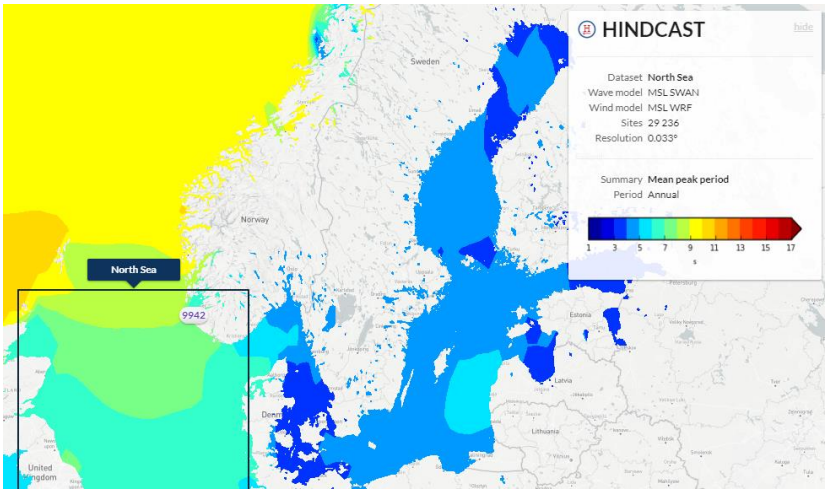

Figure 16. Mean peak period.

6 Potential flow theory – deep and shallow water waves

In this section of the report, it is shown the sketch of deep and shallow waters that our design might encounter on its route. This is done considering the potential flow theory and the results are drawn in the profile of Ondo.

Ondo's route encounters relatively shallow water in the Baltic Sea thus shallow water waves may be present. Below on Ondo profile are sketched waves with height 5 m and length 50 m - Figure 17. These type of waves appear in Baltic Sea in stormy autumn/winter periods.

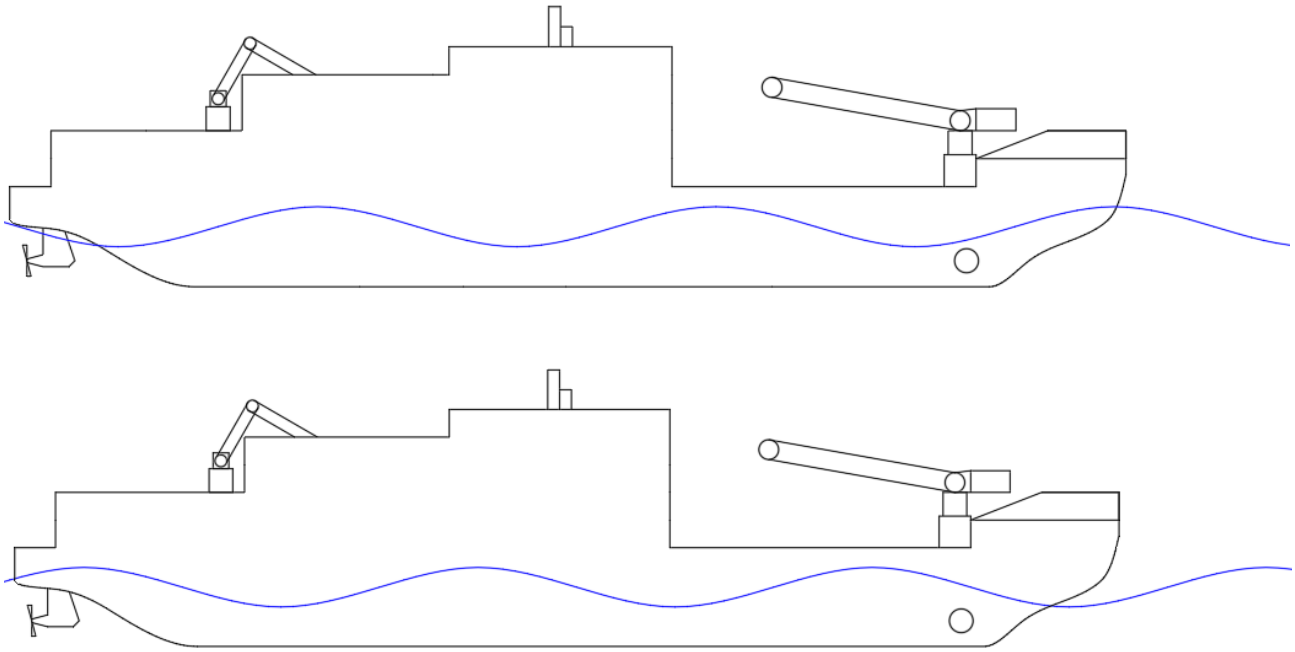

Figure 17. Shallow waves in Baltic Sea.

North Sea consists of deep water thus Ondo will encounter deep-water waves as well. Here, significant wave height is assumed to be 7 meters or more which is realistic for North Sea stormy conditions. In Figure 18 is drawn wave with height 8 m and length 90 m.

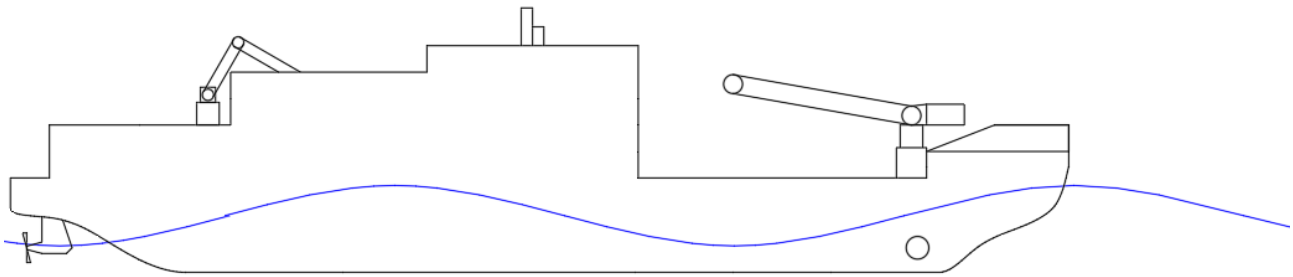

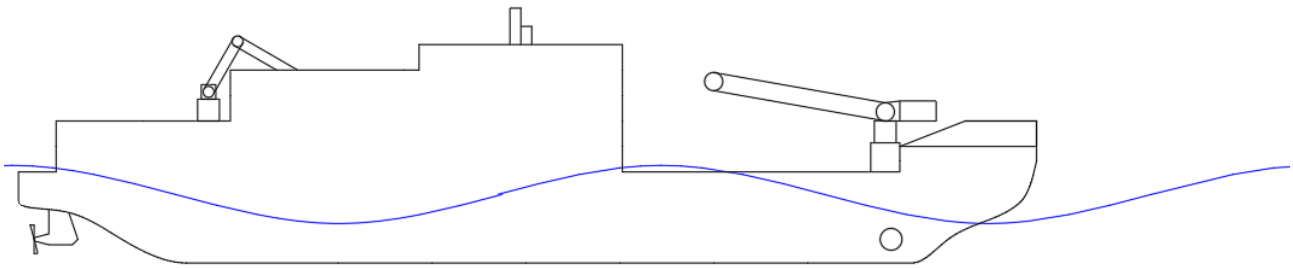

Figure 18. Deep-water waves in North Sea.

7 Wave spectra

A wave spectrum represents the wave energy (or wave amplitude) distribution of individual wave frequencies in a stationary sea state.

According to DNV GL, the wave spectra most relevant for ships are the two parameter Pierson-Moskowitz (PM) and JONSWAP wave spectra. These are unidirectional wave spectra referred to as single peak one-dimensional wave spectra, i.e. without wave energy spreading. Consequently, as recommended by the class society which has been used throughout our design project (DNV GL), one of the abovementioned wave spectra will be chosen.

According to the book by Ochi "Ocean Waves – The Stochastic Approach", the Pierson-Moskovitz spectral formulation (Pierson and Moskovitz 1964) was developed from analysis of measured data obtained in the North Atlantic by Tucker wave recorders installed on weather ships. Analysis was carried out only on selected wave records considered to have been acquired in fully developed seas. On the other hand, the JONSWAP spectrum is described to have been based on an extensive wave measurement program known as the Joint North Sea Wave Project carried out in 1968 and 1969 along a line extending over 160 km into the North Sea from Sylt Island (Hasselmann et al. 1973). The spectrum represents wind-generated seas with fetch limitation, and wind speed and fetch length are inputs to this formulation. The JONSWAP spectrum is the product of the Pierson-Moskovitz spectrum by a factor called the peak enhancement factor.

In fact, by analysing the wave conditions which Ondo has to face during a typical voyage (Section 1) it will navigate in the Baltic, North and Norwegian Seas as it goes up north to an arctic region of choice to do research and the worst-case scenario is seen in January (Section 5.2). This is when the wave conditions are the worst as the significant wave height is the highest among the year.

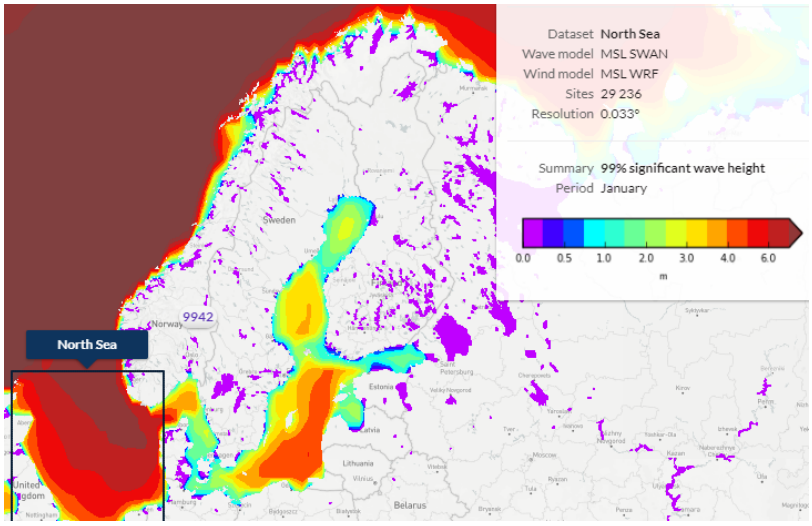

Figure 19. Significant wave height in January.

From Figure 19, where is shown the significant wave height throughout the route of Ondo in January which, for instance, represents the conditions the ship will face after coming back to its home port in Helsinki after doing research in the Arctic. Here it is seen that the maximum significant wave height it will encounter is of around roughly 7.0 metres which takes place in regions of the North and Norwegians Seas.

Next, we can look at statistic regarding the peak period of the waves in regions relevant for Ondo. A colourful plot containing the average peak period of waves is shown in Figure 20 and this is taken as an approximation of the significant wave period.

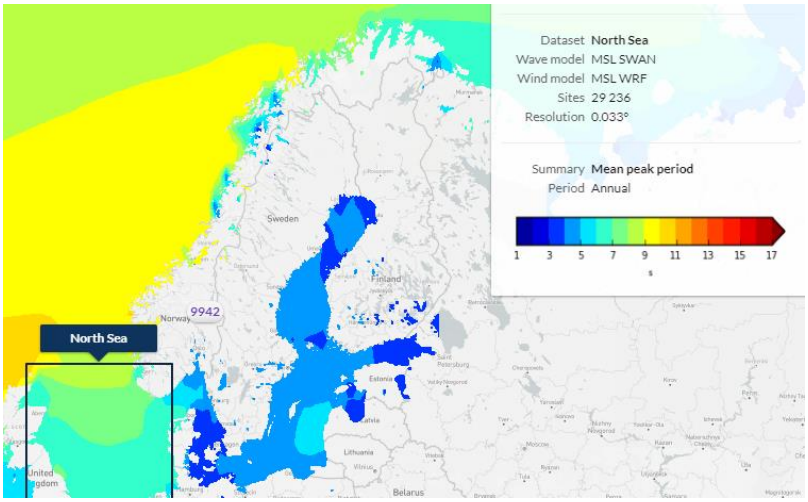

Figure 20.Average significant wave period (approximation).

From Figure 29 it can be seen that the average peak period, which is taken as the significant wave period, is set between 7 and 10 seconds in the North and Norwegian Seas where the wave height conditions were found to be the worse (highest) in Figure 19. For practical reasons, let us take the significant wave period to be considered as 10 seconds.

To sum up, the significant wave height which will be considered is H_S = 7.0 metres and the significant wave period is T_S = 10 seconds.

The route of Ondo being considered here will consist of both open water (in the Norwegian Sea and further North), where fetch is not limited by land and by areas where the fetch is limited (such as the Baltic Sea, the Danish Straights and a big part of the North Sea). Additionally, some experiments have shown that JONSWAP-spectrum represents wind sea characteristics in open waters more accurately than Pierson-Moskovitz spectrum (Hasselmann, 1973), which is due to shape-stabilisation caused by quadruplet wave-wave interactions, which redistribute the wave energy. As DNV GL refers in their rules, JONSWAP-spectrum is widely used among the engineering community (Holthuijsen, 2007). Consequently, we find that the most adequate wave spectra to represent the wave conditions Ondo will encounter is the JONSWAP-spectrum. This will be analysed in some further detail from now on.

The JONSWAP wave spectrum is formulated as a modification of the PM wave spectrum, and JONSWAP represents a developing sea state in a fetch limited situation:

$$S_J(\omega) = A_\gamma S_{PM}(\omega)\gamma^{\exp(-0.5(\frac{\omega-\omega_p}{\sigma\omega_p})^2)}$$

where:

γ = non dimensional peak shape parameter

σ = spectral width parameter

σ_a for $\omega \leq \omega_p$

σ_b for $\omega > \omega_p$

$A_\gamma = 1 - 0.287ln(\gamma)$ is a normalising factor

Average values for the JONSWAP experimental data are γ = 3.3, σ_a = 0.07, σ_b = 0.09.

Additionally, class regulations say that the JONSWAP wave spectrum is expected to be a reasonable model if:

$$3.6 < T_p / \sqrt{H_s} < 5$$

This even gives more reasoning to our choice of wave spectra as the ratio shown above between the significant wave period and the square root of the significant wave height, in our case shown, lays exactly in that range:

$$3.6 < T_p / \sqrt{H_s} = 10 / \sqrt{7} \approx 3.78 < 5$$

As understood, the PM wave spectrum is the basis of the JONSWAP wave spectrum. Therefore, the PM wave spectrum for a fully developed sea is shown and is given by:

$$S_{PM}(\omega) = \frac{5}{16} H_S^2 \omega_p^4 \omega^{-5} \exp(-\frac{5}{4}(\frac{\omega}{\omega_p})^{-4})$$

where:

ω = wave frequency in rad/s

ω_p = spectral peak frequency = $2\pi / T_p$, in rad/s

Having all this input defined, we can then use MATLAB to get the plot of the JONSWAP wave spectrum that we are considering (using the average values obtained from experimental data). Figure 21 is the basis spectrum for Figure 22, as explained previously.

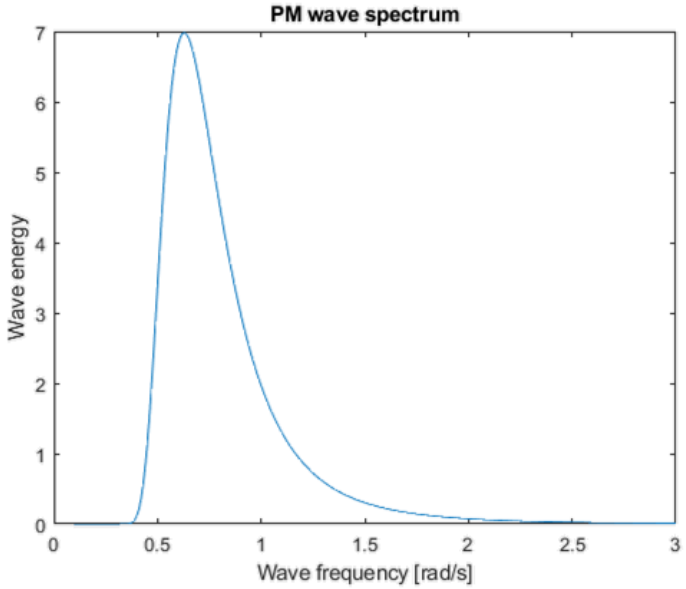

Figure 21. PM wave spectrum.

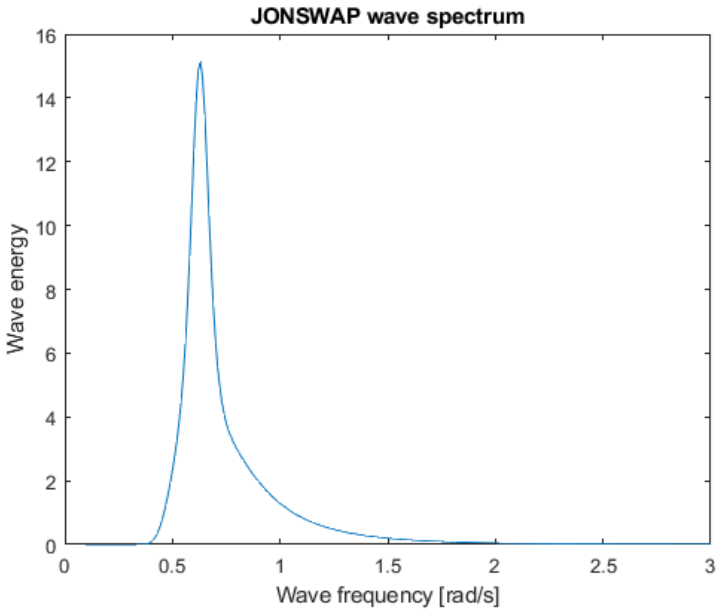

Figure 22. JONSWAP wave spectrum.

Figure 22 represents the JONSWAP wave spectrum we have taken as described in DNV GL regulations in Class Guideline, DNVGL-CG-0130, corresponding to Wave Loads (edition January 2018). From the plot of the wave

spectrum shown it is found that the peak wave energy is found to be equal to approximately 15 and it refers to a have frequency of around 0.63 rad/s, the spectral peak frequency. The wave energy is found in a very narrow band of frequencies. It can be said that the energy is located from 0.5 to 1.5 rad/s. In addition, comparing both wave spectrums in Figure 21 and Figure 22 it is concluded that in the latter one, the peak energy is more than double and in the first one the energy is slightly more dispersed throughout the wave frequencies.

7.1 Joint distribution of significant wave height and period

Joint environmental models are required for a consistent treatment of the loading in a reliability analysis and for assessment of the relative importance of the various environmental variables during extreme load/response conditions and at failure.

Different approaches for establishing a joint environmental model exist. The Maximum Likelihood Model (MLM) (Prince-Wright, 1995), and the Conditional Modelling Approach (CMA) (e.g. Bitner-Gregersen and Haver, 1991), utilise the complete probabilistic information obtained from simultaneous observations of the environmental variables. The MLM uses Gaussian transformation to a simultaneous data set while in the CMA, a joint density function is defined in terms of marginal distribution and a series of conditional density functions. According to DNV GL, the CMA joint model is recommended. The significant wave height is modelled by a 3-parameter Weibull probability density function:

$$f_{H_s}(h) = \frac{\beta_{Hs}}{\alpha_{Hs}}\left(\frac{h-\gamma_{Hs}}{\alpha_{Hs}}\right)^{\beta_{Hs}-1}\exp\left\{-\left(\frac{h-\gamma_{Hs}}{\alpha_{Hs}}\right)^{\beta_{Hs}}\right\}$$

And the zero-crossing wave period conditional on H_s is modelled by a lognormal distribution:

$$f_{T_Z|H_s}(t\,|\,h) = \frac{1}{\sigma t\sqrt{2\pi}}\exp\left\{-\frac{(\ln t-\mu)^2}{2\sigma^2}\right\}$$

Where the distribution parameters μ and σ are functions of the significant wave height.

The parameters from the above equation can be found in the DNV GL rules – Environmental Conditions and Environmental Loads. In this classification's society rules, the world is divided into several regions (Figure 23) where the significant wave height is modelled using the probability functions shown. The operational profile being studied here, and which has been presented previously includes the nautical zones numbers 1, 4, 5 and 11. The specific parameters for the different nautical zones within the operational profile shown are presented in Figure 24 (in red). For the various nautical zones defined, it is assumed that:

$$\gamma_{Hs} = 0$$

$$\mu = 0.70 + a_1 H_s^{a_2} \text{ and } \sigma = 0.07 + b_1 e^{b_2 H_s}$$

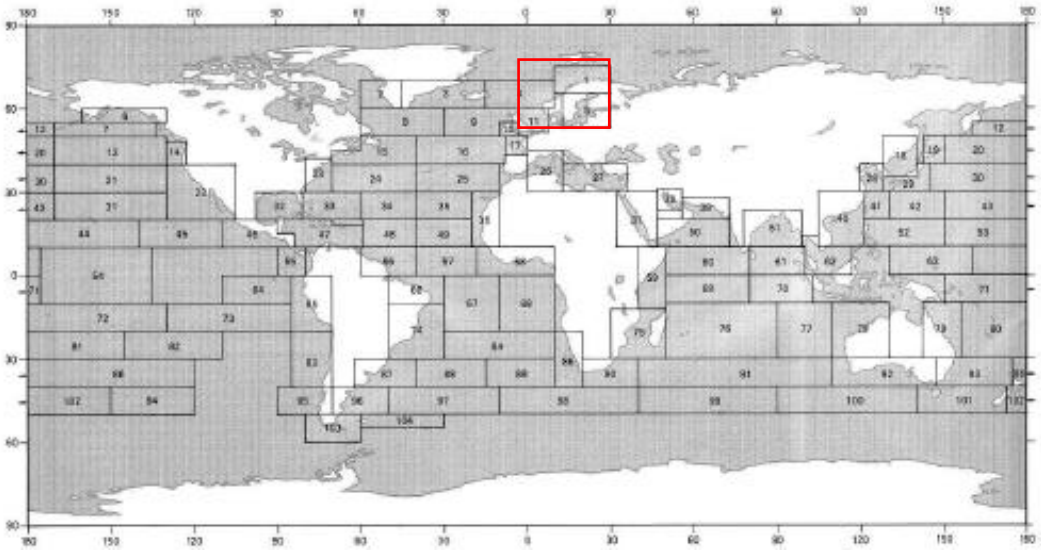

Figure 23. Nautic zones for estimation of long-term wave distribution parameters (DNV GL).

Area	α_s	β_s	a_1	a_2	b_1	b_2
1	2.33	1.33	0.974	0.205	0.1263	-0.0201
2	1.96	1.34	0.994	0.175	0.1414	-0.0238
3	2.74	1.35	1.127	0.160	0.1255	-0.0912
4	2.84	1.53	1.125	0.150	0.0978	-0.0074
5	1.76	1.59	0.828	0.167	0.3449	-0.2073
6	2.76	1.45	1.128	0.154	0.0964	-0.0066
7	3.39	1.75	1.256	0.118	0.0809	-0.0069
8	3.47	1.57	1.272	0.114	0.0728	-0.0015
9	3.56	1.61	1.260	0.119	0.0755	-0.0054
10	2.45	1.37	1.036	0.181	0.1166	-0.0137
11	2.19	1.26	0.935	0.222	0.1386	-0.0208

Figure 24. 2-parameter Weibull parameters and Log-Normal distribution parameters for Hs and Tz.

As the significant wave height and period considered until now are for regions 4 and 11, these will be analysed here:

- Region 4

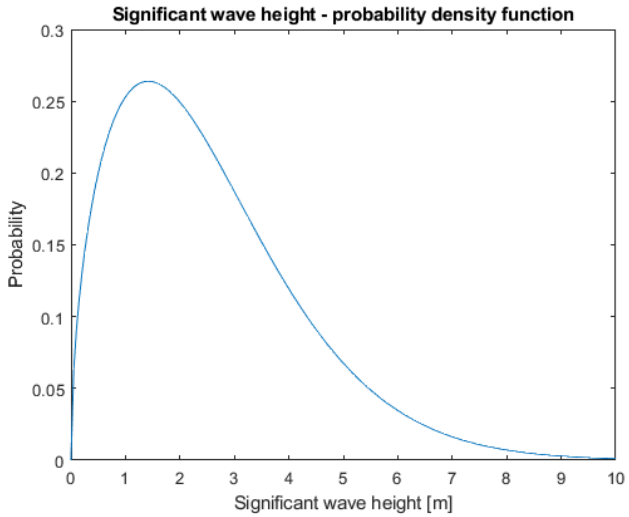

Figure 25. Significant wave height - probability density function.

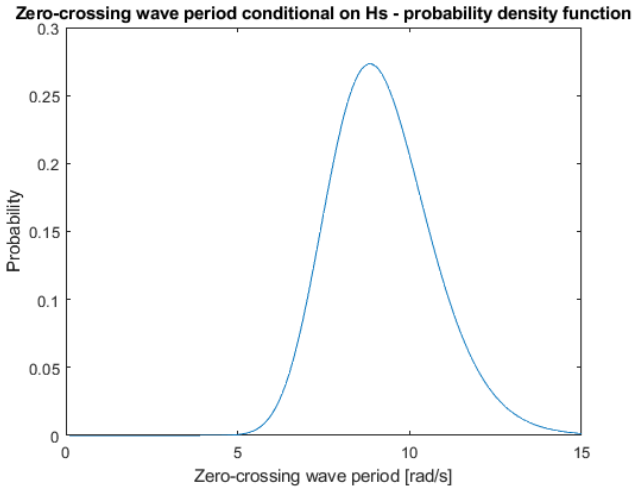

Figure 26. Zero-crossing wave period conditional on Hs - probability density function.

In Figure 25 can be seen the long-term probability of wave heights, in metres, taking into consideration the scatter diagram from region 4. From the probability density function, it can be concluded that the probability of the wave height exceeding 7 metres (significant wave height being studied) is of 98%. Consequently, waves greater than the significant wave height considered are rare. On the other hand, the probability density function of the zero-crossing wave period conditional to the significant wave height of 7 metres is shown in Figure 26.

- Region 11

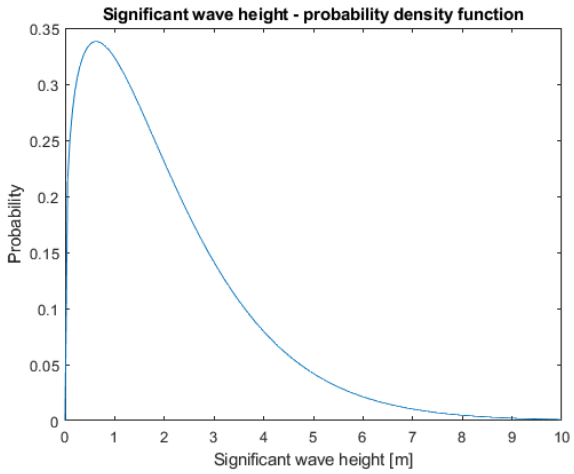

Figure 27. Significant wave height - probability density function.

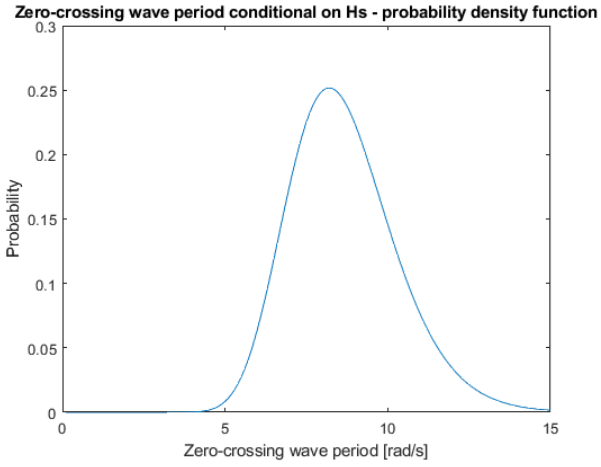

Figure 28. Zero-crossing wave period conditional on Hs - probability density function.

Here, in Figure 27 can be seen the long-term probability of wave heights, in metres, taking into consideration the scatter diagram from region 11. From the probability density function, it can be concluded that the probability of the wave height exceeding 7 metres (significant wave height being studied) is of 98.34%. Consequently, waves greater than the significant wave height considered are, just like previously, rare. On the other hand, the probability density function of the zero-crossing wave period conditional to the significant wave height of 7 metres is shown in Figure 28.

8 Extreme events

Extreme events include several types of phenomena such as rogue waves, tsunamis, etc. In this section, we will consider only rogue waves as these are more related to the scope of this Ship Dynamics course.

Rogue waves, also known as freak, monster, episodic, killer, extreme or abnormal waves, are unusually large, unpredictable and suddenly appearing surface waves that can be extremely dangerous to ships. They are distinct from tsunamis, which are caused by the displacement of water due to other phenomena, such as earthquakes, and are often almost unnoticeable in deep waters.

Rogue waves are usually defined as waves whose height is more than twice the significant wave height, which is defined as the mean of the largest one third of waves in a record. This means that the rogue are unusual large waves for a given sea state. These types of waves do not have a single distinct cause but occur where physical factors such as high winds and strong currents cause waves to merge (constructive interference/interaction) to create a single extremely large wave. An example of a record having a rogue wave is shown next in Figure 29.

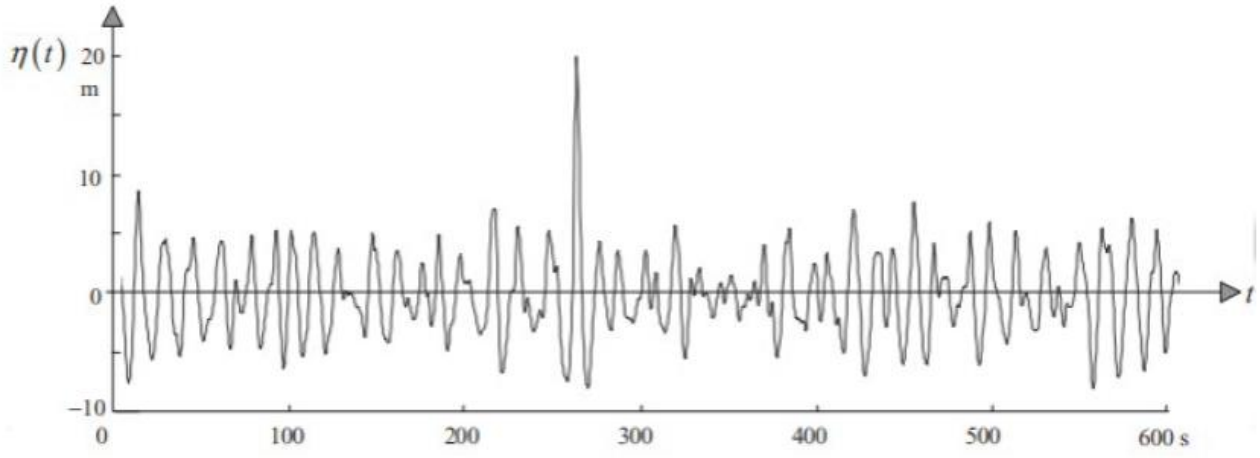

Figure 29. Wave record showing a rogue wave.

The occurrence of rogue waves has a dependence on the operational area due to different possible physical mechanics of rogue wave generations. However, no nautical area is free from suffering a rogue wave or an extreme event as it depends on the sea state.

From data available, it is seen that there have been registered a couple of rogue waves in the North Sea which is a region well within the operational profile of Ondo being considered. Therefore, we believe that there is somewhat likelihood that our design might, at some point face the influence of this type of extreme event. Referring back to Figure 25 and Figure 27, it was seen that having a wave height in the long-term much higher than the significant wave height of 7 metres (found to be the most demanding situation, during the

beginning of the year, in January) is very rare and thus the probability of occurring a wave with height more than twice the significant wave height is nearly zero.

Looking at the *Metoceanview* website where were found the significant wave height and period considered period, we can only obtain an estimation of the 10-, 100- and 1000-year wave height that Ondo would find in the regions it is operating. For the case of Ondo, a ship, the latter two do not make sense due to the typical lifetime of a ship which is set at around 20 years. Let us therefore look at the 10-year wave height estimation for the regions of the Baltic, North and Norwegian Seas. The annual results are shown in Figure 30.

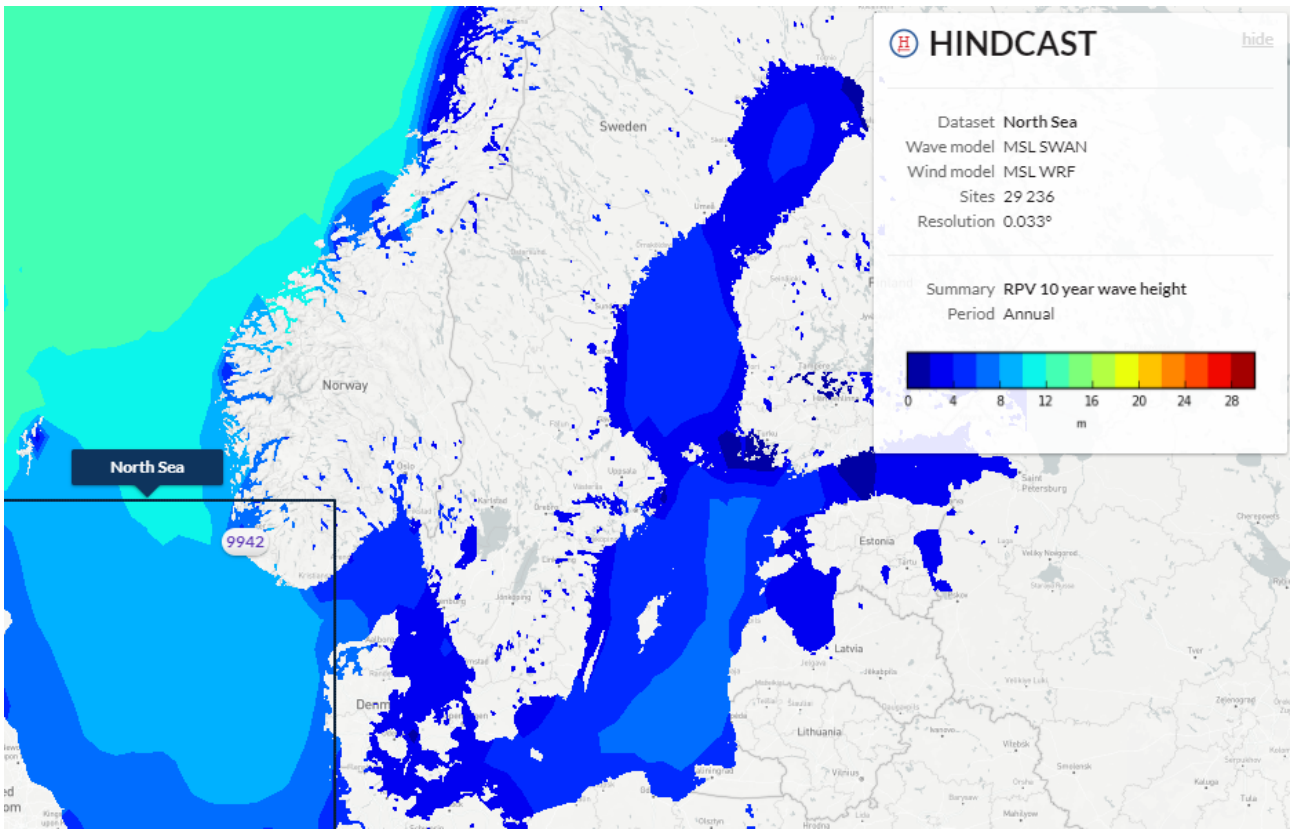

Figure 30. 10-year wave height estimation (Metoceanview).

From Figure 30 it is seen that the 10-year wave height maximum in the region which is of interest for Ondo is set at 17 metres. This is, in fact, much higher than the significant wave height considered previously (7 metres). Consequently, this might be something to consider in more in-depth analysis of the wave conditions to encounter in this operational profile.

9 Main components of Equations of Motion and mission

A ship when moving in water may experience motions in all six degrees of freedom. These are shown in Figure 31. Consequently, six equations of motion are necessary to describe the dynamic behaviour of a ship.

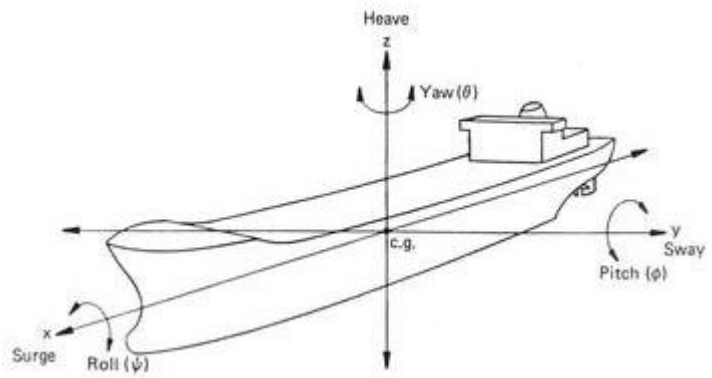

Figure 31. Six degrees of freedom of a ship.

The ship rigid body motions are linear displacements, also called translations (surge, sway, and heave), and rotations (roll, pitch, and yaw). The linear and rotational displacements for all the six degrees of freedom in regular waves, are represented by simple harmonic functions, and these are presented below:

$$\text{Surge: } x = x_a \cos(\omega_e t + \varepsilon_{x\varsigma})$$

$$\text{Sway: } y = y_a \cos(\omega_e t + \varepsilon_{y\varsigma})$$

$$\text{Heave: } z = z_a \cos(\omega_e t + \varepsilon_{z\varsigma})$$

$$\text{Roll: } \phi = \phi_a \cos(\omega_e t + \varepsilon_{\phi\varsigma})$$

$$\text{Pitch: } \theta = x_\theta \cos(\omega_e t + \varepsilon_{\theta\varsigma})$$

$$\text{Yaw: } \psi = \psi_a \cos(\omega_e t + \varepsilon_{\psi\varsigma})$$

In the above equations, the left-hand side is the dynamic response in question, the first factor on the right-hand side of the equations represent the amplitude of the response, ω_e is the encounter frequency, t is time and the ε -term accounts for the phase shift. By using this formulation for the displacement functions, it is important to note that we are assuming regular waves and the linear theory. By making these assumptions, the total motion given at any point of the ship is then evaluated by superposition. Consequently, this is a very

relevant and important assumption since it allows to describe motions in irregular waves by superimposing regular waves. In addition, the displacements are evaluated at the centre of gravity of the ship, as shown previously in Figure 31.

Velocity and acceleration of the motion is an essential parameter of each one of the equations of motion. These can be easily obtained from the assumed harmonic motion of each component by derivation. Time first derivative of displacement gives velocity, and second derivative in relation to time gives the respective acceleration. This computation is shown below:

$$\mathrm{A} = \mathrm{A}_a \cos(\omega_e t + \varepsilon_{\mathrm{A}\varsigma})$$

$$\dot{\mathrm{A}} = -\omega_e \mathrm{A}_a \sin(\omega_e t + \varepsilon_{\mathrm{A}\varsigma}) = \omega_e \mathrm{A}_a \cos(\omega_e t + \varepsilon_{\mathrm{A}\varsigma} + \pi/2)$$

$$\ddot{\mathrm{A}} = -\omega_e^2 \mathrm{A}_a \cos(\omega_e t + \varepsilon_{\mathrm{A}\varsigma}) = \omega_e^2 \mathrm{A}_a \cos(\omega_e t + \varepsilon_{\mathrm{A}\varsigma} + \pi)$$

where A may refer to any of the six degrees of freedom (surge, sway, heave, roll, pitch, or yaw).

Newton's second law is the basis for the ship equations of motion:

$$(m + a)\ddot{x} + c\dot{x} + kx = F(t)$$

where *m* is the ship's mass, *a* the added mass, *x* the displacement, *c* the hydrodynamic damping, *k* the stiffness and *F(t)* an excitation due to external environment.

Both the added mass and hydrodynamic damping coefficients are a function of frequency of oscillation. However, added mass depends primarily on the shape of the ship's hull, the type of motion (linear or rotational), and the direction of the motion. Therefore, added mass differs from just mass since mass is a quantity independent of motion. (Hirdaris, 2021). On the other hand, hydrodynamic damping is related to the viscosity of the fluid. Added mass is proportional to acceleration whereas hydrodynamic damping is proportional to velocity.

The last remaining term to be discussed, kx, related to the restoring force. In ship dynamics, the restoring forces are analogous to spring stiffness in mechanical systems. In the case of a ship, the existence of restoring forces depends on the degree of freedom being considered. More precisely, there is a restoring force in heave, roll and pitch motions. These are discussed more in the following section. Thus, for the equations of motion for surge, sway, and yaw, $k\mathrm{x} = 0$.

In the case of Ondo, the vessel we are designing, ship motions have an extremely big effect on its mission. The most essential ones are here highlighted briefly:

- Having a helicopter landing platform, motions shall be controlled in a way that landing is possible, and it can be done in safe conditions according to regulations.
- When doing offshore supply missions, cargo shall not be damaged due to excessive motions. For instance, excessive roll, heave, and pitch may lead to cargo shifting which may then compromise the delivery of cargo in the required conditions.
- While being dynamically positioned offshore to pursue research, conditions onboard shall be such that research missions can be conducted. For instance, excessive oscillations are not allowed so that personnel can work safely and do their work properly.
- Passenger comfort is a key issue. They shall feel comfortable and safe so that their experience onboard Ondo is unforgettable.
- Having a small impact in environment is an essential mote for Ondo. Therefore, motions shall be kept in a way that maximum possible efficiency is achieved so that least possible propulsion energy is used. For instance, added resistance shall be minimised.

From the points highlighted above, it was seen how important ship motions and their equations are to the mission of Ondo. For instance, ship motions and their effect on the mission of the ship must be well debated so that good design choices can be made with an objective of improving the way Ondo succeeds in its tasks.

In the next section of this report, we will have a look at each equation of motion independently and make reasoning in terms of design choices that might help Ondo to achieve its mission.

10 Effects on Equations of Motion

Here, the simplified equations of motion for a ship with port/starboard symmetry (like the case of Ondo), are shown. The equations used have been taken from Lloyd's (1998) and some terms have been further simplified using the lecture notes of the Ship Dynamics course. Each equation of motion and the effect of the general arrangement, hull form, and operational profile of our ship on them is discussed.

Lloyd's (1998) presents in tabular format the dependency of the equation of motion of each degree of freedom in terms of the added mass, damping coefficients, and the stiffness coefficients. This can be seen in Table 1 and Table 2.

Table 1. Added mass and damping coefficients in the equations of motion for a ship with port/starboard symmetry.

Velocity and acceleration	surge force i=1	sway force i=2	heave force i=3	roll moment i=4	pitch moment i=5	yaw moment i=6
surge j=1	✓	$zero_2$	*small*	$zero_2$	*small*	$zero_2$
sway j=2	$zero_3$	✓	$zero_3$	✓	$zero_3$	✓
heave j=3	*small*	$zero_2$	✓	$zero_2$	✓	$zero_2$
roll j=4	$zero_3$	✓	$zero_3$	✓	$zero_3$	✓
pitch j=5	*small*	$zero_2$	✓	$zero_2$	✓	$zero_2$
yaw j=6	$zero_3$	✓	$zero_3$	✓	$zero_3$	✓

Table 2. Stiffness coefficients in the equations of motion for a ship with port/starboard symmetry.

Displacement	surge force i=1	sway force i=2	heave force i =3	roll moment i=4	pitch moment i=5	yaw moment i=6
surge j=1	$zero_1$	$zero_1$	$zero_1$	$zero_1$	$zero_1$	$zero_1$
sway j=2	$zero_1$	$zero_1$	$zero_1$	$zero_1$	$zero_1$	$zero_1$
heave j=3	*small*	$zero_2$	✓	$zero_2$	✓	$zero_2$
roll j=4	$zero_3$	*small*	$zero_3$	✓	$zero_3$	*small*
pitch j=5	*small*	$zero_2$	✓	$zero_2$	✓	
yaw j=6	$zero_3$	✓	$zero_3$	✓	$zero_3$	✓

In the above tables, a tick (*√*) means that the value is significant, *zero₁* means that it is zero by geography, *zero₂* that it is zero due to symmetry of the hull, *zero₃* is zero for small motions and *small* means it can be neglected.

Consequently, considering all the information acquired, from Table 1 and Table 2 it is possible to conclude that the surge equation of motion is the only one which does not depend on parameters coming from the other degrees of freedom, when considering that small influences can be neglected. On the other hand, sway depends on both roll and yaw, heave on pitch, roll on sway and yaw, pitch on heave, and yaw on sway and roll. When concluding this, we are considering that the motions taking place are small thus, for larger motions this would lead to much more complex definition of the problem, and that the sea state can be described by a certain wave spectrum which would lead to less severe sea conditions (geographical factor in Lloyd's).

In general, it is seen that there is no coupling between the vertical plane motions and the lateral plane motions. This allows the vertical and lateral plane motions to be considered independently.

Let us then have a look at each one of the equations of motion simplified to a ship like Ondo, with hull symmetry. The equations are assumed uncoupled (i.e., coefficients related to other degrees of motion are set to zero) from each other, so that only terms which we can explain at this point come up. For this reason, it must be kept in mind the simplifications that have been done and that the equations of motions would, in fact, be much more complex than what appear here. This is done through Sections 10.1 to 10.6.

10.1 Surge

Surge is the translational motion in the forward and back direction (along the x-axis of the ship). The uncoupled linear equation of motion for surge is:

$$(m + a_{11})\ddot{x} + b_{11}\dot{x} = F_{w10}\sin(\omega_e t + \gamma_1)$$

Here $(m + a_{11})\ddot{x}$ is the sum of the mass and added mass induced inertial forces, respectively; $b_{11}\dot{x}$ is the damping force for surge motion and $F_{w10}\sin(\omega_e t + \gamma_1)$ indicates the wave exciting force (related to surfing in wave crest, for example). As it can be seen in the equation, surge motion does not include a restoring force.

The thrust delivered by the two Azipods installed at the aft of Ondo are the main source involved in surge motion. Additionally, steering and waves can cause the ship to move forward and backwards.

10.2 Sway

Sway is the translational motion of the ship in the side-to-side direction (along the y-axis). The uncoupled linear equation of motion for sway is:

$$(m + a_{22})\ddot{y} + b_{22}\dot{y} = F_{w20}\sin(\omega_e t + \gamma_2)$$

Here $(m + a_{22})\ddot{y}$ is the sum of the mass and added mass induced inertial forces, respectively; $b_{22}\dot{y}$ is the damping force for sway motion and $F_{w20}\sin(\omega_e t + \gamma_2)$ indicates the wave exciting force (related to drifting, for example). From the equation describing the sway motion it is seen that it does not involve any restoring force as in the previous case (surge).

In the case of Ondo, both Azipods and the bow thruster positioned at the fore of the ship can induce sway motion. In addition, steering also plays an important role (coming from the direction that the Azipod flow is in relation to the water flow along the hull). These features, as explained in the first assignment of this course, are extremely important in the case of Ondo so that it has good manoeuvrability when in ports and also when performing research operations by making use of its Dynamic Positioning System. This DPS system is important in terms of countering the external surge and sway motions (by means of the Azipods and bow thruster).

10.3 Heave

Heave is the translational motion of the ship in the vertical direction (along the z-axis). The uncoupled linear equation of motion for heave is:

$$(m + a_{33})\ddot{z} + b_{33}\dot{z} + \rho g A_w z = F_{w30}\sin(\omega_e t + \gamma_3)$$

Here $(m + a_{33})\ddot{z}$ is the sum of the mass and added mass induced inertial forces, respectively; $b_{33}\dot{z}$ is the damping force for heave motion and $F_{w30}\sin(\omega_e t + \gamma_3)$ is the exciting force. $\rho g A_w z$ is the hydrostatic restoring force which comes from the change in displacement of Ondo due to the heave motion. Looking at this restoring force, it is possible to see that the size of the waterplane area has a reasonable influence. Thus, higher the waterplane area is, larger the heave restoring force will be. As only small motions are considered here (assumption done in the beginning of this section by Lloyd's), it can be assumed that the waterplane area does not change considerably. Therefore, restoring force is nearly constant.

In addition, the initial position, or in other words, the position of Ondo in vertical terms when not suffering from heave motion, is dependent on its displacement. Therefore, the initial condition will depend on the loading conditions of Ondo (e.g. port departure or arrival) which is tightly related with how much cargo is being transported and how full are the tanks of the ship.

10.4 Roll

Roll is the rotational motion of the ship around the surge axis (around x-axis). The uncoupled linear equation of motion for roll is:

$$(I_{xx} + a_{44})\ddot{\phi} + b_{44}\dot{\phi} + \rho g \nabla_0 GM_0 \phi = M_\phi$$

Here $(I_{xx} + a_{44})\ddot{\phi}$ is the sum of the ship inertia and added mass induced inertia, respectively; $b_{44}\dot{\phi}$ is the damping force for roll motion and $\rho g \nabla_0 GM_0 \phi$ is the roll restoring force. M_ϕ represents the external moment applied to Ondo (caused by waves or wind, for example).

Roll is an extremely important type of motion to account for since there are many factors that can cause roll motion and excessive heeling may lead to the ship capsizing. Moreover, roll motion can put both cargo and passengers/crew into danger. In addition, crew and passengers might suffer from motion sickness due to the roll motion. This effect on passengers and crew is more noticeable in decks higher in the superstructure and are mostly due to high values of transversal metacentric height. (Ruponen, 2020). Thus, a compromise must be found between both the transverse metacentric height (related to initial stability) and the height of the superstructure so that effects on personnel are not common.

By analysing the roll restoring force it is concluded that the force is larger for ships with a larger transversal metacentric height, GM_0. Furthermore, a greater initial displacement volume ∇_0 leads to greater restoring force for roll motions. In terms of the vessels operating profile, this means that we can expect the ship to be less prone for roll in a heavy loading condition as she sails deep whereas the dry ship-condition is much more easily rolled. To tackle this problem of having too small draught, ballast water is used to acquire reasonable stability.

Cargo shifting affects significantly the ship's stability in terms of roll. This because the shifting of loosen cargo will lead to additional external moments being applied to the ship. Consequently, this might lead to an increase in the roll amplitude. For this reason, cargo onboard Ondo shall be well attached to their position when dangerous sea conditions are prone to be present. Also, the effect of free water surface must be considered. Very large and wide tanks shall be kept at minimum so that the corrected metacentric height is not reduced considerably. Therefore, a good design of tanks in terms of the general arrangement of the ship must be kept in mind.

The rotational moment of inertia is defined mostly by the hull shape, in addition to main dimensions (such as length, breath and draft). Furthermore, the weight distribution coming from the general arrangement (cargo compartments and ballast tanks location, for instance) also have an important role in the calculation of this rotational moment of inertia.

All in all, to have a well-designed ship, the resonant frequency of the structures of Ondo must be kept away from critical frequencies given by the scatter diagram of the operational area of the ship to be designed (operational profile).

10.5 Pitch

Pitch is the rotational motion of the ship around the sway axis (around the y-axis of the ship). The linear equation of motion for pitch is:

$$(I_{yy} + a_{55})\ddot{\theta} + b_{55}\dot{\theta} + \rho g \nabla_0 GM_L \theta = M_\theta$$

Here $(I_{yy} + a_{55})\ddot{\theta}$ is the sum of the ship inertia and added mass induced inertia, $b_{55}\dot{\theta}$ is the damping force for pitch motion and $\rho g \nabla_0 GM_L \theta$ is the restoring force. M_θ is the external moment around the sway axis.

The pitch motion may sometimes result in slamming. This is an extremely important and dangerous phenomenon because the waves slamming on the bottom of the hull may cause extreme loads and vibrations on the structure. As Ondo has an icebreaking bow (spoon-shaped-bow), the hull angles are relatively small and that is why we must expect the vessel to face slamming. This kind of event will certainly happen when navigating in open waters for instance, when going north for research and when travelling from the northern to southern hemispheres and vice-versa. This is an example of how pitch motions must be minimised considering the operational profile of Ondo.

Here once again, the restoring force depends on the initial displacement of the ship. Higher the displacement, higher the restoring force will. Therefore, like in the roll motion case, the loading condition of Ondo will have a big impact on the pitch motions. In addition, the longitudinal metacentric plays a role in defining the restoring pitch force. Here, higher the longitudinal metacentric height, higher will be the restoring force.

The rotational moment of inertia once again influences this equation of motion, which is affected by the hull shape and general arrangement (in terms of load distribution along Ondo).

10.6 Yaw

Yaw is the rotational motion of the ship around the heave axis (around the z-axis). The linear equation of motion for yaw is:

$$(I_{zz} + a_{66})\ddot{\psi} + b_{66}\dot{\psi} = M_\psi$$

where $(I_{zz} + a_{66})\ddot{\psi}$ is the sum of the ship inertia and added mass induced inertia, respectively; and $b_{66}\dot{\psi}$ is the damping force for yaw motion. M_ψ is the external moment around the heave axis. This rotational motion differs from the two previous ones (roll and pitch) as there is no restoring force.

The yaw motion is manipulated by, for instance, the bow thruster and the two Azipods of Ondo. This is done by the aid of steering. When performing research using the Dynamic Positioning System, yaw might be a motion which needs to be kept at minimum.

Once again, the rotational moment of inertia for this degree of freedom has similar implications as in the previous two cases.

To sum up, each one of the equations of motion here analysed have effects coming from the general arrangement, operational profile, and hull form of Ondo. For instance, the general arrangement has a great effect on weight distribution on board Ondo, which affect the righting lever and metacentric height (related to stability). The metacentric height affects the restoring matrix of the equations of motion. Furthermore, with a high metacentric height, excessive accelerations may occur which is something unwanted due to danger and difficult working conditions. Added mass terms are highly affected by the hull form (for instance, main dimensions) as it defines the interaction which takes place between the ship and surrounding water. Operational profile influences in terms of loading conditions. Moreover, operational profile also has an influence in the encounter frequency of waves (dependent on direction of waves and relative heading of Ondo, and relative velocity of Ondo and waves).

11 Seakeeping analysis model

Seakeeping analysis is an important part of the ship design spiral. It must be known beforehand how well and how safely a ship will operate in its defined conditions (operational profile). During seakeeping analysis, issues like maximum speed in a seaway, routing, sea induced loads, people's comfort and safety on board, and safety of the ship from capsizing are investigated.

One of the tools to predict ship seakeeping at early design stage is computations using numerical methods. These methods are embedded in different seakeeping analysis softwares. At this point, available softwares are MaxSurf, BV Hydrostar, and NAPA.

The aim of this assignment is to perform a seakeeping analysis of group's project ship. Our project ship, called Ondo, is fully designed in NAPA software. Hull surface is in NAPA format and when exporting it in order to use in other softwares errors came up frequently. As the group is well acquainted and familiar with NAPA software for seakeeping analysis, it was decided to make the main analysis using NAPA. In parallel, BV HydroStar is also used by taking as a starting point Ondo's model but a shorter and less detailed analysis is made due to the issues explained before. MaxSurf software was tried as well but errors in importing the hull model made us step aside from it.

The first definitions for NAPA seakeeping model are main dimensions (Figure 32) and hull surface (Figure 33) of Ondo's project. This is made automatically, and error free thanks to NAPA project format whereas usage of other softwares gives problems of exporting/importing the ship model.

Reference length (LPP)	131.701	m
Reference breadth (B)	20.90	m
Design Draught (T)	7.500	m
Length over all (LOA)	140.204	m
Length to Breadth Ratio (LPP/B)	6.301	
Breadth to Draught Ratio (B/T)	2.79	

Figure 32. Ondo's main dimensions.

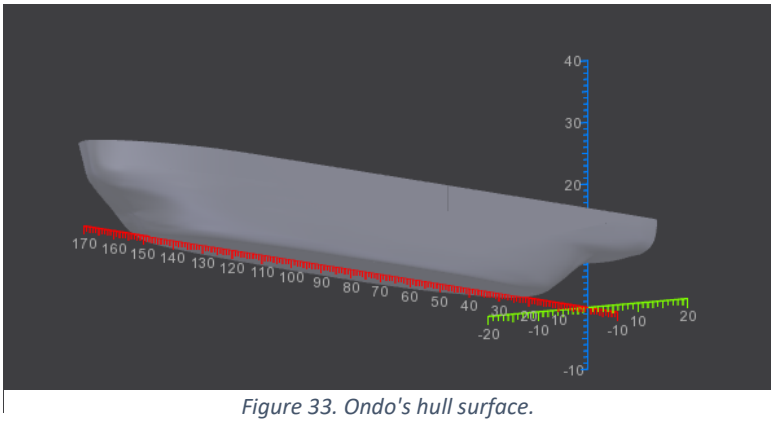

Figure 33. Ondo's hull surface.

Afterwards, the method to perform the seakeeping analysis shall be selected. NAPA has both Strip and Panel Methods as options. To understand these methods and their differences Chapter 4 “Seakeeping” of book “Practical Ship Hydrodynamics” by Volker Bertram was selected.

The Strip Method is to be the standard tool for ship seakeeping computations. Method is two-dimensional based and performs linear potential-flow computations. It is very efficient, robust, and relatively accurate in low to moderate sea states.

On the other hand, the Panel Method is fully three-dimensional. This considers non-linearities and is used for seakeeping analysis aiming at rough sea conditions.

The assignment task asks for a seakeeping analysis considering a worst-case scenario of ship operation. Thus, a rough sea conditions is considered and consequently, the Panel Method has been chosen to proceed with the analysis.

Moving forward with the Panel Method analysis, then the panelisation of Ondo’s hull surface is required to be done. This consists of panel segmentation operations for ship bow and stern according to pre-defined templates. Number of panels is chosen to be the software’s maximum possible so that the hull surface is represented in the most accurate possible way. This done, we get a total number of panels equal to 2000. The result of these operations is the ship model used in NAPA seakeeping analysis panel method, shown in Figure 34. Here, the part highlighted with green represents the bow section and with blue is the stern section of the seakeeping model.

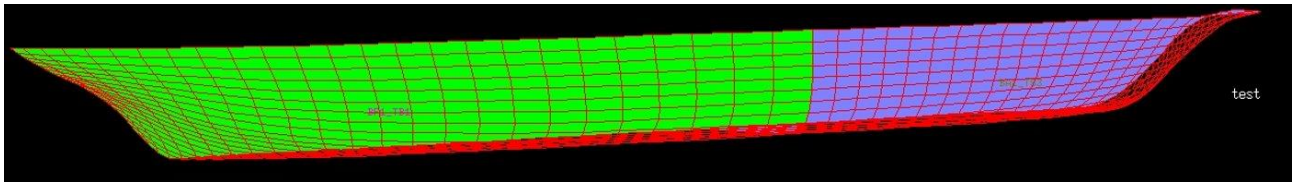

Figure 34. NAPA seakeeping analysis model.

In addition to the input values referred to previously, some additional parameters regarding Ondo are still required. Knowing the hull surface panels, it is required to define the ship’s floating position. Ondo’s design draft is 7.5 m at both aft and fore. Metacentric height is defined to be 1 m. Speeds at which analysis is performed are defined to be 0 knots (drifting), 10 knots (around half-forward), and 16 knots (design speed). Seakeeping analysis is carried out in deep water. Heading angles are to be calculated at 45° increment.

11.1 Additional seakeeping model simplifications

In the ship designer's quest for producing efficient, functional hull forms, numerical panel method is used as a powerful method. Their ability to accurately predict motions and wave patterns of conventional vessels has made them invaluable as a design tool. In the green function panel method, the three -dimensional flow around the hull is calculated in order to obtain the pressure, forces, and moments acting on the wetted hull surface. As the method is three-dimensional the approximations inherent in strip theory (inviscid fluid, slender ship, rigid hull, moderate speed, small motions, wall-sided sections, deep water, no effect of the hull on waves, etc…) are avoided. The computation is made on the centre of each panel so that it is assumed that there is no flow through. Flow irregularities occurring at the boundaries of the panels are smoothened by distribution of sources. Laplace equations and radiation, bottom or infinite depth and linearised free-surface conditions are considered.

In addition to these simplifications or assumptions made which are inherent to the seakeeping method used (panel method), also simplifications in terms of Ondo's hull and appendages itself are made. For instance, the four passive anti-roll tanks on board Ondo are not taken into account, the analysis is made without considering the propulsion systems and their interaction with the flow around the hull, free surface effect from tanks is neglected (although it can affect significantly motions) and distribution of load along the ship is neglected and taken as distributed in a uniform way.

12 Response Amplitude Operators calculation

Response Amplitude Operators are calculated in regular waves. Then, to assess response in irregular waves the principle of superposition of waves is used.

After NAPA has performed its seakeeping analysis a report is printed out. From the report a user can take seakeeping calculations he is interested in.

Response Amplitude Operators are being calculated for 3 different speeds and 5 heading angles defined as referred previously. One of NAPA's pre-defined features is that frequency which is RAO's graphs X-axis is represented by another frequency unit which is the square root of division – length between perpendiculars divided by wavelength.

There are 5 RAOs for motions. The translational ones consist of sway and heave, and the rotational ones are roll, pitch, and yaw. Surge's RAO is null (0).

12.1 RAOs at speed 0 knots (drifting)

12.1.1 Translational motions – sway and heave

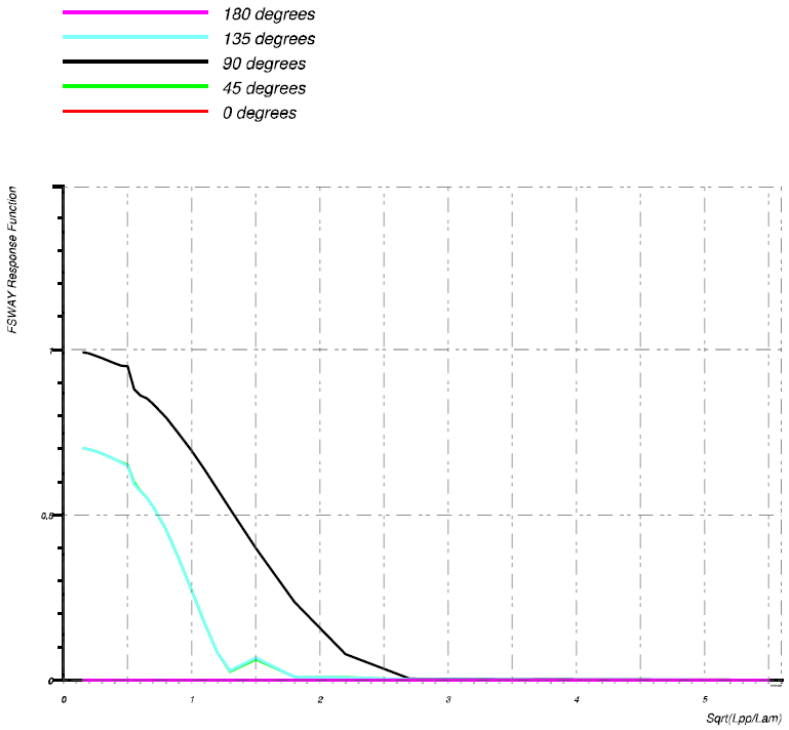

Figure 35. RAOs for sway in drifting condition at different headings.

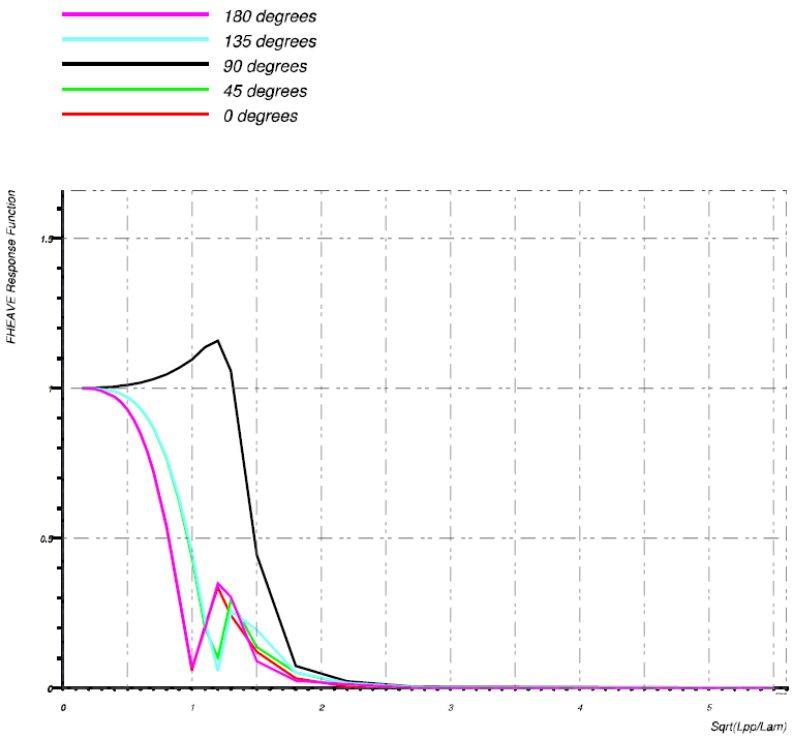

Figure 36. RAOs for heave in drifting condition at different headings.

12.1.2 Rotational motions – roll, pitch, and yaw

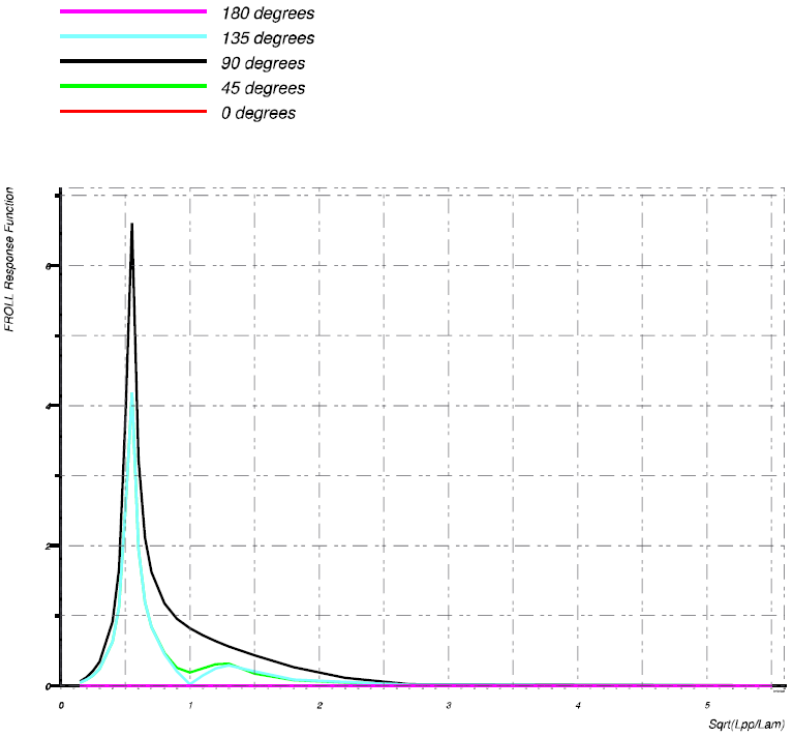

Figure 37. RAOs for roll in drifting condition at different headings

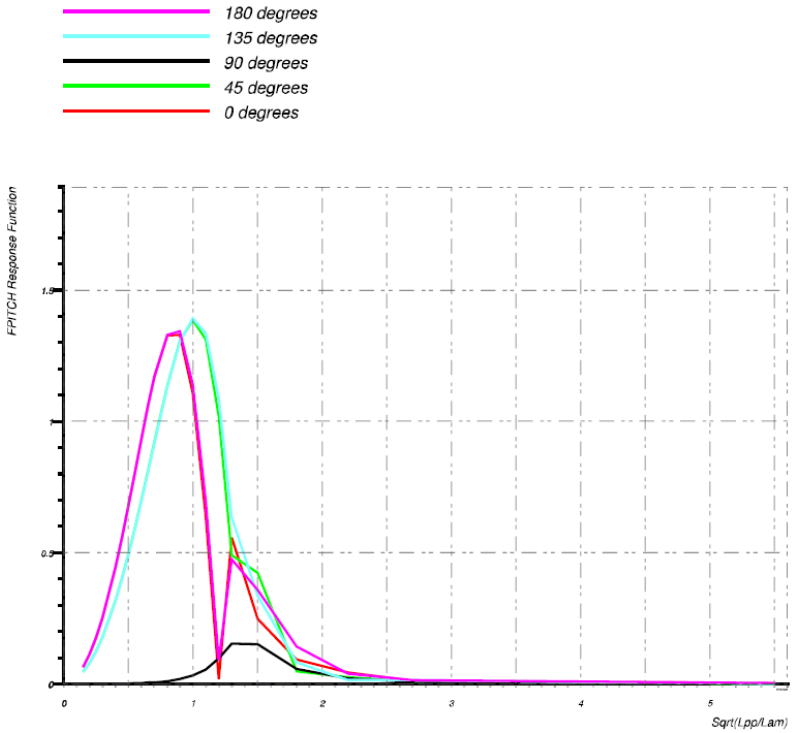

Figure 38. RAOs for pitch in drifting condition at different headings

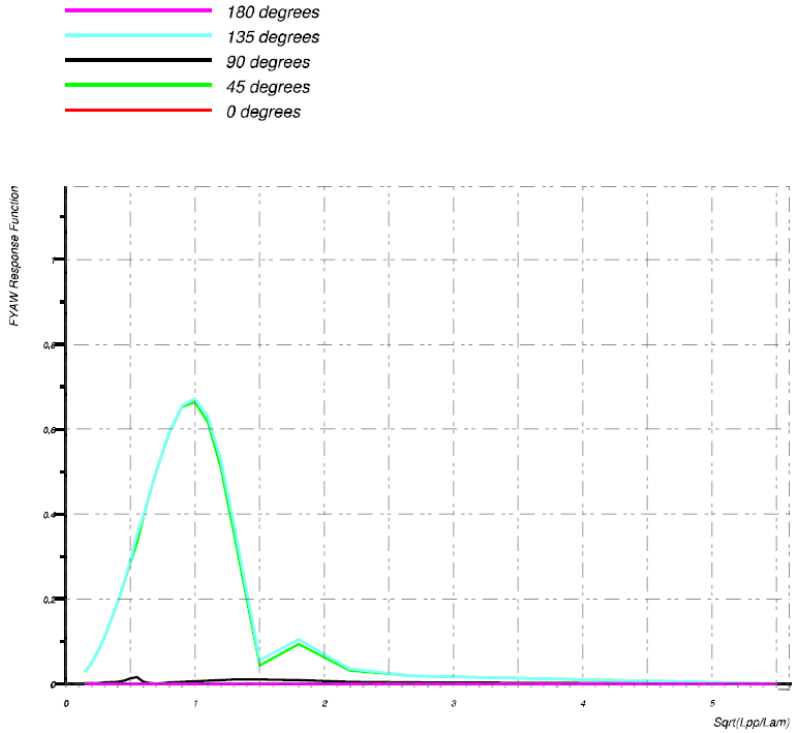

Figure 39. RAOs for yaw in drifting condition at different headings.

12.2 RAOs at speed 8 knots – half forward

12.2.1 Translational motions: sway and heave

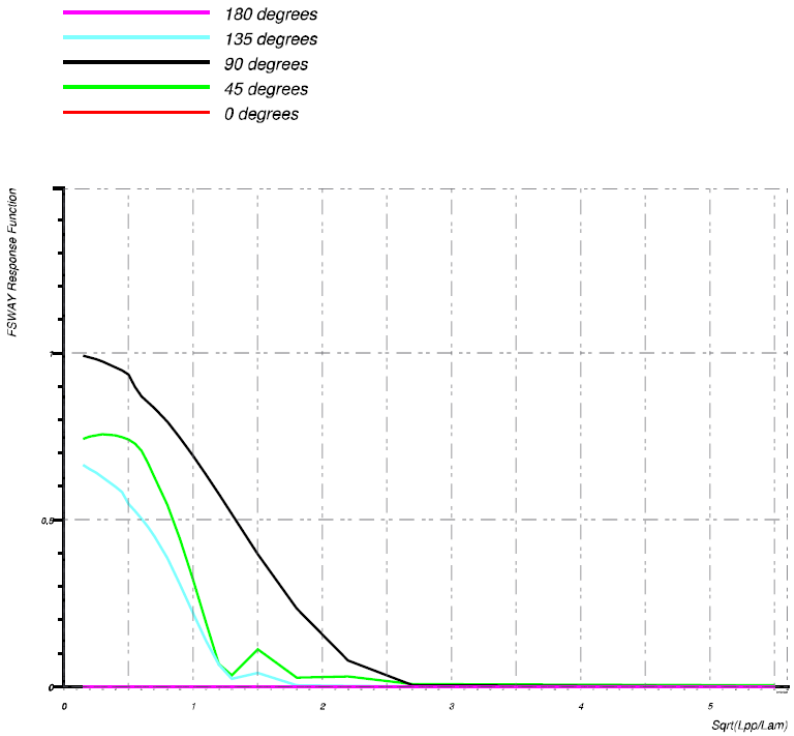

Figure 40. RAOs for sway in half forward condition at different headings.

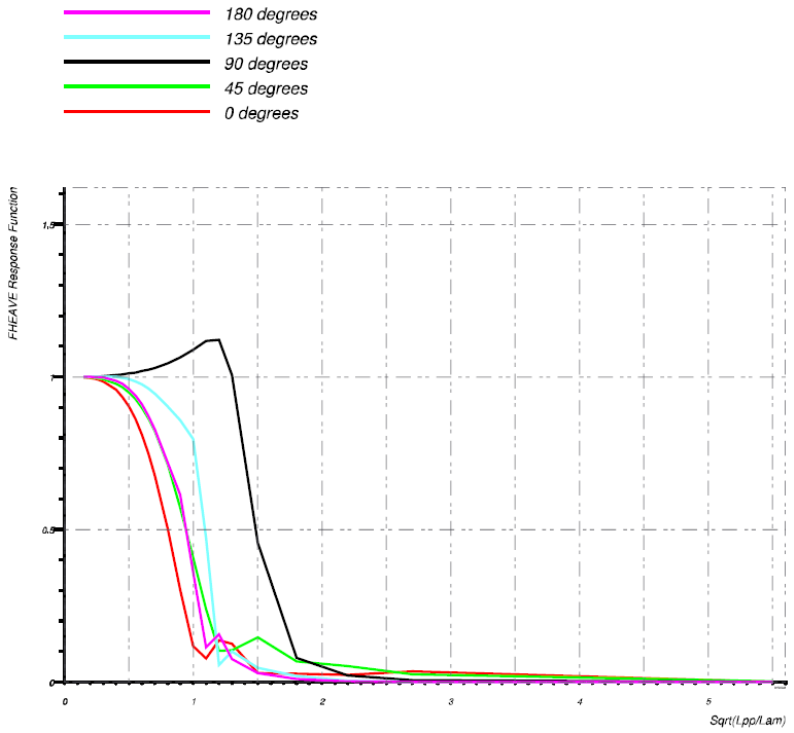

Figure 41. RAOs for heave in half forward condition at different headings.

12.2.2 Rotational motions: roll, pitch, yaw

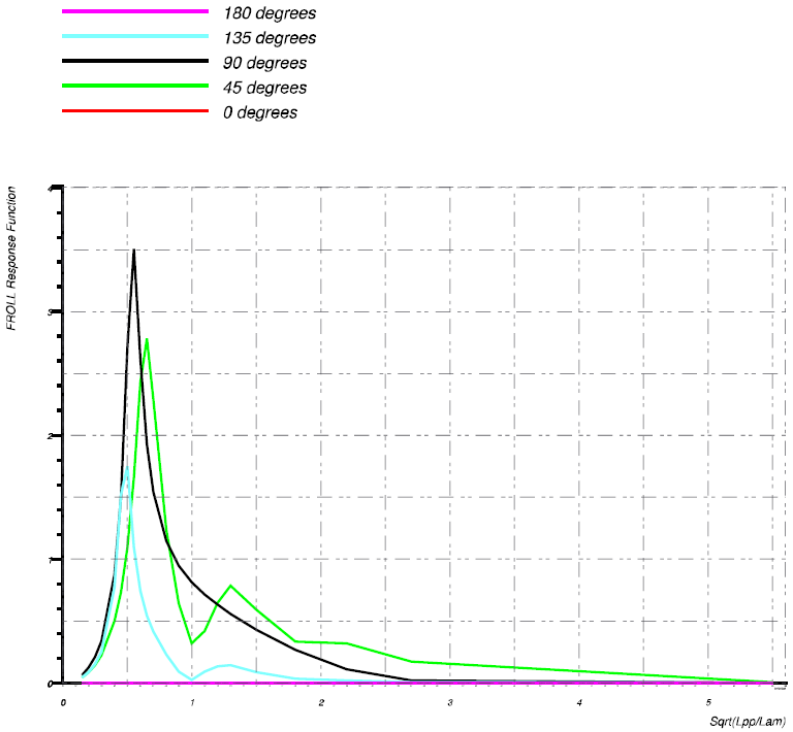

Figure 42. RAOs for roll in half forward condition at different headings.

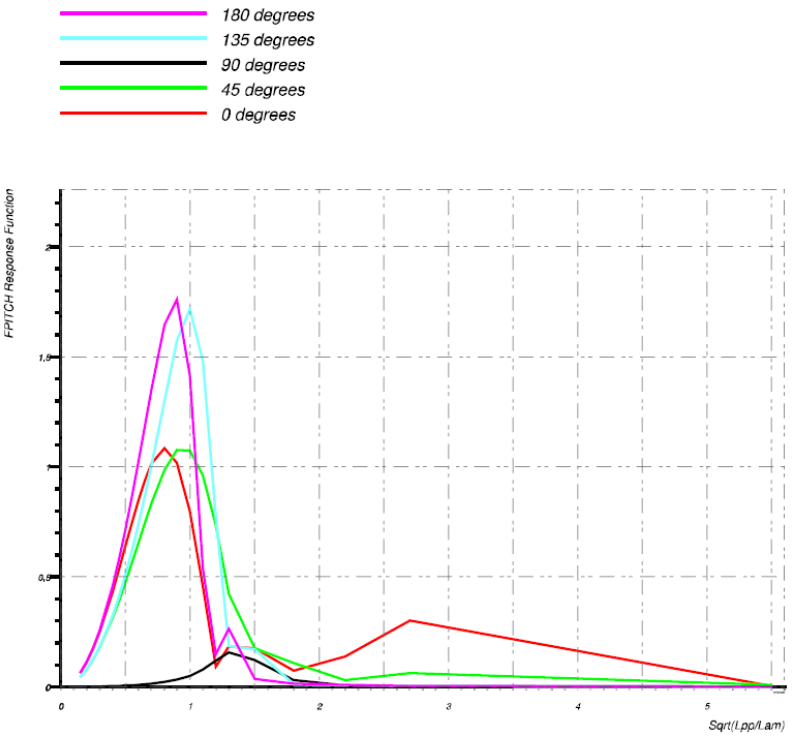

Figure 43. RAOs for pitch in half forward condition at different headings.

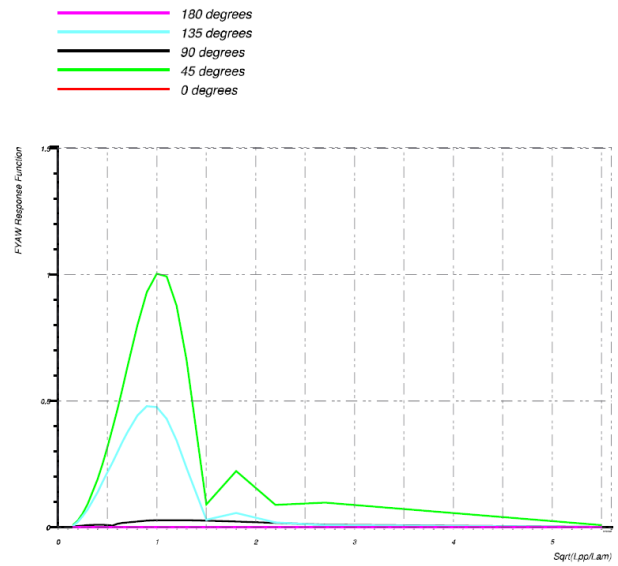

Figure 44. RAOs for yaw in half forward condition at different headings.

12.3 RAOs at speed 16 knots – design speed

12.3.1 Translational motions: sway and heave

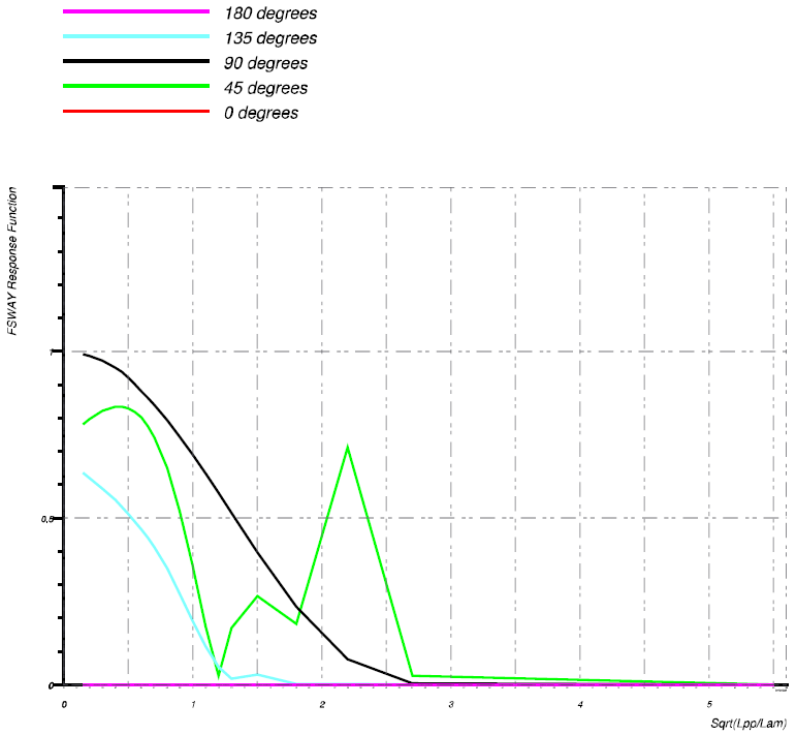

Figure 45. RAOs for sway in design speed condition at different headings.

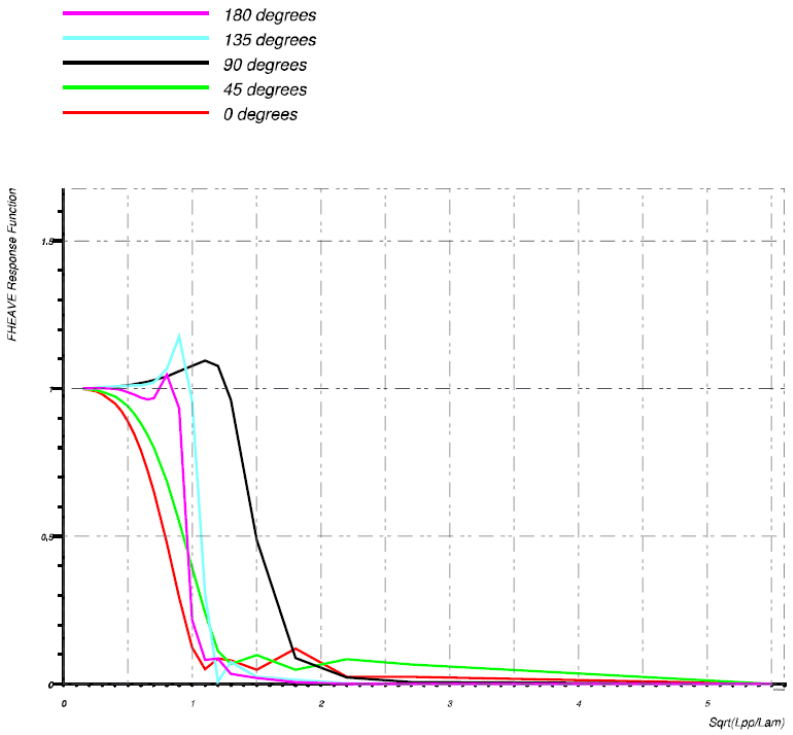

Figure 46. RAOs for heave in design speed condition at different headings.

12.3.2 Rotational motions: roll, pitch, and yaw

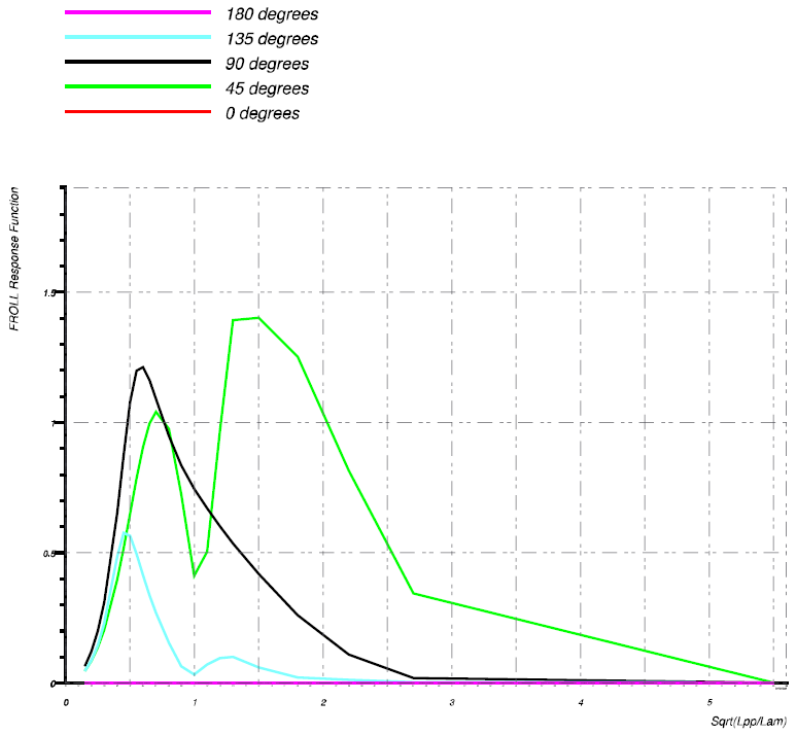

Figure 47. RAOs for roll in design speed condition at different headings.

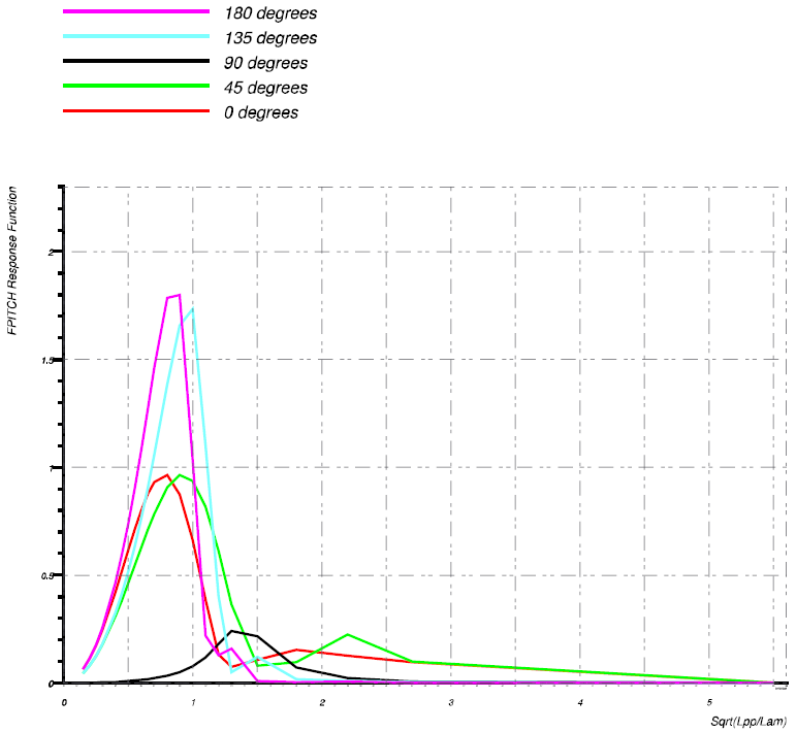

Figure 48. RAOs for pitch in design speed condition at different headings.

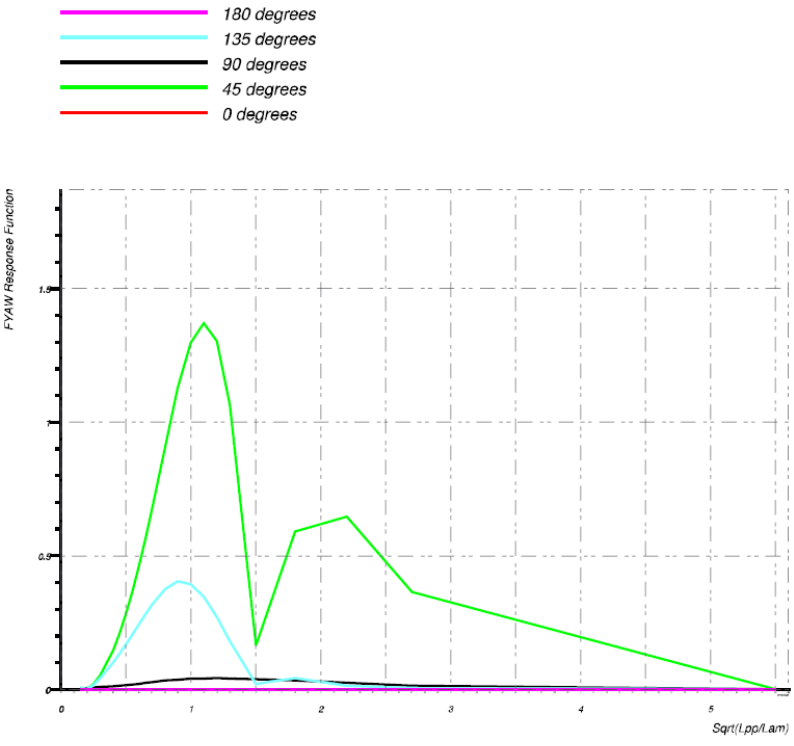

Figure 49. RAOs for yaw in design speed condition at different headings.

12.4 RAOs short discussion

Let us now make an analysis to the transfer functions for each degree of freedom presented in the previous section of this report.

Sway motion RAO, in general, does not show notable local peaks and the response amplification decreases as the frequency is increased. At 0 knots speed, only for 180 and 135 degrees the RAO is different than zero. As the speed of Ondo increases, more headings appear to influence the response and at design speed, at heading of 45 degrees the behaviour of the sway RAO changes and presents two well defined peaks.

Heave response is largest clearly with waves longer than the length of Ondo (approximately). It is quite intuitive that the RAO tends to unity in long waves, since the vessel follows the wave profile in these situations, resulting in quasi-static response. On the other hand, if the wave frequency is relatively big, waves are short, and the vessel is not able to respond at all to the wave motions. In fact, this statement applies to all degrees of freedom (in general), except for yaw in oblique seas at higher speeds (half forward and design speed). There is a second maximum in response in most of the RAO when the vessel is drifting.

Roll motion is arguably the most interesting out of the six degrees of freedom, as described in the previous assignment of this course. This is due to its problematic nature of being difficult to dampen and excessive roll motions causing the ship to capsize. The shape of roll's RAO brings sense to this issue. There is a notable peak in the RAO at the natural frequency of the roll motion of the vessel (more notable in drifting and half forward speed), resulting in considerably large roll motions around this frequency. As expected, the peak is higher for beam seas and when the ship is still. The effect of ship's speed is notable since roll damping increases as the speed of the vessel is increased (Section 10.4). How this peak in the RAO of roll can be mitigated, lowered, or changed its natural frequency has been discussed in Section 3. For instance, passive anti-roll tanks are a solution which has been considered in Ondo. However, calculations here presented do not consider the increase of damping effect of these additional factors.

Also pitch response has a notable local peak giving reasoning to the existence of a resonance frequency. This resonance frequency is somewhat close to the one relating to roll resonance. The speed and heading have some influence on pitch response and, for beam seas the response (RAO) is much smaller in comparison to other headings.

Yaw motion at design speed condition shows a clear resonance frequency for heading of 45 degrees. In this situation the motion is seen to be amplified. As vessel's speed increases, the value of RAO decreases and keeps at all times below one (including heading of 45 degrees).

13 Motions and global loads

13.1 Motions

Here, all motions and global loads are calculated for selected sea spectra, which is taken as worst-case scenario in North Atlantic. Prediction of motions and loads for 3 hours maximums is made.

For this purpose, NAPA seakeeping analysis can calculate response in irregular waves. The user defines significant wave height, zero crossing periods and wave spectra to be used in response calculation. For worst case spectra in North Atlantic modified Pierson-Moskowitz spectra is used. Significant wave height at this region for worst case scenario is chosen to be 16.5 metres and zero crossing period of 12.5 seconds.

Output of calculations are significant response functions at different headings and speeds. Here will be shown significant response functions at design speed of 16 knots and then motions polar plots at same speed.

13.1.1 Translational motions: sway, and heave

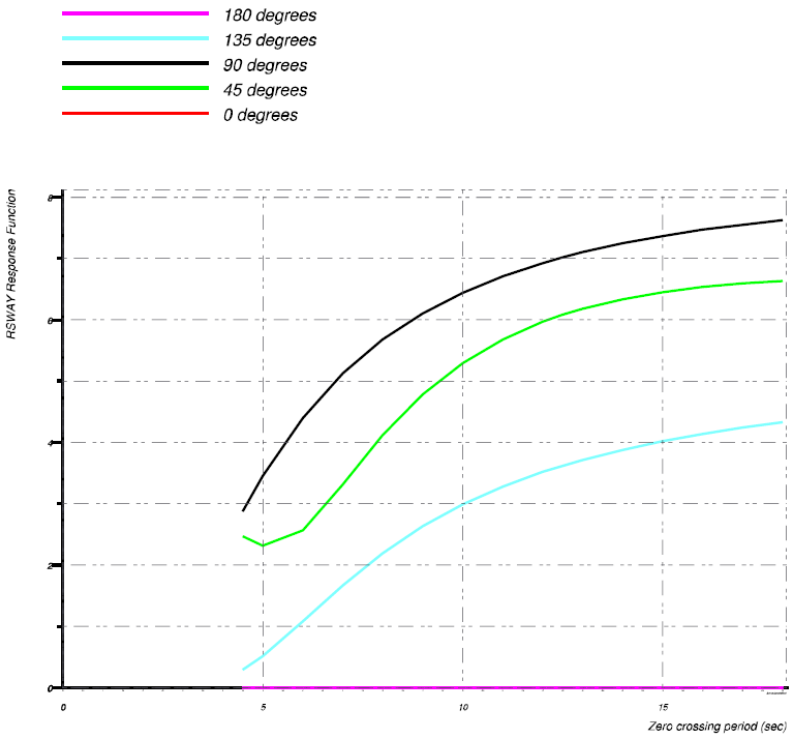

Figure 50. Motion response for sway.

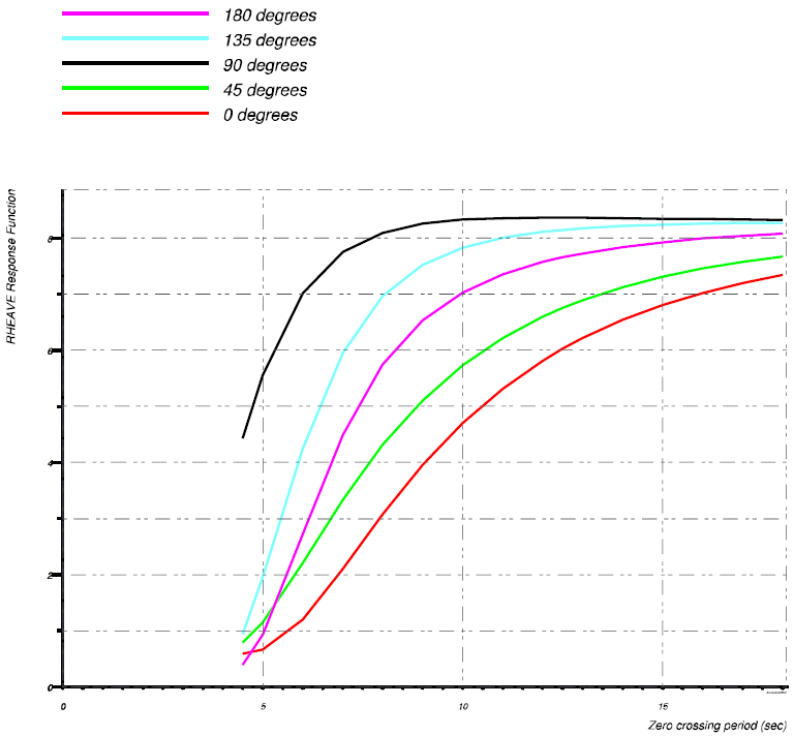

Figure 51. Motion response for heave.

13.1.2 Rotational motions: roll, pitch, yaw

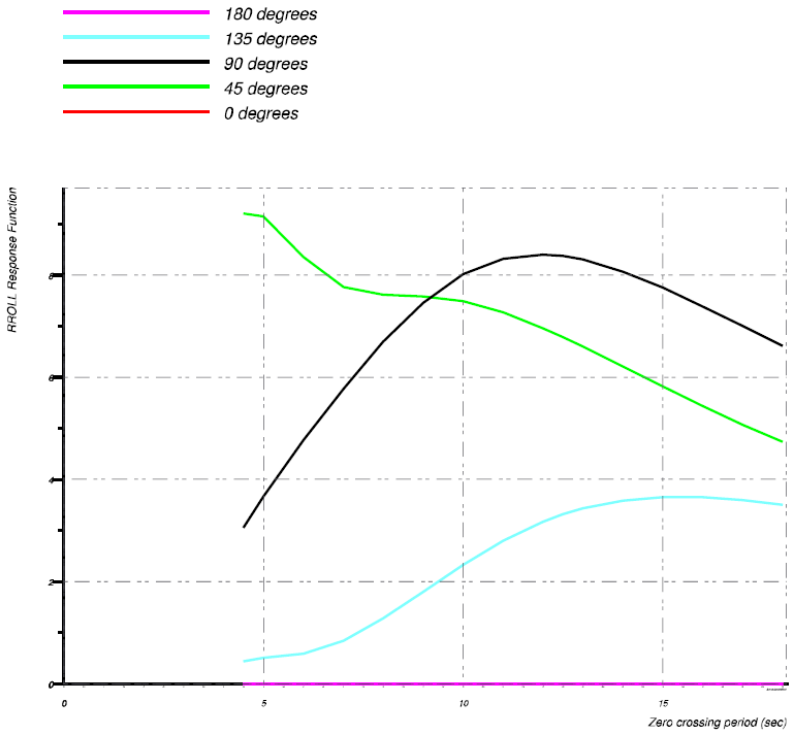

Figure 52. Motions response for roll.

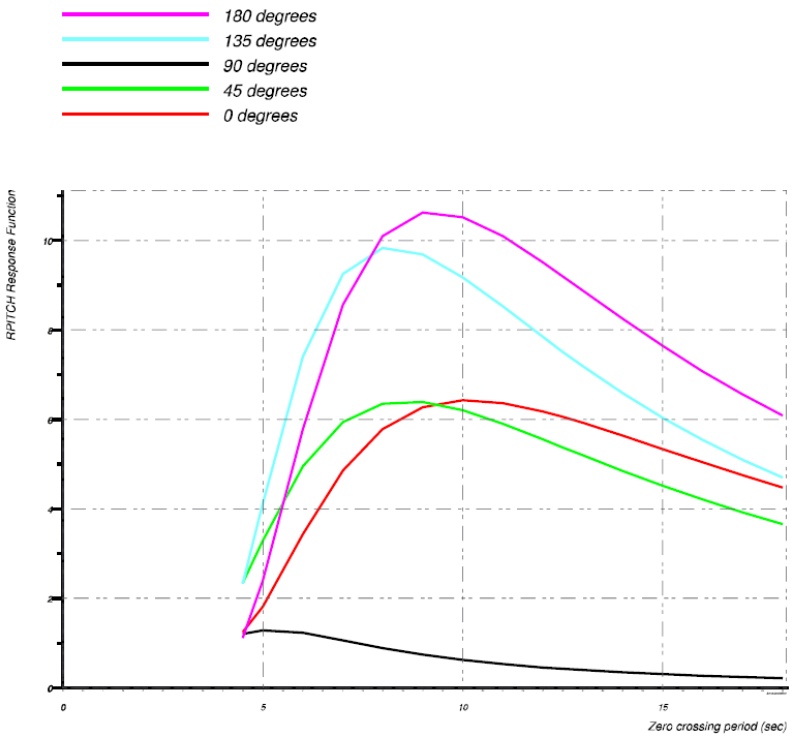

Figure 53. Motions response for pitch.

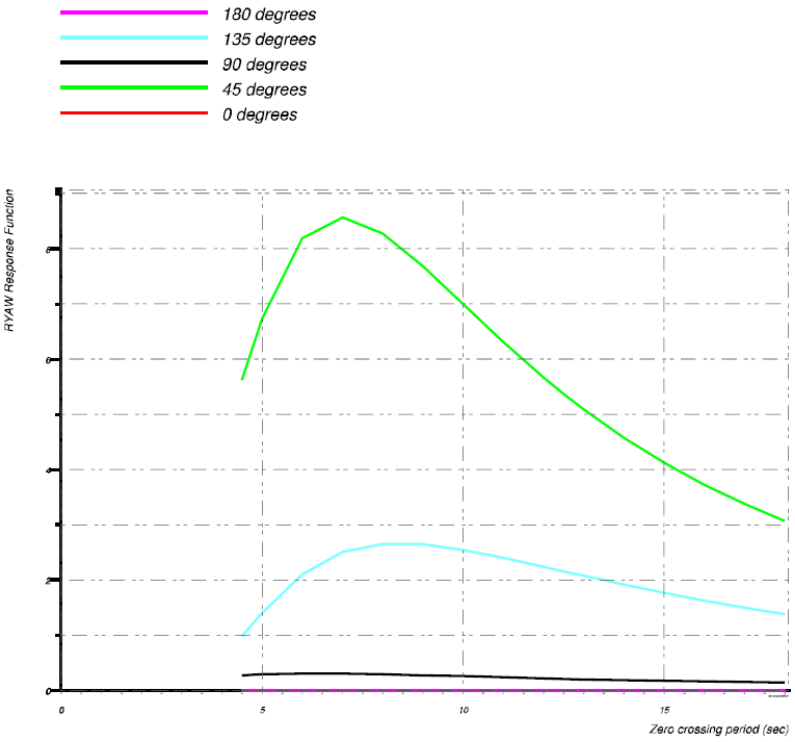

Figure 54. Motions response for yaw.

Using significant response functions, it is possible to obtain motion which depend on zero crossing period of wave.

For better understanding and visualisation of motions, polar plots can be used. These are plotted at design speed of 16 knots and are shown down below. These motions (red line) are calculated based on significant wave height of 16.5 m and zero crossing period of 12.5 s.

13.1.3 Translational motions: sway, heave (polar plots)

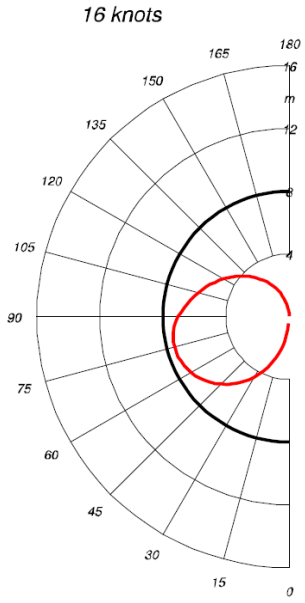

Figure 55. Polar plot for sway.

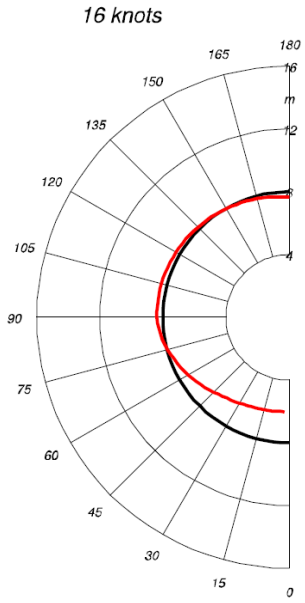

Figure 56. Polar plot for heave.

13.1.4 Rotational motions: roll, pitch, yaw (polar plots)

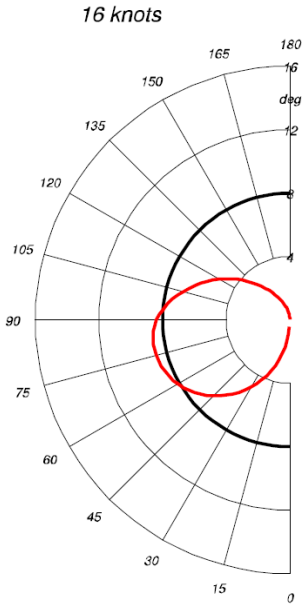

Figure 57. Polar plot for roll.

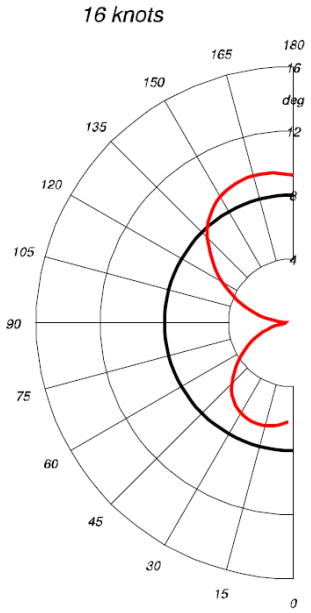

Figure 58. Polar plot for pitch.

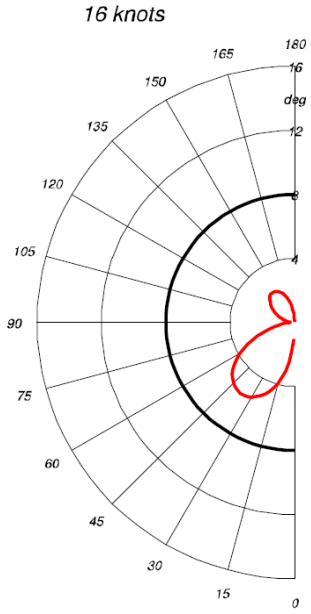

Figure 59. Polar plot for yaw.

From the polar plots shown in Figure 55 to Figure 59, it is seen that motions for the worst-case scenario being considered for Ondo are quite reduced (considering the sea conditions). For instance, all rotational motions are situated below a threshold of 8 degrees. It is seen that for example pitch is most significant motion in head seas and it can be said that yaw is affected very little, in general. Then attention must be paid to roll motion in beam seas. However, this is found to be very well below the imposed limit by class rules being used in the project. Last but not least, heave has noticable motion which can cause unpleasant accelerations on board. Here, special attention must be considered.

As seen in the analysis done using the previously presented polar diagrams and explained shortly in the above paragraph, at design speed Ondo can be described as seaworthy. However Ondo's speed can change in sea which also leads to change in motions. Motion which highly depends on speed change is roll according to NAPA analysis. Roll polar plot at speeds 0, 8, 16 knots is given in Figure 60. It is clearly seen that at drifting or low speeds roll motion is very significant. At drifting and beam seas roll angle can go up to 25°. However, according to regulations this value is still well within the allowed limit. Therefore, in terms of roll motion (angle) no issues arise at this point.

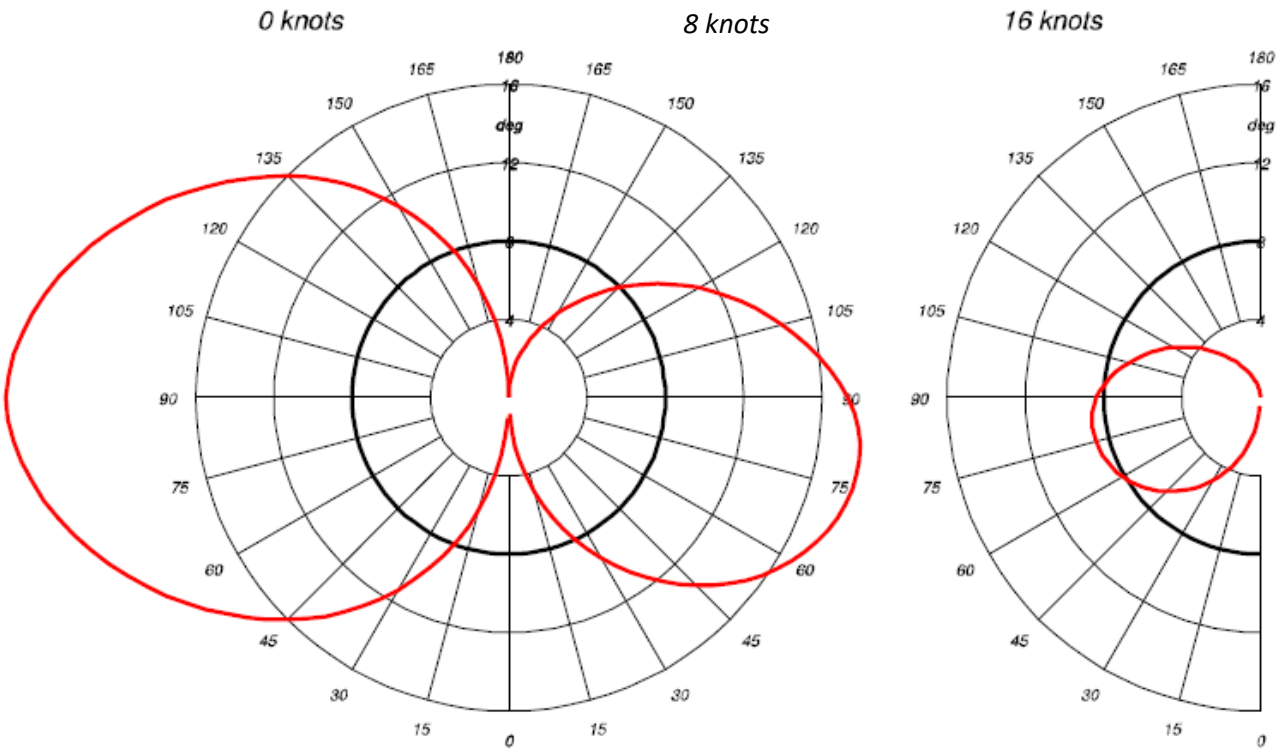

Figure 60. Roll polar plots for 0, 8, and 16 knots.

13.2 Global loads

Global loads calculated in NAPA are vertical bending moments in irregular waves using strip theory method. They are calculated for wave with significant wave height of 1 m. 1 m is the default value in NAPA and to change it, some NAPA coding in order to develop a reasonable Macro is required in which Ondo group does not have enough experience at this point.

In **Erro! A origem da referência não foi encontrada.** Figure 63 and **Erro! A origem da referência não foi encontrada.**Figure 62 are shown the shear force and vertical bending moment, respectively, related to the input spectra discussed previously. This is related to regular waves and are shown as functions of the adimensionalised parameter already referred to previously (square root of Lpp by wavelength). On the other hand, Figure 61 shows the vertical bending moment as a function of the zero-crossing period applied in Ondo when considering irregular waves. Here, it was not possible to export shear force results from NAPA.

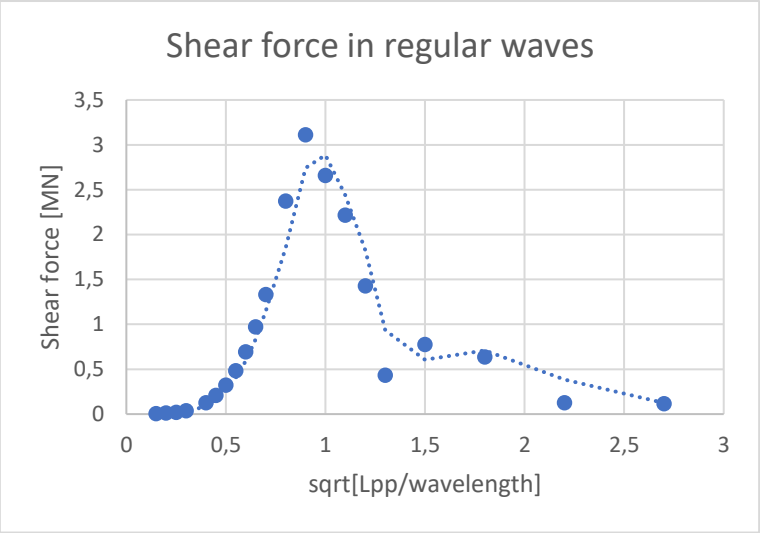

Figure 63. Shear force in regular waves.

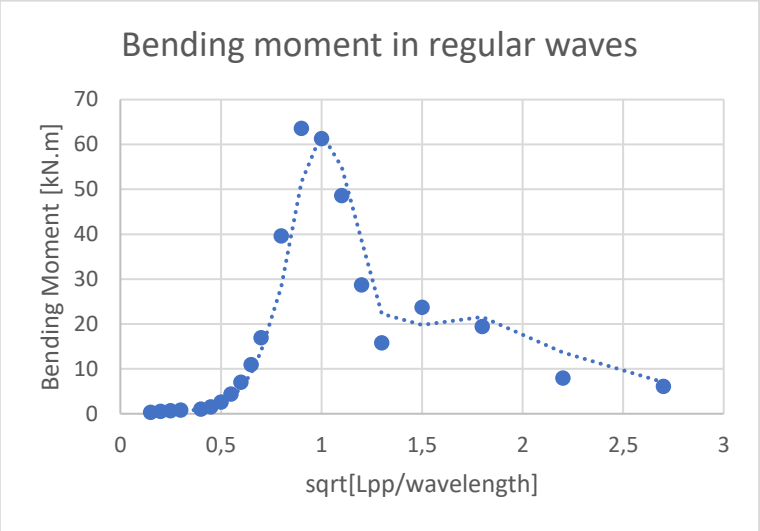

Figure 62. Bending moment in regular waves.

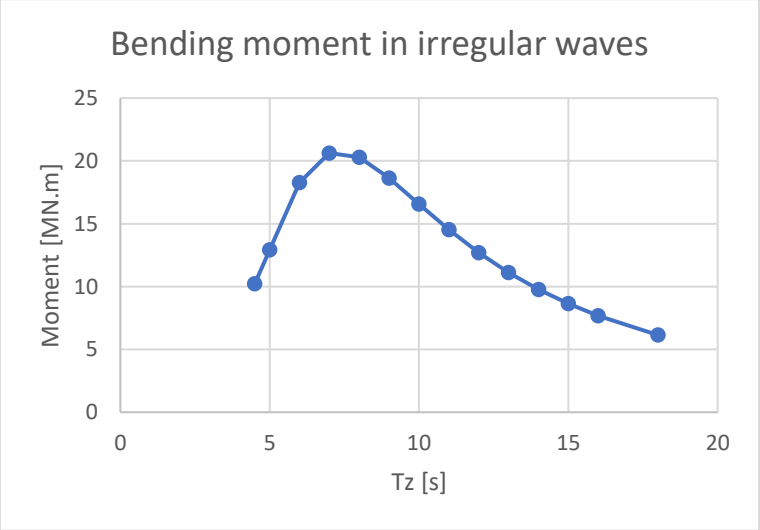

Figure 61. Bending moment in irregular waves.

From the results presented previously in Figure 61 and Figure 62Figure 63 it is possible to see that both the shear forces (in regular waves) and vertical bending moment (in regular waves) show their maximum values when the wavelength is equal to the length between perpendiculars of Ondo. Thus, in regular waves, the maximum shear force is found to be 2.75 MN and the vertical bending moment equal to 60kN.m. On the other hand, Figure 61 shows that the maximum value of vertical bending moment in irregular waves is attained when the zero-crossing period is 7 seconds and its value equals to 21MN.m. Thus, it is found that in irregular waves the vertical bending moment is 350 times greater.

Consequently, the difference found in terms of load depending on whether regular or irregular wave conditions are studied show the importance of making a meaningful seakeeping analysis. In fact, if only regular waves would have been considered, the results would have been critically low in comparison to what they would be in real life. A next step in terms of seakeeping analysis would be to be able to utilise the wanted spectrum in load calculations so that accurate results could be used in structural strength definition, for instance.

In this next part of the report, some computations using BV HydroStar are presented. This is shown as additional material as it gave the whole group some good insight on another software prone to be used in seakeeping analysis.

14 BV HydroStar seakeeping analysis

14.1 RAOs for motions

This software can calculate design wave for a selection of RAOs and associated Load Combination Factor (LCF) for another set of RAOs. Starspec systematically computes 3 types of design waves: Regular waves, Irregular waves, Response Conditioned Waves. In this analysis the Irregular waves has been used for motion analysis. The calculation has been done for worse selected sea spectra.

Estimation of sea state is studied using a set of measured ship responses, a parametric description of directional wave spectra (a generalised JONSWAP model) of the ship responses. Finding the forces on the ship when it is forced to oscillate in still water conditions. The forces are divided into added mass forces due to having to accelerate the water along with the ship, damping (hydrodynamic) forces due to the oscillations creating outgoing waves which carry energy away from the ship, restoring forces due to bringing the buoyancy/weight and moment equilibrium out of balance.

In this analysis translational motions (sway, surge, heave) of Ondo model are as follow:

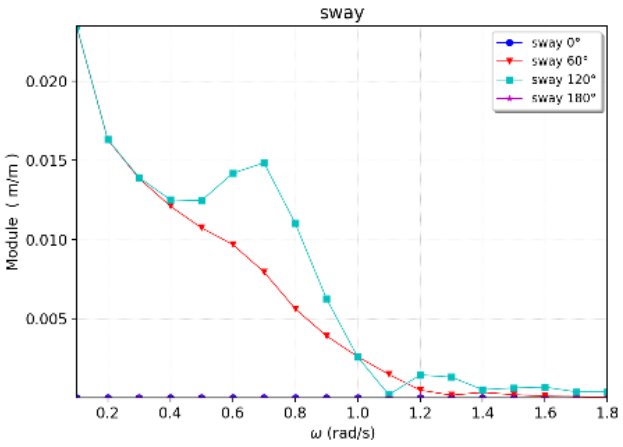

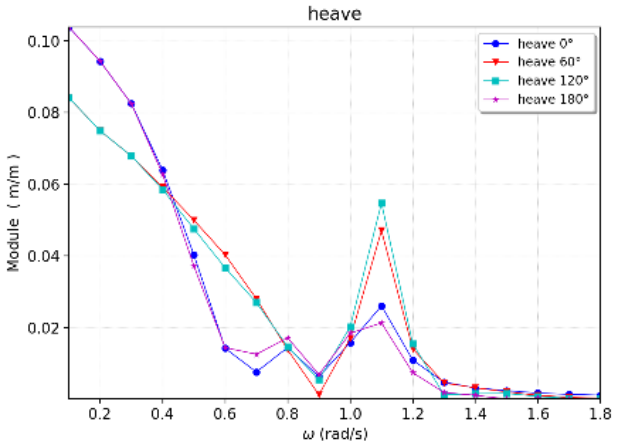

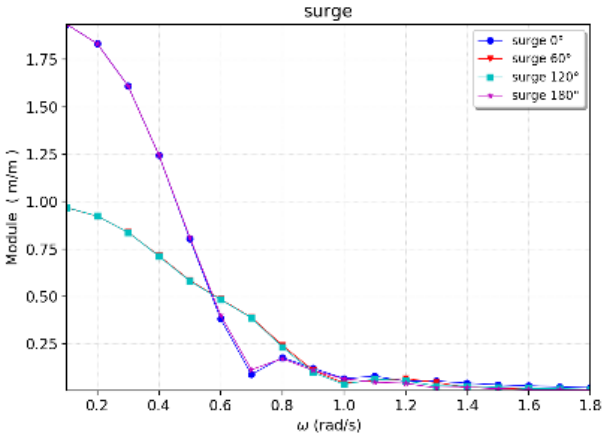

Figure 64. Translational motions: sway, surge, heave.

In this analysis the rotational motions (roll, pitch, yaw) of Ondo model are as follow:

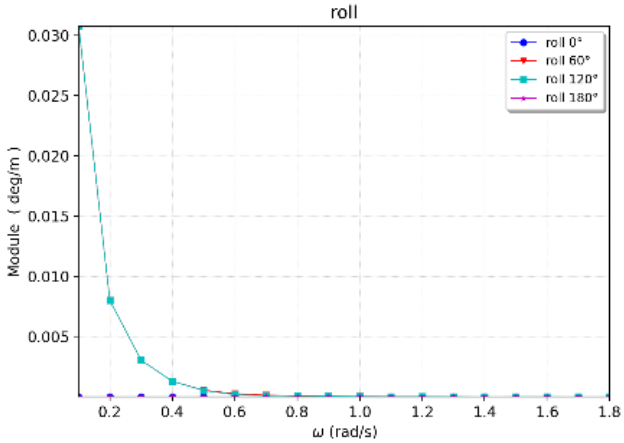

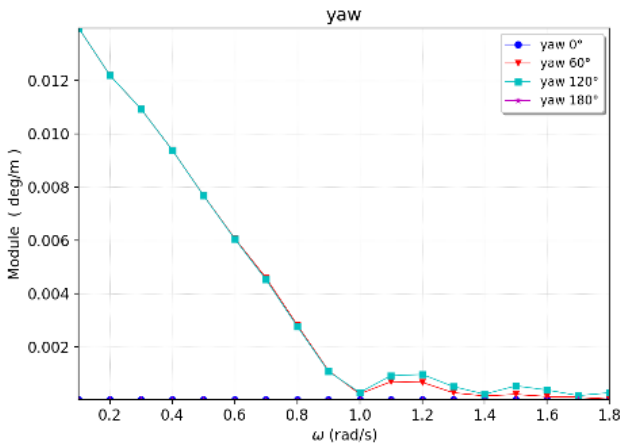

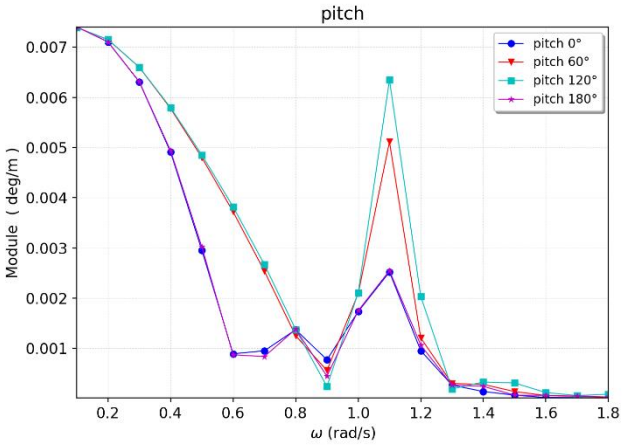

Figure 65. Rotational motions: roll, pitch, yaw.

There are various numerical methods for predicting the wave induced motions and loads. All methods require proper modelling and correct execution parameters in order to produce reliable results. For seakeeping assessments there are two main categories of 3D panel methods: — Free surface Green's function methods requires mesh of the wetted hull. Only the simple Neuman-Kelvin free surface conditions, can be handled. Fake solutions may occur for certain wave frequencies called irregular frequencies corresponding to the modes inside the hull. This is a particular challenge for short waves. Results containing irregular frequencies need to be excluded and confirmed by inspections of RAOs, which should not contain spikes. — Rankine methods require panels on the free surface in addition to the hull. These methods introduce more flexibility with respect to handling of physical free surface conditions, which is in particular important for resolving the flow for blunt ships in case of forward speed. Rankine methods are applicable for air cushion supported ships.

All non-linear methods apply some simplifications of the physics. For practical simulations, it is important to select a method which balances requirements of accuracy and computational time. This selection depends on the type of response and the available computer capacity. As a consequence, there is a large variety of non-linear sea-keeping methods. The most common methods are: — Non-linear hydrostatics and Froude-Krylov based methods. In this analysis the Froude-Krylov method has been used.

These methods are based on linear solvers with the exception that hydrostatic pressure and the undisturbed incident wave pressure are integrated over the instantaneous wetted hull. The wetted hull is defined by only considering the ship motions and the incident wave profile. Non-linear strip theory is similar to the above method but can include non-linear radiation and diffraction forces by considering the instant submergence of each 2D section. The 2D theory neglects important physical effects. Weak scatter non-linear panel methods take into account the effect of large incident wave in a simplified way. Panels are distributed on the incident wave surface and the instantaneous wetted hull. The flow field is linearized with respect to this

control volume. Hence, the method accounts for non-linear radiation and diffraction effect, e.g. of bow flares. This method is considerably more robust than fully non-linear pane.

In this analysis, the panel method has been used as a screening tool for seakeeping assessments of ships moving. The calculation has been done for worse selected sea spectra. Predict motions and loads 3 hours maximums. 3-D panel method has been used to analyse of motions of Ondo model, see the following figure:

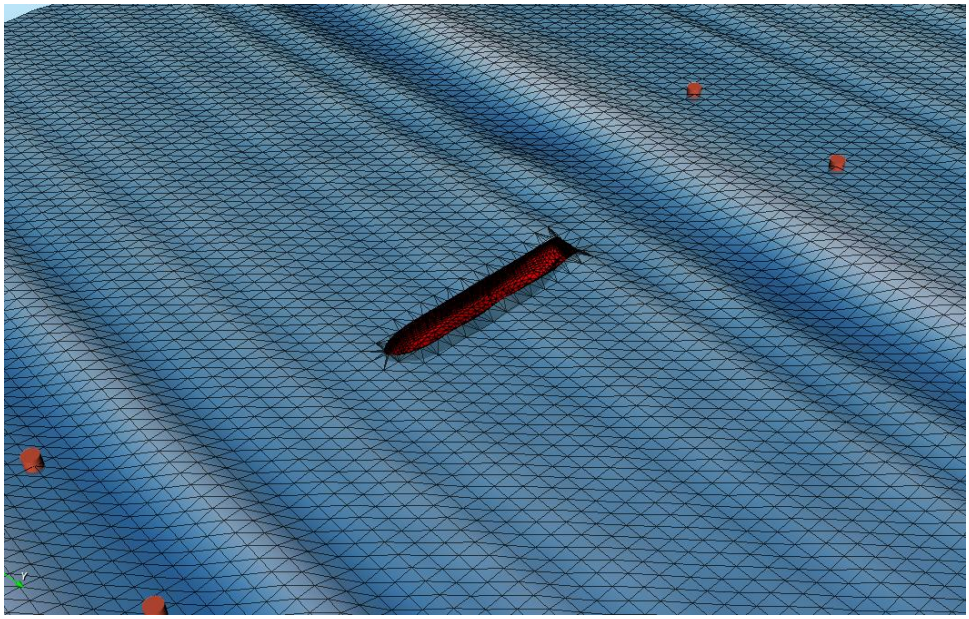

Figure 66. Panel method used for motions in irregular waves for Ondo model.

15 Seakeeping criteria assessment

Seakeeping criteria are assessed in this final report as well. This is done by means of NAPA, the software which has been used to model Ondo as well as compute motions and loads in previous sections.

By taking into consideration the operational profile of our project ship, we are considering as scatter diagram one related to North Sea. Information regarding this diagram can be found in NAPA manuals and it is shown in Figure 67.

	H13	TZ1	TZ2	TZ3	TZ4	TZ5	TZ6	TZ7	TZ8	TZ9	TZ10	TZ11	TZ12
1	11.00	0	0	0	0	0	0	0	0	0	0	0	0
2	10.00	0	0	0	0	0	0	1	1	0	0	0	0
3	9.00	0	0	0	0	0	0	1	1	1	0	0	0
4	8.00	0	0	0	0	0	1	2	2	1	1	0	0
5	7.00	0	0	0	0	0	2	4	4	2	1	0	0
6	6.00	0	0	0	0	1	4	9	7	4	1	0	0
7	5.00	0	0	0	0	2	11	19	14	6	2	1	0
8	4.00	0	0	0	0	6	27	39	26	10	3	1	0
9	3.00	0	0	0	1	17	63	73	40	13	3	1	0
10	2.00	0	0	0	3	49	121	99	40	10	2	0	0
11	1.00	0	0	0	19	86	94	41	10	2	0	0	0
12	0.00	50	150	250	350	450	550	650	750	850	950	1050	1150

Figure 67. North Sea scatter diagram - NAPA.

The seakeeping criteria to be defined are evaluated for three different speeds, already used in the previous assignment. These include the (0 knots), half forward (8 knots) and design speed (16 knots). Additionally, seakeeping performance is also evaluated according to headings. These are defined in 45 degree-step headings going from 0 to 180 degrees, where the latter one represents the condition of head seas.

The seakeeping criteria to be assessed are:

- Seasickness;
- Roll angle;
- Pitch angle;
- Vertical acceleration;
- Lateral acceleration.

The selection of these criteria have been made by means of literature where also recommended values for maximum limits are given. Table 3 gives the limiting values for each seakeeping criteria considering Bhattacharyya (1978) and McCauley (1976).

Table 3. Seakeeping criteria limits.

Seakeeping criteria	Maximum limit
Seasickness	20%
Roll angle	8 degrees
Pitch angle	3 degrees
Vertical acceleration	4 m/s^2
Lateral acceleration	2 m/s^2

In the next sections, the seakeeping criteria are checked for each heading and vessel speed. A small analysis is made for each situation.

15.1 Drifting (0 knots)

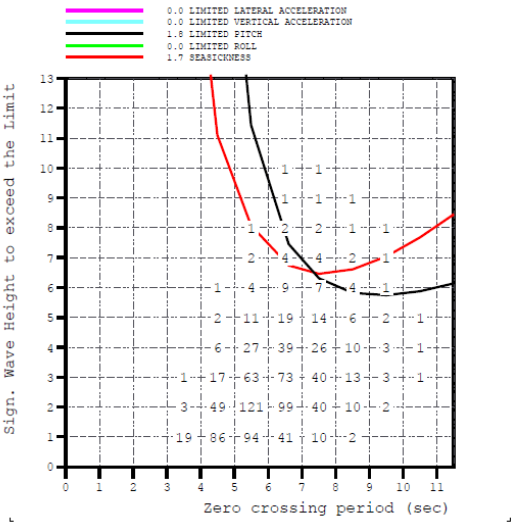

0 degrees

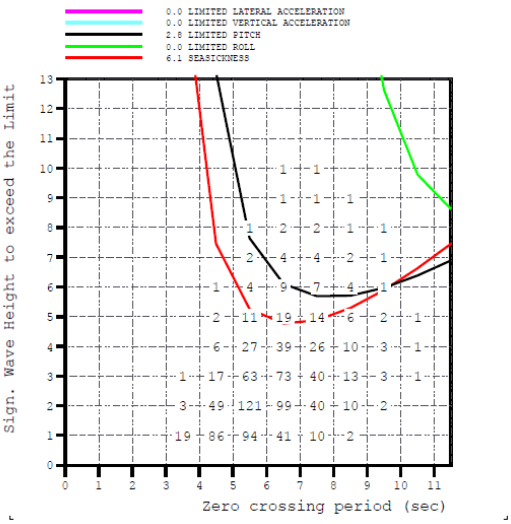

45 degrees

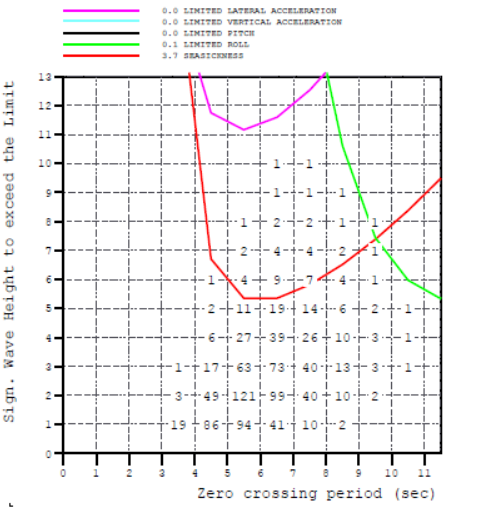

90 degrees

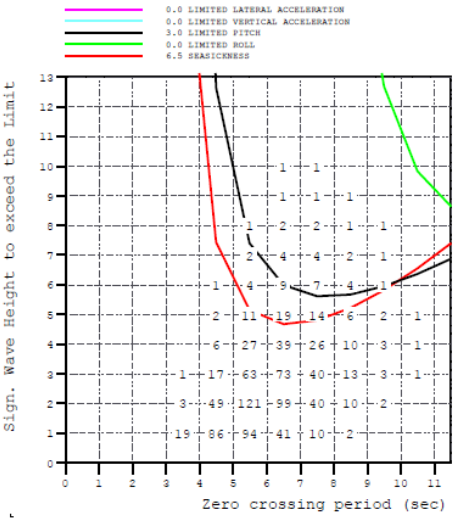

135 degrees

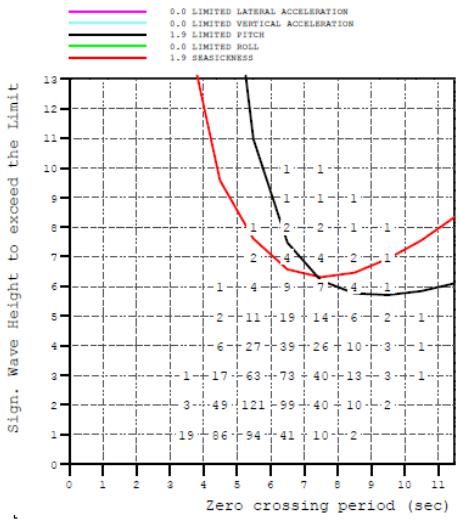

Figure 68. Seakeeping criteria for headings and 0 knots.

From the plots presented in Figure 68 is seen that both criteria regarding accelerations (vertical and lateral) are met for the scatter diagram being considered for each heading analysed at the drifting speed of 0 knots. Limited roll angle (to 8 degrees) becomes a concern only for beam seas (90 degrees heading). However the exceedance of this limit takes place only at very low probability (0.1%) for waves with high zero crossing period (9 seconds) and a significant wave height of 7-8 metres.

On the other hand, limited pitch and seasickness take place with greater frequency. Actually, for every heading analysed this situation may take place for a specific range of zero crossing period and significant wave height. Seasickness criteria is exceeded with 6.1 % probability in our reference operational area in headings of 45 degrees. For other headings this value decreases significantly but does not become impossible. Probability of occurrence of passing pitch angle limit takes place less frequently than for the previous criteria. Once again, the most favourable heading for Ondo to experience excessive pitch motions at 0 knots is 45 degrees and here the probability of exceeding the defined criteria is 2.8%, which is notably lower than for the seasickness (6.1%).

All in all, at drifting conditions, for instance when in dynamically positioned operations, Ondo seems to have good seakeeping properties. In fact, to pass the limit values for the three criteria described, the significant wave height has to be quite high according in relation to the scatter diagram used.

15.2 Half forward (8 knots)

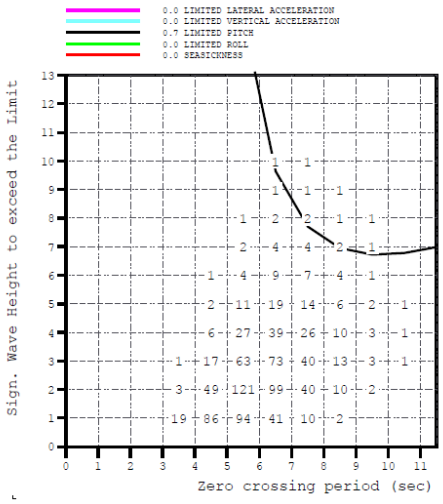

0 degrees

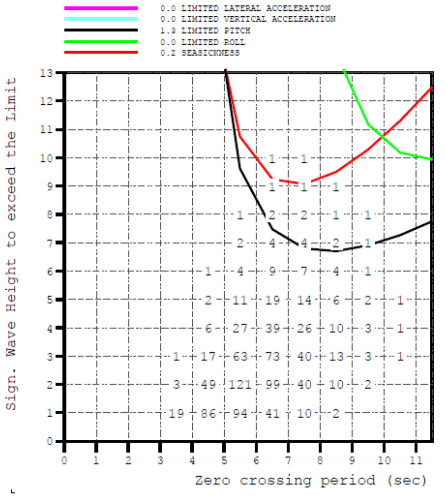

45 degrees

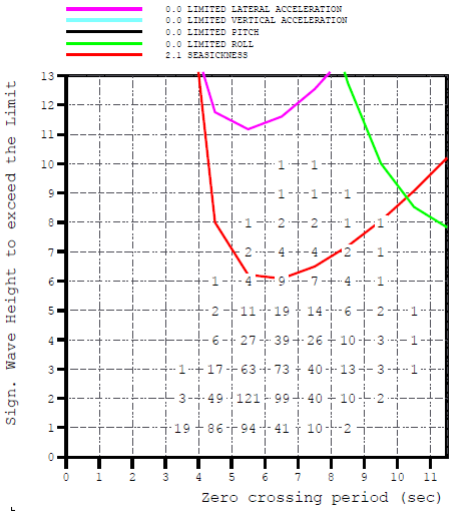

90 degrees

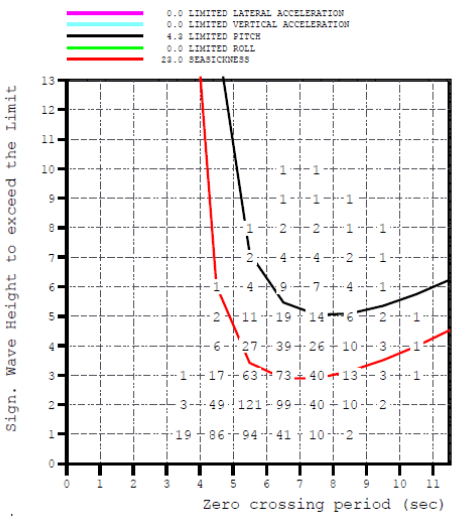

135 degrees

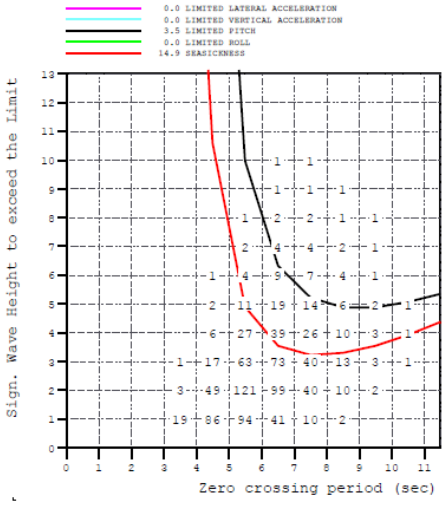

180 degrees

Figure 69. Seakeeping criteria for headings and 8 knots.

From the plots presented in Figure 69 is seen that once again, both criteria regarding accelerations (vertical and lateral), in addition to roll angle limitation, are met for the scatter diagram being considered for each heading analysed at the half forward speed of 8 knots. On the other hand, depending on the heading Ondo is taking, seasickness and limited pitch may become an issue.

Pitch criteria is an issue for all headings analysed except for beam seas (90 degrees heading). For 0- and 45-degree headings, breaking the limit of 3 degrees of pitch takes place very rarely as their probability is around only 1%. For 135 and 180 headings, this frequency increases slightly to around 4%.

On the other hand, seasickness criteria is broken at each heading except for 0 degrees. For headings of 45- and 90-degrees, the occurrence of seasickness is extremely low. However, for 135- and 180- degree headings, seasickness becomes a frequent issue as it occurs with 23 and 15% probabilities, respectively.

To sum up, the criteria which are relevant at half forward speed are the ones regarding to pitch motion and seasickness. As analysed previously for drifting condition, we saw that these criteria were better met. Therefore, as guidelines given to the crew, considering that heading cannot be changed due to defined course/route to be taken, the speed of the vessel may be reduced in order to minimise situations uncomfortable for people on board.

15.3 Design speed (16 knots)

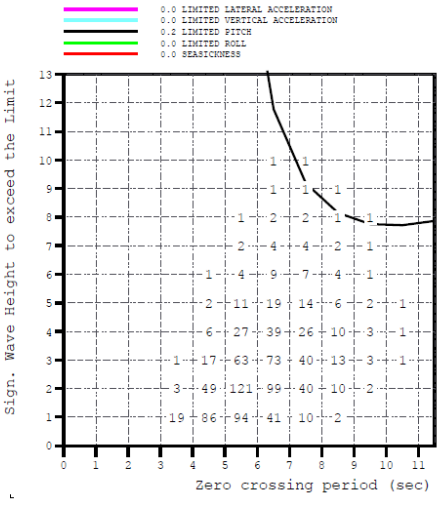

0 degrees

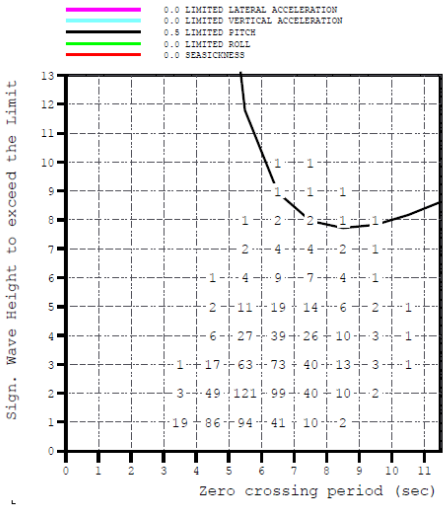

45 degrees

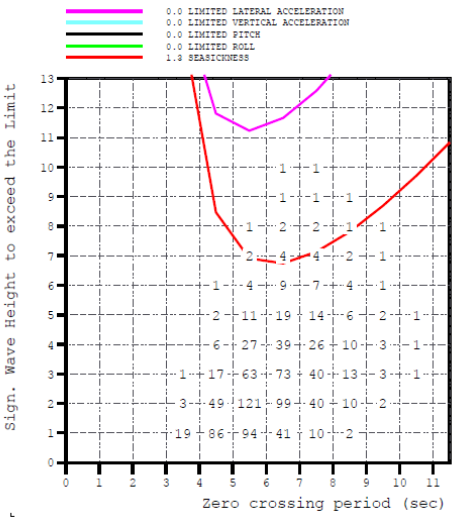

90 degrees

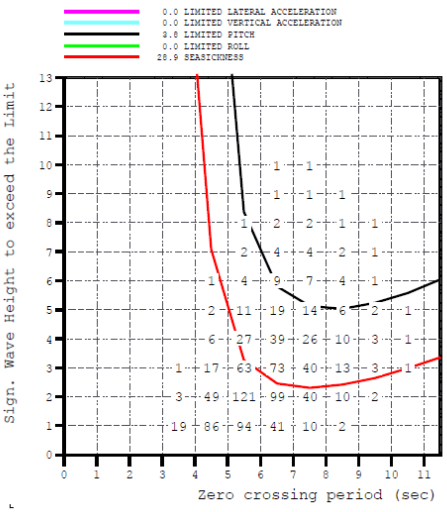

135 degrees

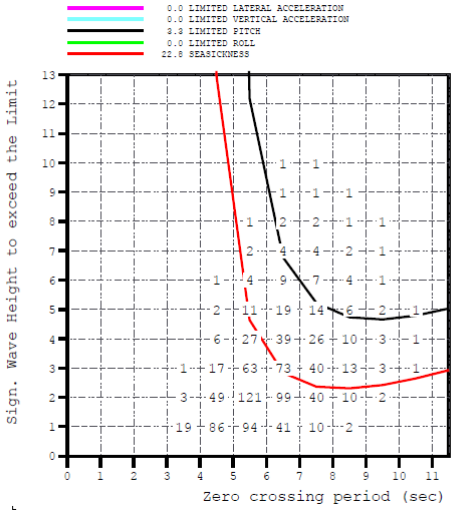

180 degrees

Figure 70. Seakeeping criteria for headings and 16 knots.

As in the case of drifting condition of Ondo, also at its design speed (18 knots), the only seakeeping criteria which raise some concern are the pitch motion and seasickness limitation.

Limited pitch is concerning heading for all headings at design speed except for beam seas. The occurrence of excessive pitch motions for headings of 0 and 45 degrees is quite unlikely as its probability is well below 1%. In fact, only for very high zero crossing periods and significant wave height pitch motions may exceed 3 degrees. For 135- and 180- degree headings the occurrence increases slightly to around 3%.

On the other hand, seasickness criteria is not met for 90-, 135- and 180-degree headings. For beam seas the probability of seasickness being greater than 20% is extremely low as its probability of occurrence is only slightly over 1%, occurring when significant wave height is over 7 metres and zero crossing period is between 5 and 9 seconds. However, for 135- and 180- degree headings seasickness becomes a great concern and it

may take place very frequently, at even relatively low significant wave heights. In fact, for a heading of 135 degrees the probability of exceedance is close to 30% and in the case of head seas is 23%.

As a summary, for design speed of our project ship the seasickness and pitch motion criteria become quite concerning when in comparison to lower speeds. In fact, seasickness and excessive pitch motion may even take place at low significant wave heights (2 metres). Therefore, guidelines given to the crew of the ship must be followed so that Ondo may operate in conditions such that personnel on board can work and enjoy their time. For instance, as seen in the previous speeds of Ondo analysed, the seasickness criteria are not so concerning at low significant wave heights. Therefore, if the route course must be kept, a reduction in speed may improve passenger and crew experience on board.

16 Manoeuvring

In book “Practical Ship Hydrodynamics” by Volker Bertram Ship Manoeuvring is defined as subject which includes topics of course keeping, course changing, track keeping, speed changing. Maneuvering requirements are a standard part of ship building contract. Minimum maneuvering requirements are specified by IMO but shipowner may introduce more severe requirements.

Understanding ship maneuvering and the related numerical and experimental tools is important for the designer for the choice of maneuvering equipment of a ship. Ship maneuverability is described by main characteristics of turning ability, yaw ability, stopping ability. Stopping ability has interest for low speeds. For avoiding obstacles at high speed it is more effective to change course by turning.

Maneuverability depends on choice of maneuvering equipment of a ship. These can be rudders, fixed finds, jet thrusters, propellers, adjustable ducts, waterjets.

Maneuvering is not the same as seakeeping. Main differences are that maneuvering is investigated in shallow and calm waters, and maneuvering tests employ time-domain simulations.

To assess Ondo maneuverability, we have chosen several maneuvering tests to be computed in NAPA. Ondo has pair of Azipods which are not fully supported by NAPA maneuvering manager. In this case we were provided with macros to compute turning circle, zig-zag and stopping tests. We think these tests will provide main information about Ondo maneuverability.

During turning circle test rudder is turned at maximum speed usually to maximum angle and kept there until ship has performed a turning circle of 540°. Main parameters which are obtained during test are:

- tactical diameter;
- maximum advance transfer at 90° change of heading;
- time to change heading 90° and 180°;
- transfer loss of steady speed.

Ondo

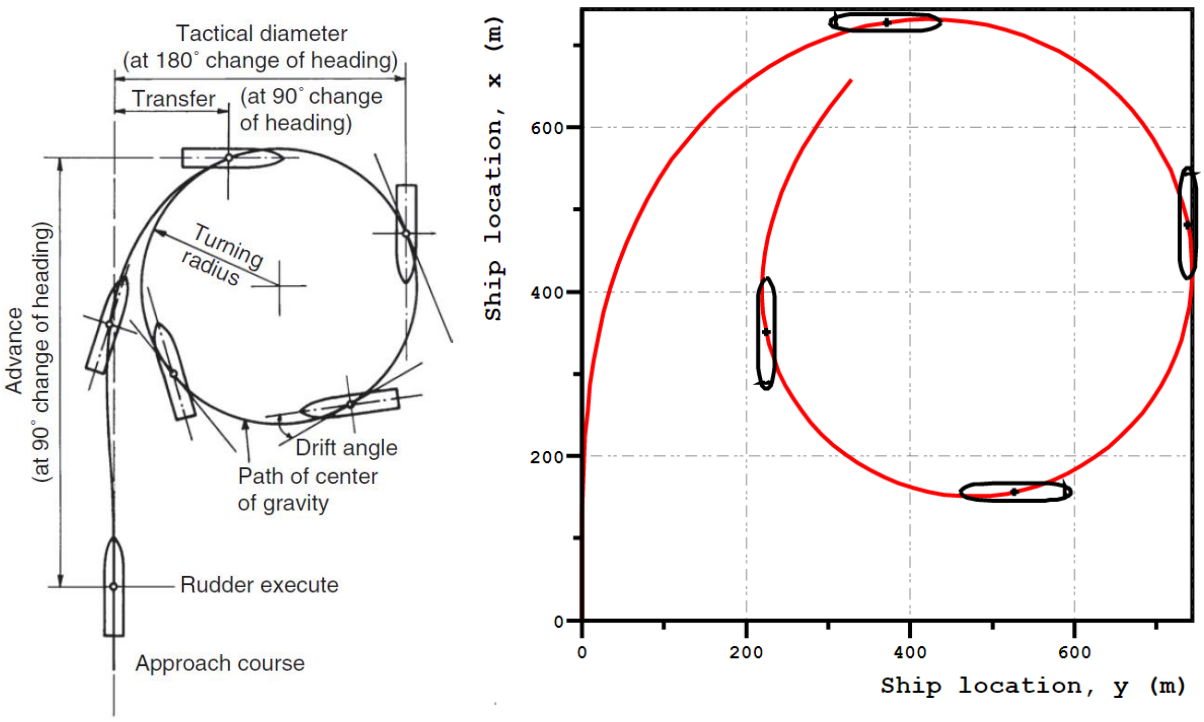

Figure 71. Turning circle test

In Ondo case NAPA turning circle test computed parameter values are:

- advance 727.6 m;
- transfer 371.2 m;
- tactical diameter 743.4 m;
- steady diameter 530.2 m;
- time for 90° turn 125 s;
- time for 180° turn 210 s;
- time for 270° turn 295 s;
- time for 360° turn 380 s.

Ondo tactical diameter has value of 5.6L which is typical value for slender ship.

During Zig-zag test rudder is reversed alternately by a rudder angle to either side at a deviation from the initial course. After a steady approach the rudder is put over to starboard (first execute). When the heading is off the initial course, the rudder is reversed to the same rudder angle to port at maximum rudder speed

(second execute). After counter rudder has been applied, the ship continues turning in the original direction (overshoot) with decreasing turning speed until the yaw motion changes direction. In response to the rudder the ship turns to port. When the heading is off the initial course to port, the rudder is reversed again at maximum rudder speed to starboard (third execute). This process continues until a total of, say, five rudder executes have been completed. Typical values for deviation are 10° and 20° from the initial course.

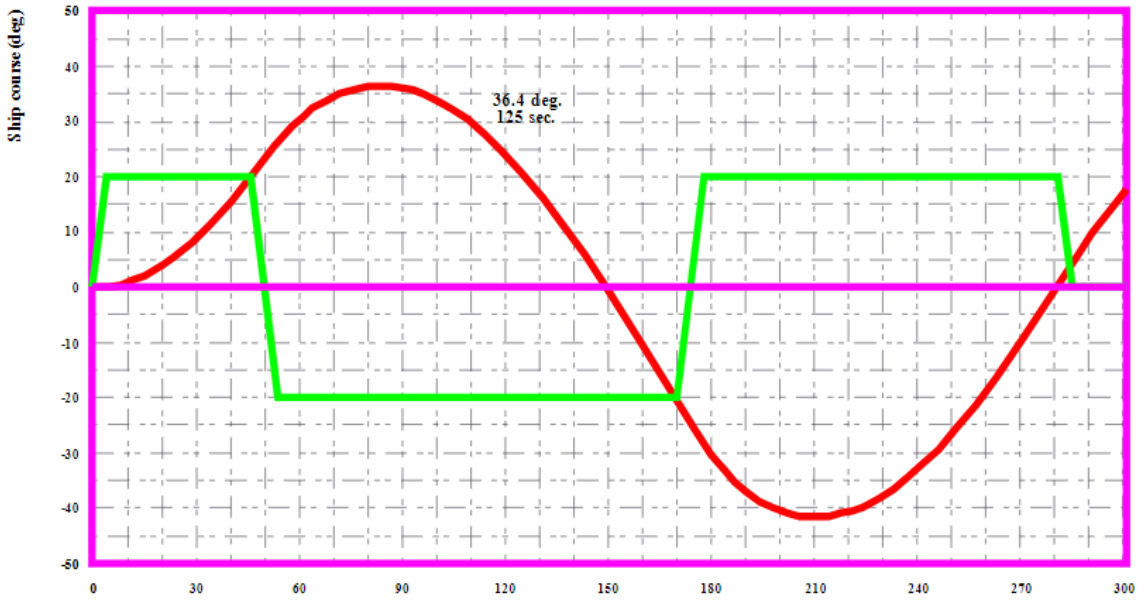

Figure 72. 10/10 zig-zag test

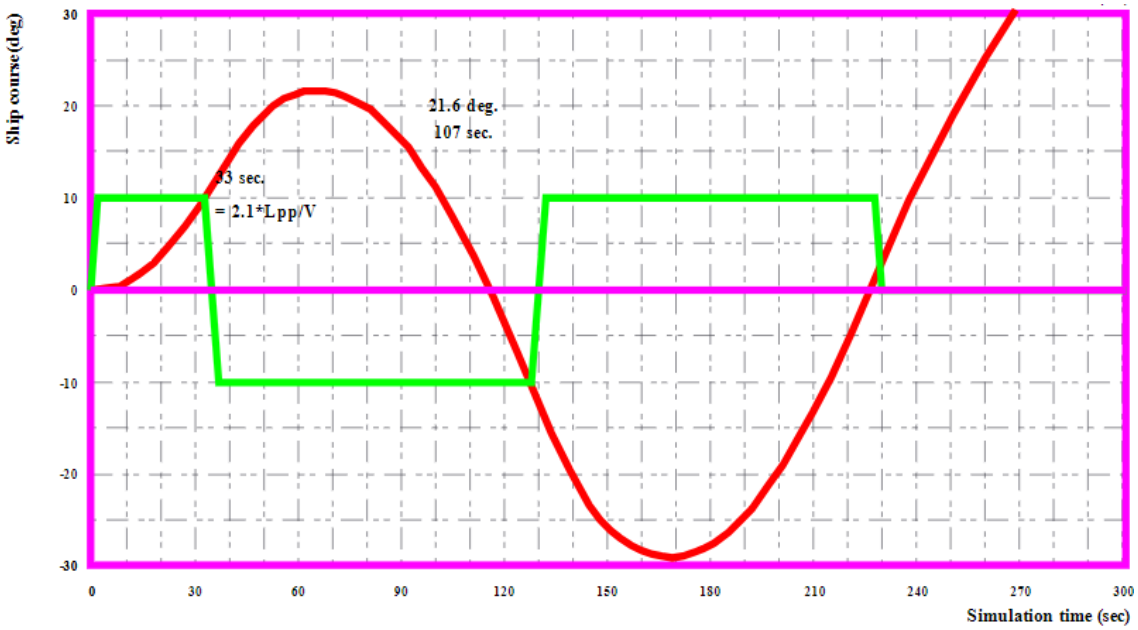

Figure 73. 20/20 zig-zag test

Z 10/10 first over shoot angle is 11.6 degrees,
which satisfies IMO criterion of 13 degrees

Non-dim length to first 10 deg. course change is 2.1*Lpp/v
which satisfies IMO recommendation of 2.5*Lpp

Z 20/20 First over shoot angle is 16.4 degrees,
which satisfies IMO criterion of 25 degrees

Figure 74. Zig-zag test results

Figure 74 shows the results obtained with the zig-zag test according to IMO criteria. There, Ondo's results of zig-zag tests at deviations 10° and 20° from the initial course satisfy fully the IMO criteria.

Stopping test is the crash-stop from full-ahead speed. The reaction to stopping maneuvers is strongly non-linear. Thus, environmental influences and slight changes in the initial conditions may change the resulting stopping track considerably. Results of the stopping maneuver are:

- head reach;
- lateral deviation;
- stopping time.

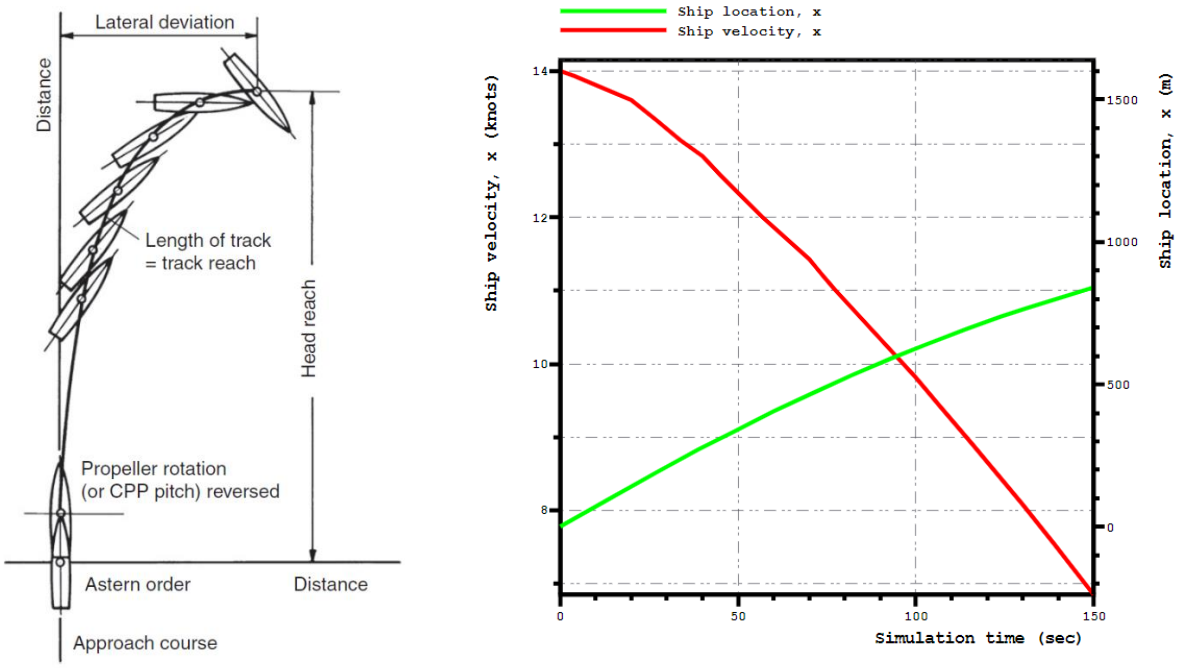

Figure 75. Stopping test

17 Added resistance

Ship resistance can be computed as:

$$R_T = R_C + R_A$$

Where R_T is the total resistance in a seaway, R_C is the resistance in calm water and R_A is the added resistance, which can be further defined into added wave resistance and added wind resistance. The portion of added resistance may in some cases be 15-30% of the total resistance and therefore it is a very important resistance component to take into account already in early design phase (Hirdaris, 2021). Added resistance can cause the performance of the vessel to drop in the seaway and lead to involuntary loss of speed, which ends up as possible economic losses.

Added wave resistance in head irregular waves was determined for the three different speeds previously mentioned (drifting, half forward, and design speed) taken into account the scatter diagram already considered previously (North Atlantic). The reference significant wave height used for this purpose was 3 metres as this is found to be a very likely sea state in our operational area (we are not looking at worst-case scenario here). Thus, as results the plots shown in Figure 76 through Figure 78 were obtained. There is shown the added resistance in irregular waves as function of the zero crossing periods considered in the North Sea scatter diagram ($H_{1/3}$ = 3 m). This is the output coming from NAPA seakeeping manager which was tool used for the computations for added resistance.

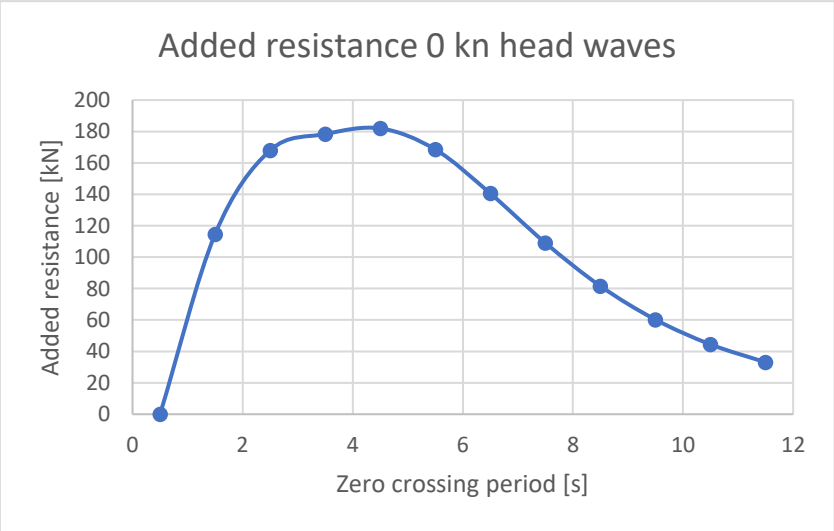

Figure 76. Added resistance at 0 knots head waves.

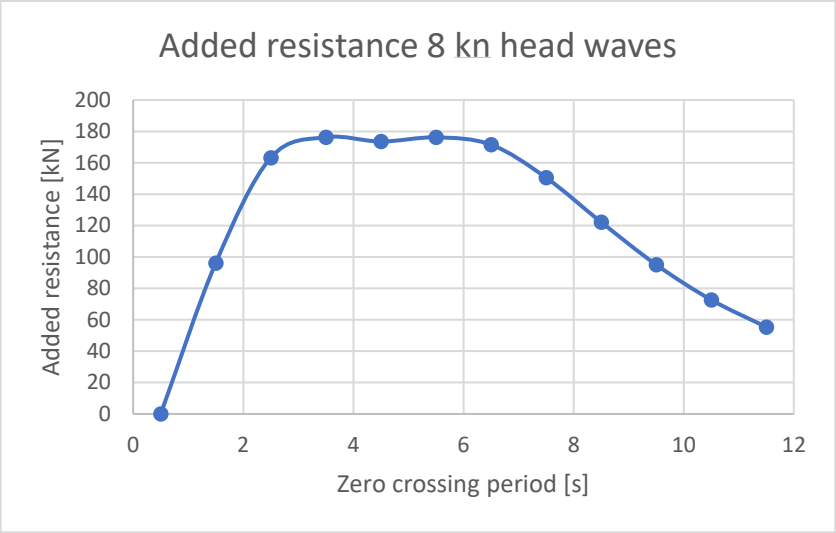

Figure 77. Added resistance at 8 knots head waves.

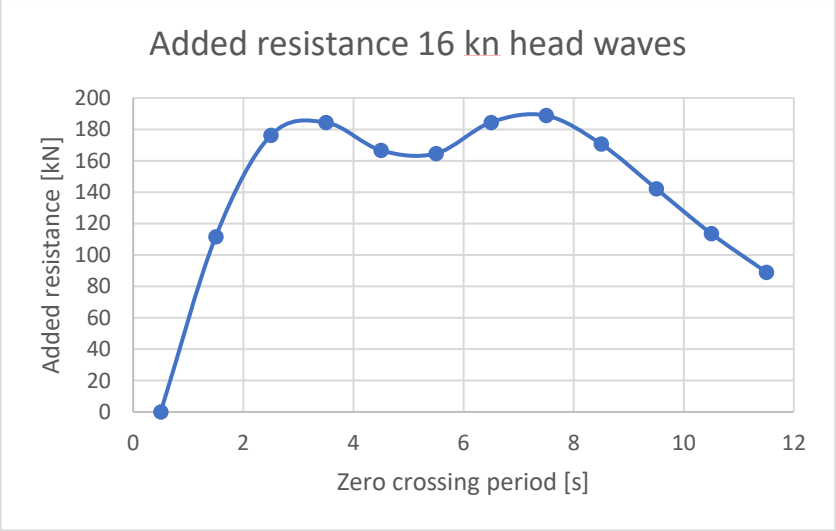

Figure 78. Added resistance at 16 knots head waves.

From the plots presented in Figure 76 to Figure 78 can be seen that the maximum value for added resistance is always situated at a specific range of zero crossing periods. For instance, the range for maximum added resistance may be given as being between 2.5 and 5.5 second. However, for the situation of design speed, the plot for added resistance shows two different peaks situated at 2.5-3.5 and 6.5-7.5 seconds, respectively. In addition, it is seen that the change in maximum added resistance (numerical value) only changes slightly with the change in speed. The maximum added resistance for the three speeds shown takes place at the design speed for a zero-crossing period of 7.5 seconds. Here, the added resistance in waves takes a value of approximately 189 kN. The results presented here seem reasonable and can be compared with results shown in Papanikolaou (2016). In fact, type of plot and tendencies of added resistance as function of zero crossing period (wave length in the article) are similar in both giving reassurance in our results.

Furthermore, we can compute the maximum added resistance value as function of speed. For this, similar plots than the ones shown previously are outputted and the maximum value found is then saved for each speed. Once again, it is found that maximum added resistance for each speed takes place in zero-crossing period range referred to previously. As result we obtained the plot shown in Figure 79 where the maximum added resistance is shown for each speed.

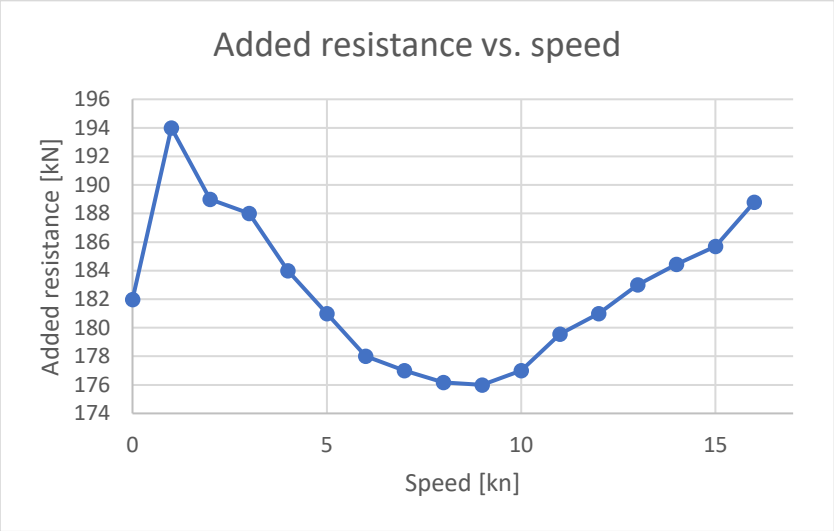

Figure 79. Added resistance as function of speed.

From the plot in Figure 79 is seen that the added resistance as function of speed of Ondo shows an interesting behaviour. First, there is a big jump from drifting condition to a speed of 1 knots. This jump takes place from 182 kN to 194 kN, respectively. Then, the added resistance follows a tendency to decrease as speed increases until a value of around 9 knots. Here, the added resistance reaches its minimum in the range of speeds considered for Ondo, by taking a value of 176 kN. By increasing the speed of Ondo further from 9 knots, the tendency of added resistance in waves changes, showing a tendency to increase. However, added resistance in waves does not reach as high value as for the case of 1 knots speed.

The results shown for added resistance as function of speed of Ondo seem reasonable. The obtained have been compared to the ones presented in Söding and Shigunov (2015). There, the plot giving the added resistance of the vessel as function of speed shows the same kind of behaviour as for the case of Ondo presented in Figure 79. First is found a reduction in added resistance in waves as speed increases until a certain threshold value. As the speed increases further from that threshold value the added resistance in waves starts increasing rapidly. Therefore, once again we can have some good insight in terms of our results being or not in line with what is found in literature.

Next, a comparison between the part of added resistance in selected wave conditions in relation to still water resistance is made. From the plot in Figure 79 we have the dependency of added resistance to the speed of

Ondo. Additionally, we have computed previously the open water resistance for Ondo in the Ship Design Portfolio course. To estimate the resistance in still open water Holltrop method was utilised.

By taking into consideration the results presented and the ones we have had beforehand from other courses where we have worked on this project ship, we can plot the total resistance of Ondo on a seaway by means of the formula presented in the beginning of this section. In summary, the total resistance can be computed as the sum of still open water resistance and the added resistance in waves. As result, the plot in Figure 80 is obtained.

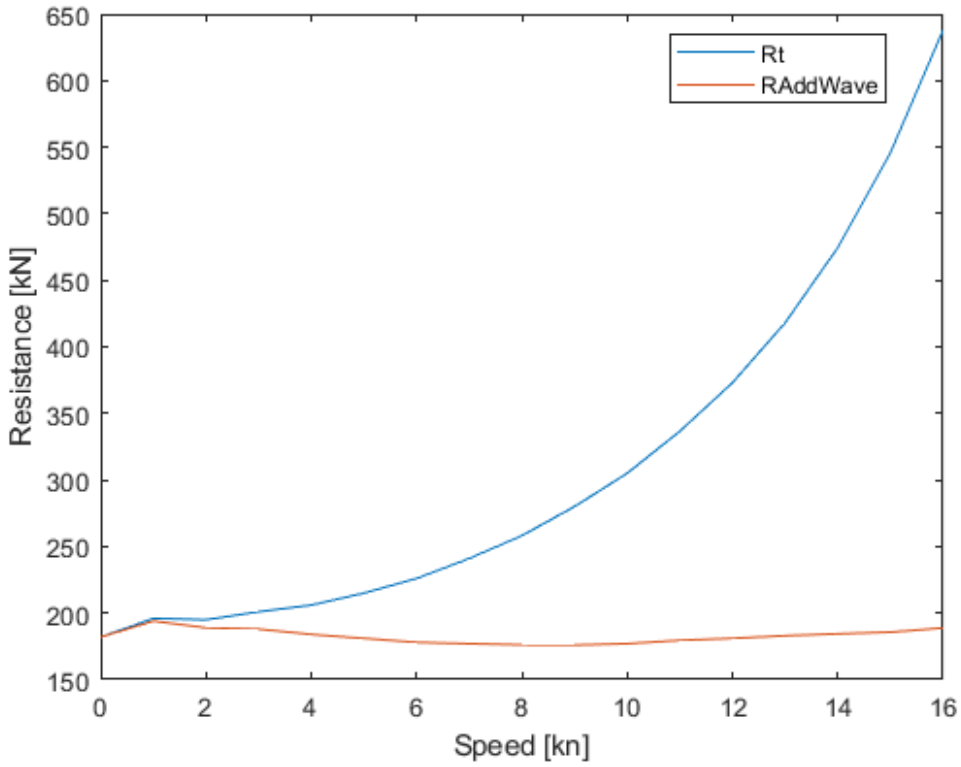

Figure 80. Total and added wave resistance as function of speed.

From the plot in Figure 80 is seen that at small speed (lower than 2 knots) the total resistance of Ondo is mostly set by the added resistance in waves. As speed increases further, the still open water resistance increases exponentially and the added resistance in waves begins to decrease. This takes place until a speed of 9 knots is achieved (Figure 79). As the speed increases above 9 knots, the still open water resistance begins its exponential growth and also added resistance in waves starts showing an increase (however at much smaller rate than the first one).

All in all, it is seen that at the design speed of Ondo (18 knots) the added resistance accounts for almost 30% of the total resistance of the ship in the seaway. On the other hand, when the speed is reduced to half (8 knots) the added resistance accounts for 60% of the total resistance. For the situation of design speed, it is possible to see that the results obtained here are well in line with what is said by Hirdaris (2021).

18 Simplifications made in analysis of Ondo. Future improvements.

Throughout the development of this ship project in the Ship Dynamics course, many were the simplifications made and this is one of the main reasons why improvements can be done.

Simplifications done during the computations include assuming that viscous damping is negligible and that waves are linear. In other words, non-linear effects have not been considered at any point. For instance, when motions become bigger, non-linear effects become important as the properties at the effective waterline of the ship do not keep constant. All in all, for a better analysis of the worst-case scenarios, non-linearities should be considered in order to account for the effect of larger motions.

In addition, some other improvement that can be done to our modelling is to consider effectively the worst-case scenario that our ship will encounter. For instance, it was considered that due to the period of the year Ondo would be navigating the worst-case scenario would take place in the North Sea. However, for a thorough analysis, all possible solutions should be analysed in order to find out which area where Ondo would operate would in fact induce the worst conditions. Furthermore, ice floes are prone to be present in the operational area of our project. This has not been considered in any of the computation or analysis carried out. Therefore, the influence of ice in the results should be further discussed. Last but not least, is also the influence of moderate wind and wind gusts both in ship motions, manoeuvrability and added resistance. It is well known that wind can have a moderate impact in these features.

In Section 3 of this report the devices implemented in our design related to ship dynamics were discussed. However, throughout the work in this course these features have not been considered in the computations. For instance, Ondo is equipped with four passive anti-roll tanks which aim at improving the seaworthiness of Ondo. Therefore, the results of the computations made might be giving worse results than what would be expected if these devices were considered.

To sum up, many were the simplifications made during the assignments in order to facilitate the work and be able to complete them in time for delivery. Thus, some project for the future is to dig more deeply to ship dynamics in terms of motion analysis, loads, seakeeping, manoeuvring and added resistance. Even in early design stage, the dynamic properties of a ship shall be well defined due to them being key issues in terms of the ship being able to carry out its job in the most effective way possible.

19 Books, articles, and lecture reflections

This chapter of the report includes the reflection regarding the additional reading done to support the assignments of the Ship Dynamics course. Different sections in this chapter concern different assignments. Reflection throughout the course was done to various books, articles, and course lecture slides.

19.1 Introduction to ship dynamics

19.1.1 Hull-Form Optimization of KSUEZMAX to Enhance Resistance Performance – Jong-Heon Park, Jung-Eun Choi and Ho-Hwan Chun

This research has been done to improve the hull-form, the size and dimensions of the ship are different from the current project. But it can be considered to improve the hull-form in the future models.

The bow and the stern hull-forms are optimized separately without altering neither, and the resulting versions of the two are then combined. Various optimization algorithms can be used to minimize (or maximize) objective functions in the CFD-based hull-form optimization. Here, objective functions are the minimum values of wave-making and viscous pressure resistance coefficients for the bow and stern. Parametric modification functions for the bow hull-form variation are SAC shape, section shape (U-V type, DLWL type), bulb shape (bulb height and size); and those for the stern are SAC and section shape (U-V type, DLWL type). Sequential quadratic programming (SQP); has been applied for the optimization algorithm. The model tests have been conducted at a towing tank to evaluate the resistance performance of the optimized hull-form. It is necessary to apply optimization techniques coupled with hull-form variation and CFD as an objective and practical hull-form design tool. The hull-form optimization using a CFD is composed of three processes which are the variation of the initial hull-form, the performance prediction via a flow analysis of a varied hull-form, and the selection of the optimized hull-form.

The hull form was altered by adding the variation calculated with a parametric modification function to the initial hull-form. The work was conducted with the bow and stern separated since the flow around the bow is more non-viscous while the flow around the stern is dominantly viscous. The objective functions for the optimization are the minimum wave-making resistance coefficient (CW) for the bow, and the minimum viscous pressure resistance coefficient (CVPM) for the stern. The SQP was used in the optimization.

The objective ship is a wide-breadth slow-speed KSUEZMAX tanker, and the principal dimensions of the full-load draft are the following.

Table 4. Principal dimensions at full-load draft of KSUEZMAX ship.

Length between perpendicular	LPP	264.0 *m*
Length on waterline	LWL	268.4 *m*
Breadth	B	50.0 *m*
Draft	T	15.0 *m*
Wetted surface	S	18,134 m^2
Displacement	∇	158,122 m^3
Block coefficient	C_B	0.7986

The optimization was conducted with the bow and stern separated. The flow around the bow is more non-viscous flow, while the flow around the stern is dominantly viscous. The stern hull-form was fixed for the optimization of the bow in which the non-viscous flow is effective, and the bow was fixed for the stern where the flow is mostly viscous. The bow and stern hull-forms obtained through these processes were combined to figure the optimal hull form. The objective function of bow hull-form optimization is a minimum CW, which can be calculated as Eq. (1) from the potential flow interpretation.

$$C_W = \frac{1}{S}\int_S c_p.n_x.dS \quad [1]$$

where Cp is the pressure coefficient non-dimensionalized by ρ (fluid density) and VS. nx is x-component of normal vector on the hull surface. SQP is applied for the optimization algorithm. SQP is an efficient, gradient-based, local optimization algorithm. This method is to find the gradient (di) at the design variable (xi) in which the objective function f(xi) decreases. Then the current design variable is moved along the direction of di. Two steps are mainly used in the iterative process. The opposite gradient of an objective function f(xi) is defined as expressed in Eq. (2).

$$d_i = -\frac{\partial f}{\partial x_i} \qquad i = 1, 2, ..., N \quad [2]$$

where N is the number of design variables. Note that the gradient at a design variable xi indicates the direction of maximum decrease in the objective function.

Table 5. Design parameter of parametric modification function to show minimum C_w of the parametric study of bow hull-form.

Parametric modification function		Design variable	Value	$C_W \times 10^3$ (ratio)
SAC shape		X_0	15	0.4364 (87.4%)
		X_1	20 (FP)	
		X_{0C}	16.25	
		ΔX at X_{0C}	-0.125	
Section shape	U-V type	Z_0	0.35	0.4204 (84.2%)
		ΔY_{Max}	-0.05	
	DLWL type	Z_0	0.30	0.4958 (99.3%)
		ΔY_{Max}	0.006	
Bulb shape	Bulb height	Z_2	0.50	0.4800 (96.1%)
		ΔB_H at Z_2	0.044	
	Bulb size	Z_2	0.50	0.4891 (97.9%)
		ΔB_S at Z_{12}	0.044	

Table 5 shows the outcome of the parametric study. The ratio shown is that of the changed hull-form CW against that of original hull-form CW. The original CW constitutes 0.4995×10 -3. The SAC modification function is the X-axis modification function of f1(X). f1(X) is expressed as a 6th-degree polynomial. Figure 81 compares the original and U-V changed hulls. This is shown together with the parametric study of the stern. Section shape (U-V type) modification function calculates the variation of the breadth [ΔY=f2(X)·f3(Y)·f4(Z)] by multiplying f2(X), f3(Y), f4(Z) which are the modification function of X-, Y-, Z-axis. Add this value to the original hull-form to generate the changed hull-form. f2(X) is the weighted function where the variation gradually increases from X0(=15) to X1(=20) and is referred to as a 4th -degree polynomial.

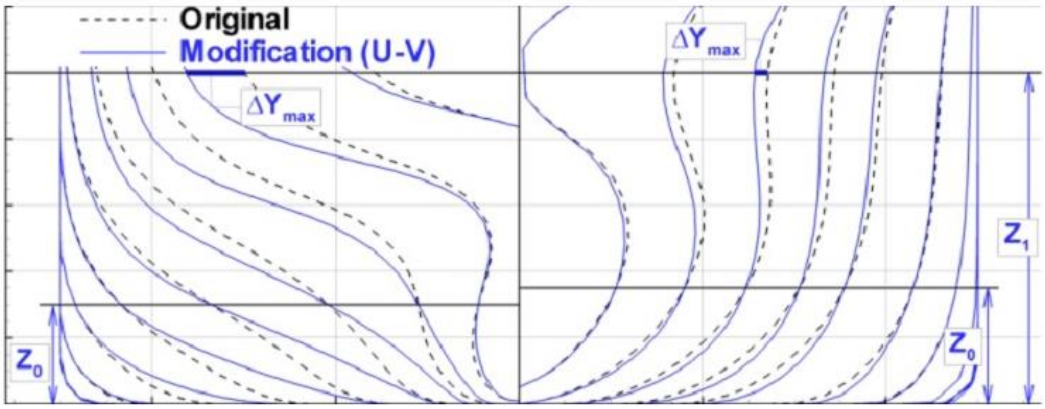

Figure 81. Design parameters for section shape modification (U-V type).

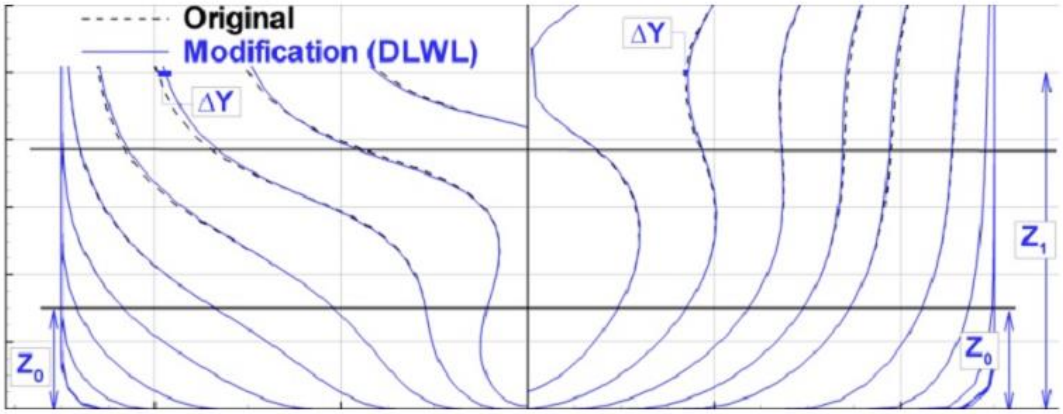

Figure 82. Design parameters for section shape modification (DLWL type).

Figure 82 compares the original and DLWL changed hulls. This is shown together with the parametric study of the stern. Section shape (DLWL type) modification function computes the variation of the breadth [ΔY=f2(X)· f5(Y)·f6(Z)] by multiplying f2(X), f5(Y), and f6(Z) which are modification function of X-, Y-, Z-axis. Add this to the original hull-form to generate the changed hull-form. f2(X) is the same as the modification function applied to the U-V type. f5(Y) is the weighted function expressed as a 6th-degree polynomial.

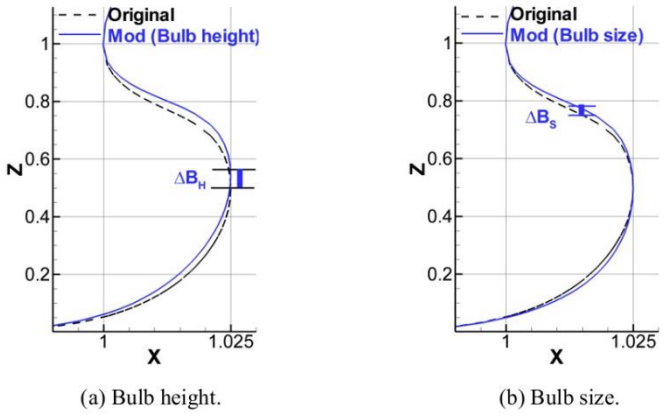

Figure 83. Design parameter for bulb height and size modification.

Figure 83(a) and Figure 83(b) compare the original hull-form and that after the bulb height and size have been altered, respectively. The bulb-height modification function computes the variation in the height (ΔZ) by multiplying f2(X), f7(Y), and f8(Z) which are modification functions of fBH (X, Y, Z). This is added to the original hull form to get the changed hull. The modification function in X-axis is weighted and is the same as f2(X) of section shape (U-V). Figure 84 presents CW contour surface and the trace to find the optimization point where two design variables of SAC and section shape modification (U-V type) are used. The solid line on the contour surface denotes the (volume) constraint. The shapes of the contour surface, and the

constraint clearly show that the domain is convex. Thus, the SQP is a suitable algorithm because the descent always points around optimum solution at any point in the given feasible domain.

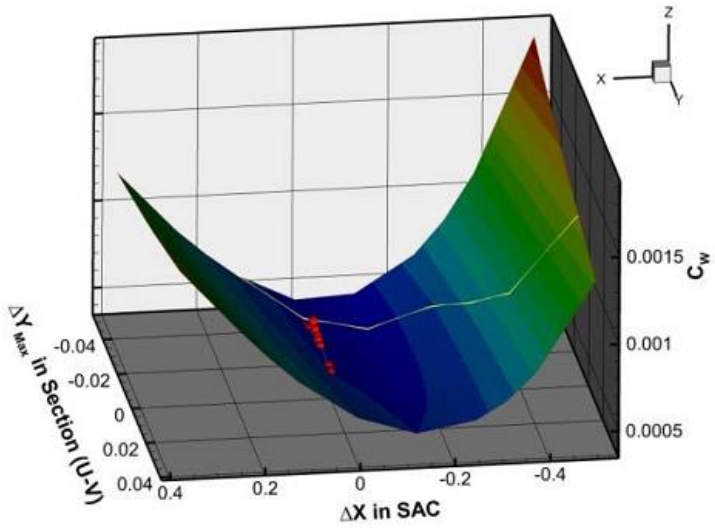

Figure 84. Contour surface of CW and design variable history.

Figure 85 shows the comparison of PE for various ship speeds between the original and optimized hull-form. The decrease in PE becomes larger at the higher velocity region than the design velocity.

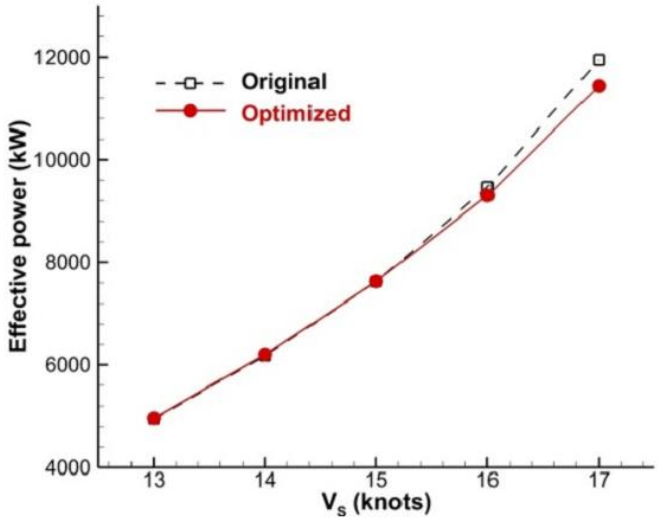

Figure 85. Comparison of effective power for various ship speeds between the original and optimised hull-form.

As a result, the modification functions to expect reducing CW are in the order of section shape (U-V type), SAC shape, bulb size, bulb height and section shape (DLWL type). However, the parametric modification functions of bulb height and size are also taken into consideration for the optimization process, though their effects are small at the parametric studies. The design variables of the bulb height and size will affect hull-form variation at widely region since those of the other modification functions are taken into consideration together. Using parametric modification functions, the initial hull form is easily deformed according to the

variations of the design parameters, which are familiar to a ship designer as design variables. The result of model test shows that the optimized hull-form brings 1.7% reduction in effective power in addition to 3.7% reduction in delivered power. Hull-form optimization taking self-propulsion conditions into consideration is suggested for further research. It has been noted that the optimized hull-form brings 2.4% and 6.8% reduction in total and residual resistance coefficients compared to those of the original hull-form. The propulsive efficiency increases by 2.0% and the delivered power is reduced 3.7%, whereas the propeller rotating speed increases slightly by 0.41 rpm.

19.1.2 Bilge-Keel Influence on Free Decay of Roll Motion of a Realistic Hull – Yichen Jiang, Ronald W. Yeung

The prediction of roll motion of a ship with bilge keels is the main topic of this article. To overcome difficulties of nonlinear characteristics of the viscous roll damping the Slender-Ship Free-Surface Random-Vortex Method (SSFSRVM) was employed to predict ship motions.

What are bilge keels? Bilge keels is the traditional passive stability enhancement system. However, they increase hydrodynamics resistance when ship rolls. Traditional pair of bilge keels is shown in Figure 86-

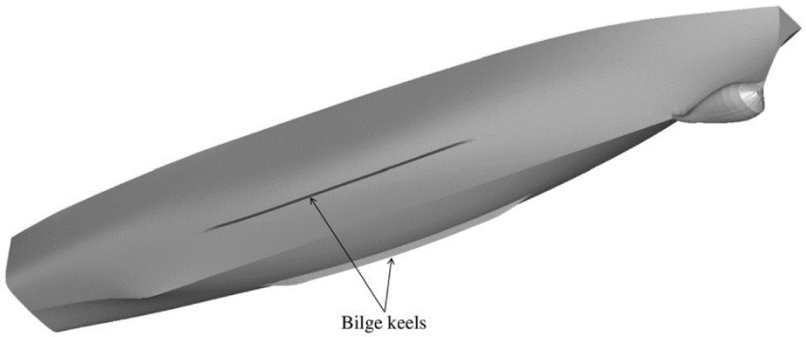

Figure 86. Bilge keels.

And how do bilge keels work? Flow separation and vortex shedding caused by bilge keels significantly affect the roll damping and hence the magnitude of the roll response decreases.

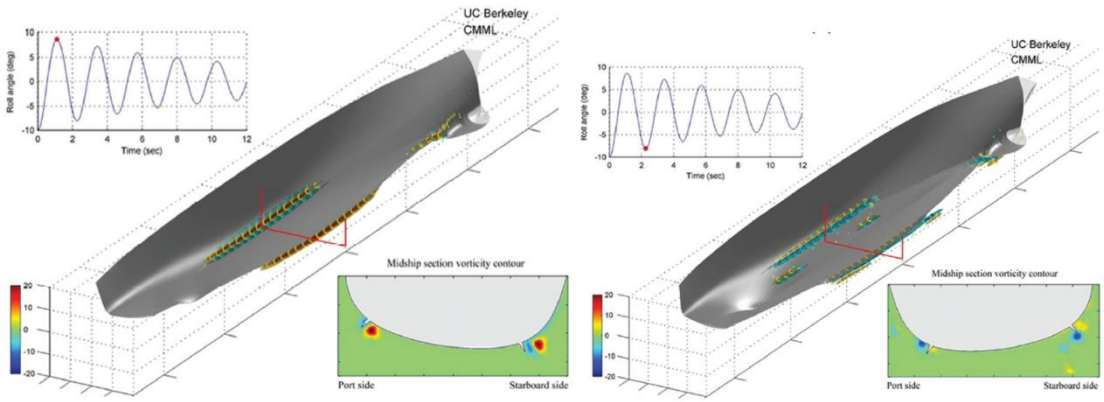

Figure 87. Bilge keels caused vorticities.

Issues of existing ship motions predicting models for example CFD is problems with mesh density and long calculating time. To solve this issue, authors developed model called Slender-Ship Free-Surface Random-Vortex Method (SSFSRVM) to predict the roll motion of a three-dimensional vessel with bilge keels. Model is a fast free-surface hydrodynamics solver and features a quasi-three-dimensional formulation involving decomposing the problem into a series of two-dimensional computational planes.

Authors model calculations and experiments show that bilge keel with larger span generates stronger counter-rotating vorticity pairs. This transfers more energy from the hull into the surrounding flow and leads to a larger decay rate. The roll decay coefficient increases with the bilge keel span, but this rate of increase is not proportional to the rate of increase of the bilge keel span. In the cases of roll motion in waves, authors found that increasing the bilge keel span effectively decreases the roll amplitude.

Bilge keels topic is directly related to Ondo ship design. Ondo must have good dynamics characteristics and bilge keels can provide them in case of roll motions.

19.1.3 Feasibility Study on Thrust Produced by Stabilizing Fins in Waves – Jerzy Edward Matusiak, Patrik Pentti Rautaheimo

This article looks at the feasibility of utilisation of wave energy, using fin stabilisers, to give additional thrust to a ship, without losing its stabilising effects. We found this article very promising to our design work as Ondo is meant to be an environmentally friendly ship. We are seeking to lowering emissions using, for example, LNG as an auxiliary propulsion fuel. The use of stabiliser fins, in addition to LNG, could bring additional benefits in lowering emissions and consequently also voyage due to additional fuel savings.

The mathematical formulations used in this research are complicated to analyse at this point due to the lack of background in ship dynamics. Therefore, the procedure and the results in general are analysed to get some interesting conclusions out from the article.

A passenger vessel with the main dimensions presented in Table 6 was used as study object in this article:

Table 6. Main dimensions of the vessel investigated.

Length; L_{pp} [m]	260.5
Breadth; B [m]	32.2
Draft; T [m]	7.8
Block coefficient; C_b	0.65
Metacentric height; GM_0 [m]	2

Three different fin configurations/locations were considered, and these are shown in Figure 88. The fins considered are all of the same kind: same rectangular form, span, constant chord length and thickness. Only the location is different within the configurations.

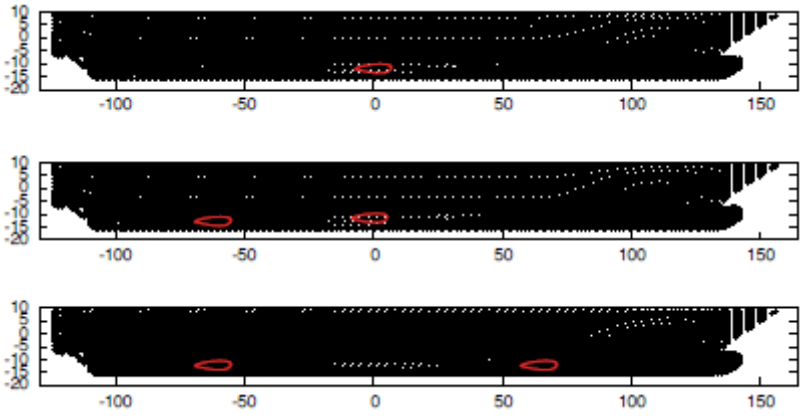

Figure 88. Fin configurations considered in the article – voyager_fin, fins_at_midship and fin4ends (from up to down, respectively).

To evaluate the potential gain of using stabilising fins in the different configurations shown in Figure 88, the thrust power of fins is related to the thrust power of propellers with fins retracted. In order to have a fair comparison of different fin arrangements, the same wave train is used for different fin configurations including both optimally controlled and fixed fins.

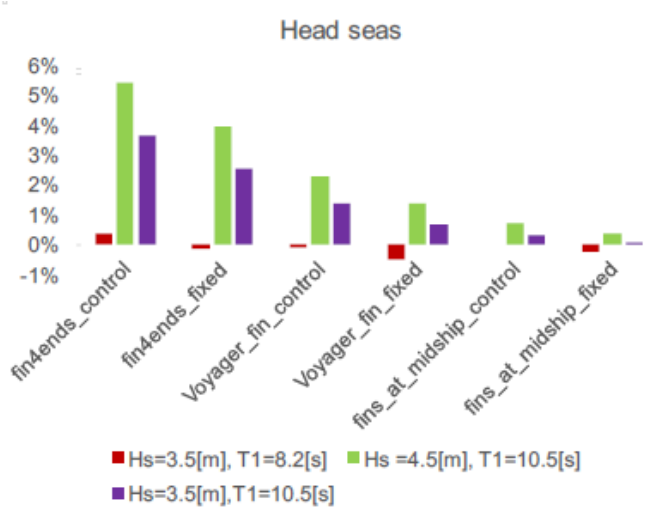

Figure 89. Fin power in relation to the thrust power of propellers. Head seas condition.

In Figure 89, it is seen the fin power in relation to the thrust power of propellers in the condition of head seas. A significant gain in power is observed in long head waves of significant height H_S = 4.5 m with two pairs of fins located at the bow and stern. With optimally controlled fins this gain is 5.5% while with fixed fins this is 4%. The gain in power seems to increase with the increase in both wave period (T1) and wave heigh (H_S). Overall, the presence of fins seems to give positive contribution to the ship's thrust, except for the use of fixed *voyager_fin* and *fins_at_midship* in short (smaller T1) and small height (H_S) waves, where it impacts negatively the thrust with a small percentage (lower than -0.5%).

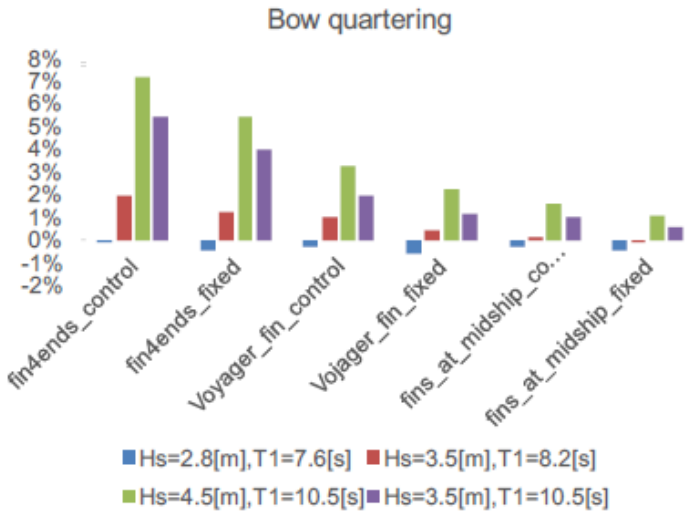

Figure 90. Fin power in relation to the thrust power of propellers. Bow quartering seas condition.

In Figure 90, just like previously, it is seen the fin power in relation to the thrust power of propellers in the condition of bow quartering seas. Changing the course (coming direction of waves) from the previous situation shown in Figure 89 to bow quartering seas brings some slight changes to the results obtained. In fact, in general, the positive contribution of the stabilisers fins increases its contribution. For instance, for the significant wave height of H_S = 4.5 m, using fins both at the stern and bow, brings savings in 7%, which is slightly higher than in the previous case. On the other hand, for the shorter and smaller waves, the contribution becomes negative, bringing additional resistance to the ship instead of decreasing it.

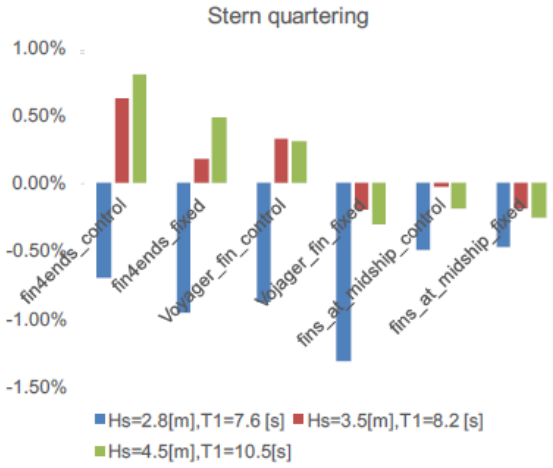

Figure 91. Fin power in relation to the thrust power of propellers. Stern quartering seas condition.

In Figure 91, it is seen the fin power in relation to the thrust power of propellers in the condition of stern quartering seas. In this condition, when there is positive influence of the stabiliser fins, there is only very limited power gain which does not even reach 1.00%. This slight contribution is verified only for the fins located at both ends of the ship and using the common voyager fin, when having optimal controlled, in wave systems with significant wave height and long waves (higher T1). All other situations lead to a negative impact which can go up to -1.25% when using the fixed voyager fins, in short and small wave systems.

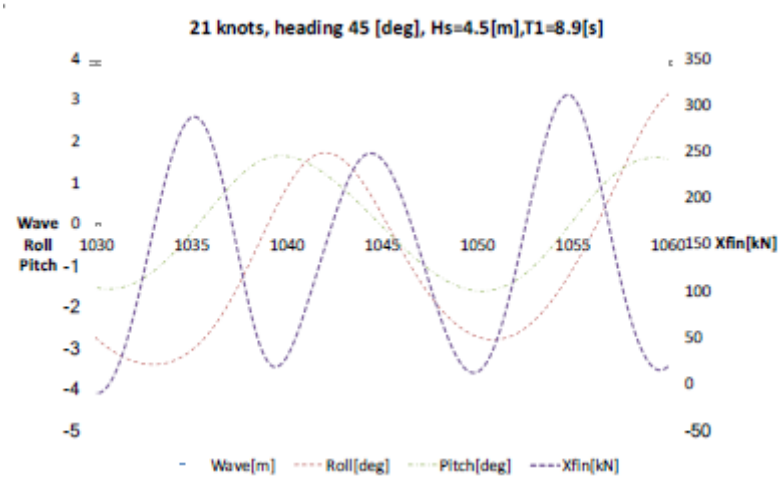

Figure 92. Thrust of four controlled fins in stern quartering seas.

In Figure 92 is illustrated the relation between thrust generated by stabilising fins and ship motion, as the time-histories of ship roll motion and thrust (X_{fin}) generated by two pairs of fins located far apart. It is seen that the ship is experiencing roll resonance, as the oscillations in roll are increasing their amplitude as time goes by. In addition, it is possible to see that fin thrust is negatively impacting at its maximum (minimum value) when the pitch motion is at its extremes (minimum or maximum pitch angle). On the other hand, when the derivative of the pitch motion is maximum in modulus, the fin thrust shows its maximum positive

influence. Consequently, this leads us to assuming that the generation of thrust by stabilising fins is coupled with the pitch motion. Thus, this also explains the better position of two pairs of fins located apart to generate thrust in head seas, as these will experience greater influence from the pitch motion.

In conclusion, the article analysed here shows that using stabilising fins in head and bow quartering long waves allow to produce some extra thrust to the ship, which may be used to ease the main machinery effort. In particular two pairs of fins, located far apart, benefit from the pitch motion component of a ship and may produce a significant thrust when compared to other fin layouts and configurations. Controlling of fins may be used to get the maximum benefit of ship motion energy transformation into propulsion energy. However, also fixed fins have a positive effect on thrust. (Matusiak, 2017).

Considering Ondo, we can have a look at the economic and environmental content of the possible application of this technology in our design. As known, Ondo is both a research and passenger vessel. Therefore, we must look at reducing to allowable values the oscillations, such as roll motions when navigating to have good comfort for passengers and to be able to do good research work onboard when in transit. Therefore, stabilising fins to damp roll motions are something to have in mind. On the other hand, as shown in the section where the operational profile of Ondo is described, this ship will navigate in the Atlantic Ocean when sailing from the Northern to the Southern Hemisphere and vice-versa. The Atlantic Ocean is known to be a critical stage in terms of wave conditions and elevated wave heights are typically reached. Consequently, making use of this additional thrust coming from the stabilising fins (which increases with wave height and period as shown previously) can have a good applicability taking into consideration the operational profile being considered.

19.2 Waves

19.2.1 Types of Ocean Surface Waves, Wave Classification

Capillary waves:

Waves affect a large number of marine activities processes that take place on and below the ocean surface. The widespread wind-generated waves are, for example, responsible for inducing considerable loads on marine structures. Ocean waves can be classified in several ways. The most intuitive and commonly used classification is based on the wave period or the associated wavelength. In Table 7, a summary of the different types of surface waves is presented with respect to wave period. The associated originating forcing and restoring mechanisms are also reported. A graphical representation is provided in Figure 93, where an idealized wave energy spectrum shows the full range of ocean wave components. The shortest-period waves, and the first to be noticed on the ocean surface when wind starts blowing, are the capillary waves. This

peculiar wavy structure is generally forced by a light breeze of speeds of about 3m/s (taken at a reference height of 10m from the water level) and assumes a fine structure of small ripples with a wavelength of less than 1.5 cm and period less than 0.1 s.

Table 7. Ocean wave classification.

Classification	Period band	Generating forces	Restoring forces
Capillary waves	<0.1 s	Wind	Surface tension
Ultragravity waves	0.1–1 s	Wind	Surface tension and gravity
Gravity waves	1–20 s	Wind	Gravity
Infragravity waves	20 s to 5 min	Wind and atmospheric pressure gradients	Gravity
Long-period waves	5 min to 12 h	Atmospheric pressure gradients and earthquake	Gravity
Ordinary tidal waves	12–24 h	Gravitational attraction	Gravity and Coriolis force
Transtidal waves	>24 h	Storms and gravitational attraction	Gravity and Coriolis force

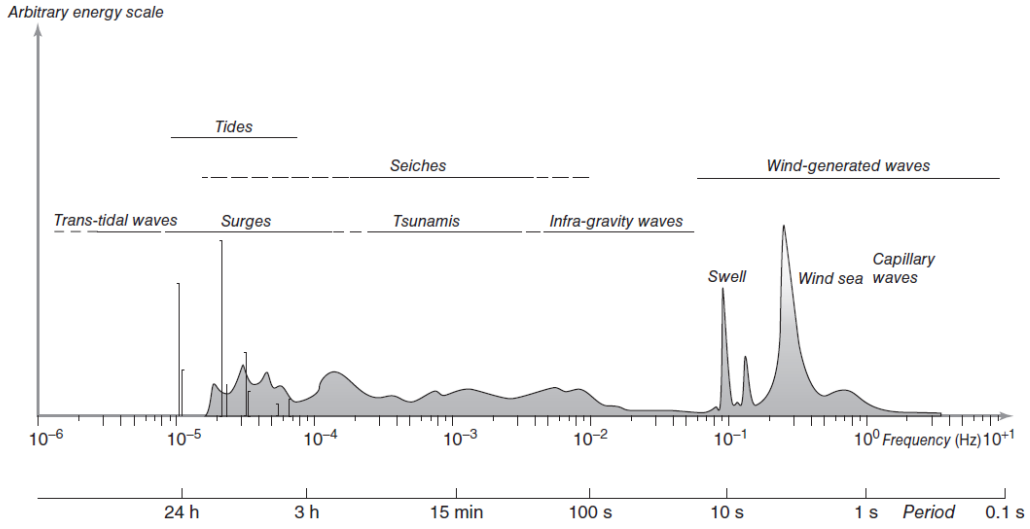

Figure 93. Frequency and period of ocean waves. (Reproduced from Holthuijsen, 2007. © Cambridge University Press, 2007.).

Under the direct effect of the local wind, many components with different wave periods, direction of propagations and phases are generated. The resulting wave field is an interaction of all these components, which generates an irregular pattern normally known as wind sea. Despite the wide period band of wind-generated waves, the dominant components of wind sea remain relatively short. During severe storm conditions, for example, the wave period increases up to maximum of approximately 10–12 s. The wave height, however, grows substantially, steepening the wave profile.

Gravity waves:

A consistent blowing of wind over a substantial fetch forces waves to become much longer than the threshold wavelength of 1.7 cm. As the wavelength grows longer than 1.5m, surface tension becomes negligible, and gravity remains the sole restoring mechanism. Under these circumstances, waves are classified as gravity waves. It is worth mentioning, in this regard, that gravity acts on wave dispersion by inducing wave phases to propagate faster than wave groups and thus reversing the effect of surface tension.

Infra-gravity waves:

Nonlinear interactions between wave components convert part of the energy associated to wind-generated gravity waves into subharmonics with periods ranging from about 20 to 30 s up to a maximum of approximately 5 min. These long oscillations, which are driven primarily by swell, are bound to the generating wave trains and are normally known as Infragravity waves. Generally, Infragravity motion observed on the continental shelf in depths ranging from 8 to 200m is a mixture of subharmonics bounded to the incident waves.

Long-Period Waves (Tsunamis, Seiches, and Storm Surges):

Well-defined waves with periods longer than 5min are routinely recorded in the ocean. Although different originating mechanisms can be responsible for such waves, meteorological conditions and earthquakes remain the primary cause. Normally, long oscillations generated by atmospheric conditions are known as seiches and storm surges, while tsunamis identify waves originated from earthquakes. Despite the long wavelength, the restoring mechanism is still dominated by gravity. Tsunamis are long waves with period varying between 1 and 20min that are generated by sudden tectonic changes to the seabed or landslides that are usually attributed to earthquakes and submarine volcanic activity. In the open ocean, tsunamis have very small amplitude and generally pass completely unnoticed. Propagation into shallower waters, however, makes wave shoal, compressing the shape of the oscillation. It is not uncommon for seismic activities and tsunamis to generate additional long-waves components (seiches) due to local geographical peculiarities. The primary causes of seiches, nonetheless, remains related to meteorological disturbances such as wind gusts or atmospheric pressure variations, which induce a resonance effect on an enclosed or partially enclosed water basins (e.g., closed seas such as the Adriatic Sea, the Baltic Sea, and the North Sea).

The range of natural periods for seiches is rather large and strongly depends on the fundamental resonance period of the water basin. In most of the seiches that occur in nature, the period T can be estimated as $T=2L/(gh)^{0.5}$, where g is the acceleration due to gravity, L the length of the basin, and h the average depth of the basin.

Tides:

The maximum tidal elevation occurs a few days after the full and new Moon as the Sun and the Moon act together (i.e., the Sun, Moon, and the Earth are aligned). This condition is known as spring tide. When the Moon is at the first or third quarter, the Sun and the Moon are misaligned by 90° and the solar gravitational force partially cancels the one exerted by the Moon. At these stages of the lunar cycle, the tidal range is at its minimum and the tide is called neap tide.

19.2.2 Spatial patterns of the wave climate in the Baltic Proper and the Gulf of Finland

The Baltic Sea is a challenging area for regional marine science. Numerical simulations of the Baltic Sea wave climate require a high spatial resolution because of the extremely complex geometry and high variability of wind fields in this basin. Numerical simulations of the Baltic Sea wave climate require a high spatial resolution because of the extremely complex geometry and high variability of wind fields in this basin. Relatively shallow areas, widely spread in this basin, may host unexpectedly high waves, formed in the process of wave refraction and optional wave energy concentration in some areas. As wave height is often proportional to wind speed squared, wave field scan be used as a sensitive indicator of changes in wind properties Storminess in the Baltic Sea region was relatively high at the beginning of the 20th century, decreased in the middle of that century and returned to the original level in the 1980s–1990s. In the international literature there is, however, highly controversial evidence about the reaction of the Baltic Sea wave fields to changes in the forcing conditions and to some extent also about the reaction of sedimentary coasts. The changes in the Baltic Sea wave climate were apparently marginal from the late 1950s until the late 1980s. The situation evidently changed in the 1990s, however, when a drastic increase in wave heights was reported off both the eastern and western coasts of the northern Baltic Proper.

Such spatially highly variable evidence suggests that wave properties indifferent regions of the Baltic Sea may reveal different patterns of temporal changes. It is well known that different sub-basins of this water body may host substantially different features of the wave climate. The anisotropic nature of the Baltic Sea wind and wave fields suggests that considerable differences between typical and extreme wave properties may also exist in the vicinity of different coasts of the Baltic Proper and the Gulf of Finland. Therefore, certain spatial structures of the wave climate may exist in separate sub-basins. A systematic turn in the wind direction (Kull 2005) may obviously lead to opposite trends in wave heights and periods on upwind and downwind coasts. It has been, however, a common implicit belief in existing studies of potential changes in the Baltic Sea wave climate that, apart from the listed variations, major changes to the wave climate have mostly the same pattern in different sea areas. The analysis is based on historical wave data and the results of numerical hind casts. As most of the available long-term wave data stem from the eastern and north-eastern Baltic Sea and the Gulf of Finland, the focus is on the eastern regions of the Baltic Sea. Finally, this information brings an evidence about differences in the patterns of changes in average and extreme wave heights and demonstrate why many such changes have gone unnoticed in the existing wave measurement network.

Long-term wave measurements and observations:

There are only a few observation and measurement sites on the eastern coast of the Baltic Sea and in the Baltic Proper covering longer time intervals. In the discussion below, we use the data from Almagrundet,

Nida, Palanga, Klaip˙eda, Vilsandi, Pakri and Narva-Jõesuu (Figure 94). Although the most reliable information about wave properties in the northern Baltic Proper stems from directional wave measurements at Bogskär in 1982–1986, in the northern Baltic Proper since 1996.

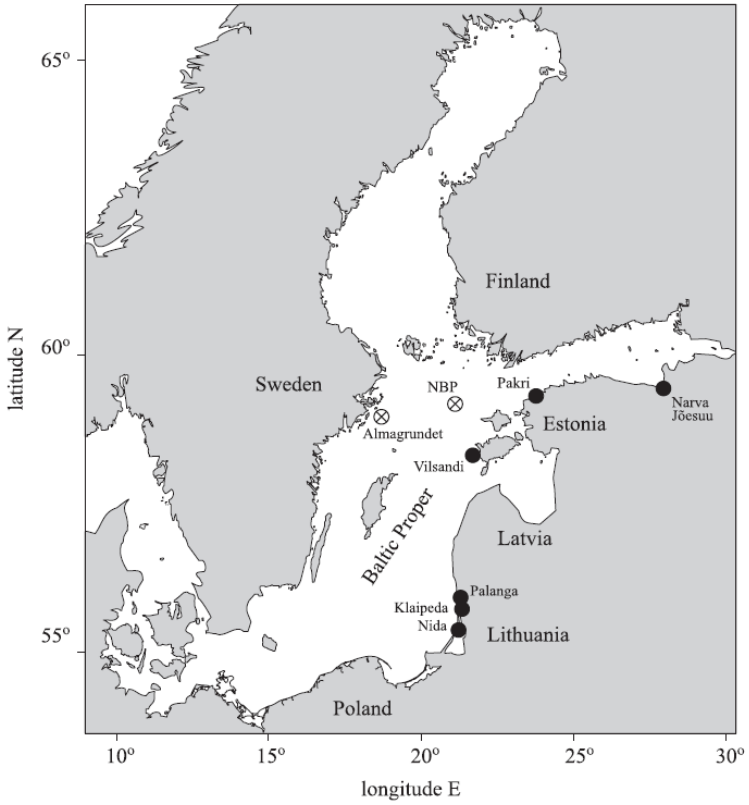

Figure 94. Locations of the long-term coastal observation sites (filled circles) and instrumental measurement sites (crossed circles) providing the data used in this study.

An estimate of the significant wave height HS was found from the 10th highest wave in a record on the assumption that wave heights are Rayleigh distributed. Although the minimum water depth at Almagrundetis about 15 m, the water at the measurement site was deep enough (about30 m) for most of the wave fields to follow the Rayleigh distribution of wave heights. The data from 1978–1995 reliably describes the wave properties in this region, while in the data gathered using another device in 1993–2003 the overall behaviour of the wave height is more or less adequate, but the periods are not useable. In general, the data constitute one of the most valuable data sets for the Baltic Sea because of the long temporal coverage and good resolution. Historically, the majority of wave information was obtained by means of visual observations. Ship-based observations of open sea wave properties are consistent with those shown by the instrumental records and have been extensively used for estimates of wave climate changes in the open ocean.

Visual wave observations from coastal sites have been less frequently used for wave climate studies. Such data pose intrinsic quality and interpretation problems. regular observations started in the mid-1950s at many locations on the eastern coast of the Baltic Sea and have been carried out using a unified procedure until today. Wave observations at three Lithuanian coastal sites started more than half a century ago but only

a small fraction of the diaries for 1992–2008 have been analysed in the international literature. The Palanga (55◦55'N, 21◦03'E) and Klaip˙eda (55◦42'N, 21◦07'E) observation sites are open to predominant wind directions from south-west to N-NW. At both sites, the water depth in the observation area (about 400–500 m from the coast) was 6–7 m and the observer was standing about3 m above sea level. The observation site at Nida (55◦18'N, 21◦00'E) was fully open to waves approaching only from west to N-NW. The observer stood on a turret located 7 m above sea level and observed waves about 700 m from the coastline where the water depth was 6–7 m. Visual observation sites on the coast of Estonia are located on the island of Vilsandi, on the Pakri Peninsula and at Narva-Jõesuu. Data from Vilsandi (58◦22'59''N, 21◦48'55''E) reasonably reflect the nearshore sea wave conditions for the predominant wind directions (south-west and N-NW) in the northern Baltic Proper and are available for 1954–2008. This site provides inadequate data for easterly winds. Waves were observed from the coast or a small pier at a distance of 200–300 m from the coast in an area, which was about 3–5 m deep. All the listed coastal sites only conditionally represent open sea conditions. The sheltering effect of the shoreline and the relatively small water depth may at times significantly alter the local wave properties compared to those in the open sea due to the shoaling, breaking and refraction of the waves. The potential distortions obviously affect the results of single observations (for example, they generally lead to a certain underestimation of wave heights) but apparently do not significantly alter the qualitative features of the overall wave statistics and evidently do not impact on the nature of long-term variations and trends in wave properties. The observer noted the five highest waves during a 5-min time interval. Both the mean height Hof these five waves and the highest single wave H_{max} were filed until about 1990. The mean wave height is normally used in the analysis; when it was missing, it was substituted by the maximum wave height. The visually observed wave height is usually a good representation of the significant wave height, whereas the estimated wave period is a few tenths of a second shorter than the peak period. The wave direction was determined in the 8-rhumb system as the approach direction of the largest wave components. The quality of the WAM wave hind cast was checked against measured and observed wave statistics using three wind data sets. MESAN wind developed by the SMHI presents hourly gridded wind information with a spatial and temporal resolution of 22 × 22 km and 3 hours, respectively. It accounts to some extent for local wind variations in rough landscapes and coastal areas. Owing to the short temporal coverage, this data was not suitable for climatological studies and was only used in model verification runs. The wave properties were calculated over several windy weeks in 2001 and 2005 using recently reanalysed wind fields developed by the European Centre for Medium-Range Weather Forecasts (ECMWF).

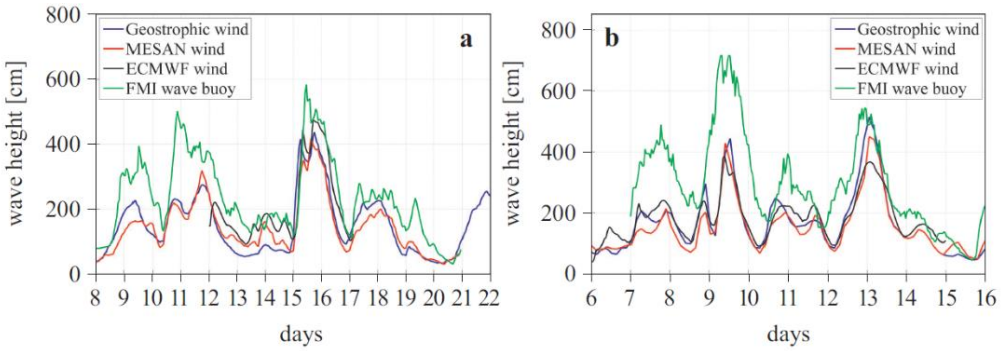

Figure 95. Measured and modelled wave heights in the northern Baltic Proper in November 2001 (left).

The overall courses of the significant wave heights simulated with the use of these winds match each other well, but none of the forcings led to a clearly better reproduction of measured wave heights (Figure 95). A typical feature of all model runs is that several storms are almost perfectly reproduced, whereas for others the model almost totally fails. The largest mismatch occurred during certain extreme wave events. For example, all the models underestimated the extreme wave events on 7–9.01.2005 by two to three metres.

Long-term wave measurements and observations:

Weekly variations in observed wave heights. The observed data sets contain several gaps for different reasons. These gaps are distributed unevenly over the years. Therefore, their presence may affect the estimated course of seasonal and even interannual variations in the wave properties. In order to suppress their influence made an attempt to replace the missing observations by the relevant climatological mean values for wave heights for single calendar days 1. These values, calculated for each calendar day over 55 years at Vilsandi and Narva-J˜oesuu and over 31 years at Pakri, course of seasonal and even interannual variations in the wave properties. In order to suppress their influence, Soomere et al. (2011) made an attempt to replace the missing observations by the relevant climatological mean values for wave heights for single calendar days. These values, calculated for each calendar day over 55 years at Vilsandi and Narva-J˜oesuu and over 31 years at Pakri, contain some noise, the level of which is the largest for the season with a relatively small number of measurements (Figure 96). The resulting values show several interesting variations in wave intensity in weekly scales, a part of which are synchronous at all three sites.

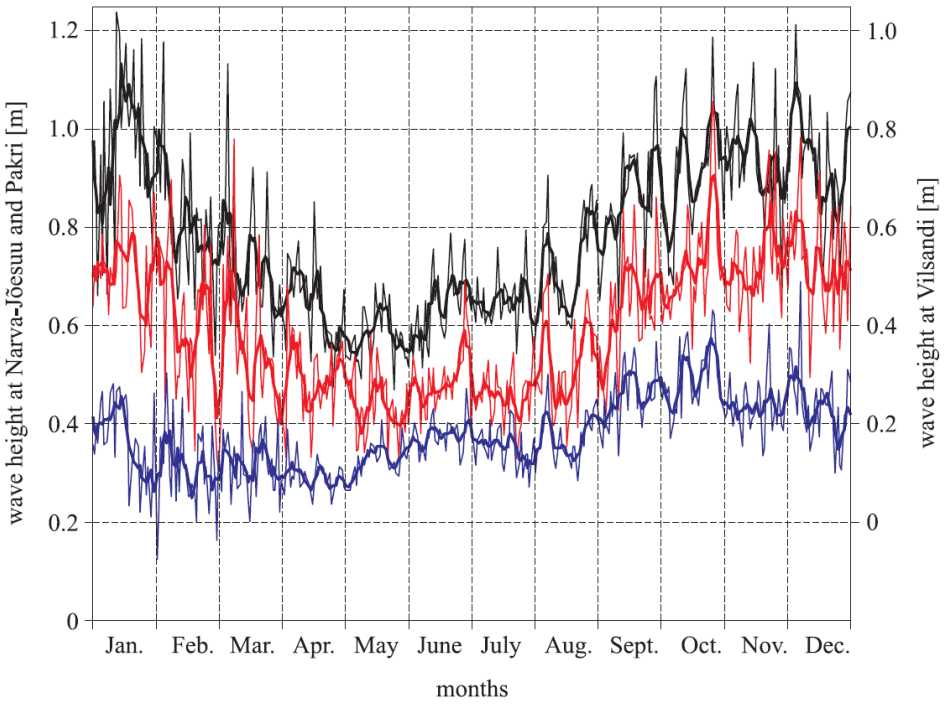

Figure 96. Climatological mean wave height at Vilsandi (black, scale at the right- hand side shifted by 0.2 m), Pakri (red) and Narva-Jõesuu (blue) over all available wave observations (thin line) and its 5-day running average (bold). Data from February 29 are merged with data from March.

Seasonal variations in observed, measured and simulated wave heights:

The presence of a strong seasonal course in the wave heights in the entire Baltic Sea region is a well-known feature that stems from the similar course in the wind speed. The seasonal cycle basically follows the annual variation in the wind speed in the northern Baltic Proper, which obviously mirrors the analogous cycle in cyclone generation over the North Atlantic. For the available data from contemporary wave measurement sites it is the strongest at Bogsk¨ar where, for example, the probability for significant wave height to exceed 1 m varies from about 90% in November to about 10% in May. It is also quite strong at Almagrundet (Figure 97), where the mean wave heights in the roughest and in the calmest months differ 2.2–2.6 times.

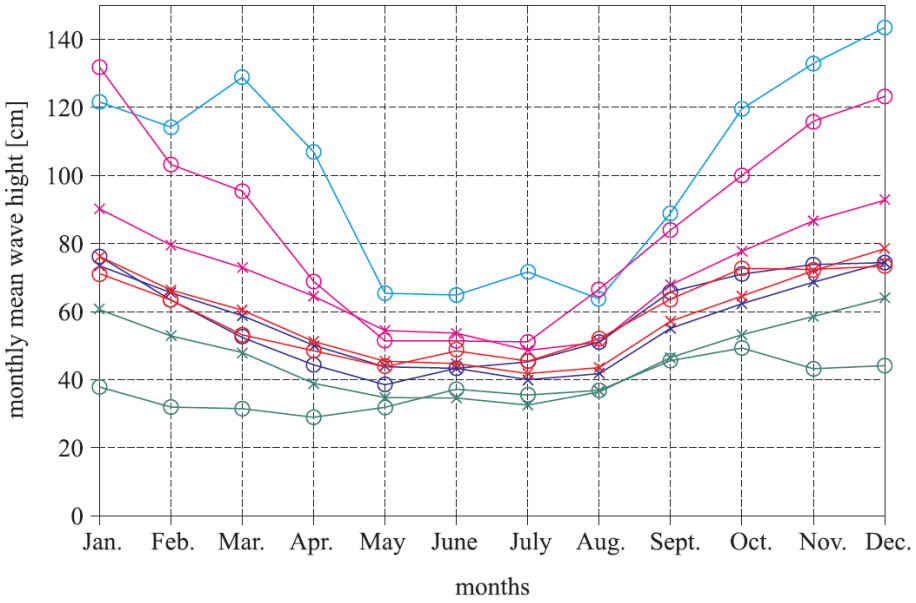

Figure 97. Seasonal variation in the monthly mean wave height at Vilsandi (blue), Pakri (red), Narva-J˜oesuu (green) and Almagrundet (magenta 1978–1995, cyan 1993–2003). Circles – observations and measurements; crosses – WAM model.

The seasonal course is somewhat less pronounced at coastal sites (Figure 97). The monthly mean wave height varies at Vilsandi from about 0.38 m during summer to about 0.75 m in winter. The highest wave activity occurs in January, and waves are almost as high from October to December. The calmest months are the spring and summer months from March to August, with a well-defined minimum in April or May. The seasonal variation at Pakri almost exactly coincides with that at Vilsandi. There is a less pronounced annual cycle in wave activity at Narva-Jõesuu (Figure 97). Variations in the annual mean wave height at Pakri are the most similar to those at Vilsandi except for the first three years of visual observations (1954–1956). The wave heights may have been overestimated at Vilsandi during the very first years of observations; however, there is some evidence that storminess was quite high in the Baltic Proper during these years. The similar variations at Narva-J˜oesuu completely follow those at Pakri for 1954–1985. In other words, the short-term (1–3) year interannual variability in the wave intensity seems to have the same pattern over a large region from the southern Baltic Proper up to the eastern part of the Gulf of Finland from the mid-1950s until the mid-1980s. This coherence is completely lost in the mid-1980s, but subsequently, both wave height trends and details of interannual variations in the wave intensity are different at Vilsandi and at Narva-Jõesuu (Figure 98). Moreover, in contrast to the period before the 1980s, years with relatively high wave intensity at Vilsandi correspond to relatively calm years in Narva Bay and vice versa. The similarity of short- term interannual variations, however, can still be tracked in the northern Baltic Proper until the end of the wave data series at Almagrundet (2003) and to a limited extent to the south-eastern sector of the Baltic Sea until 2008.

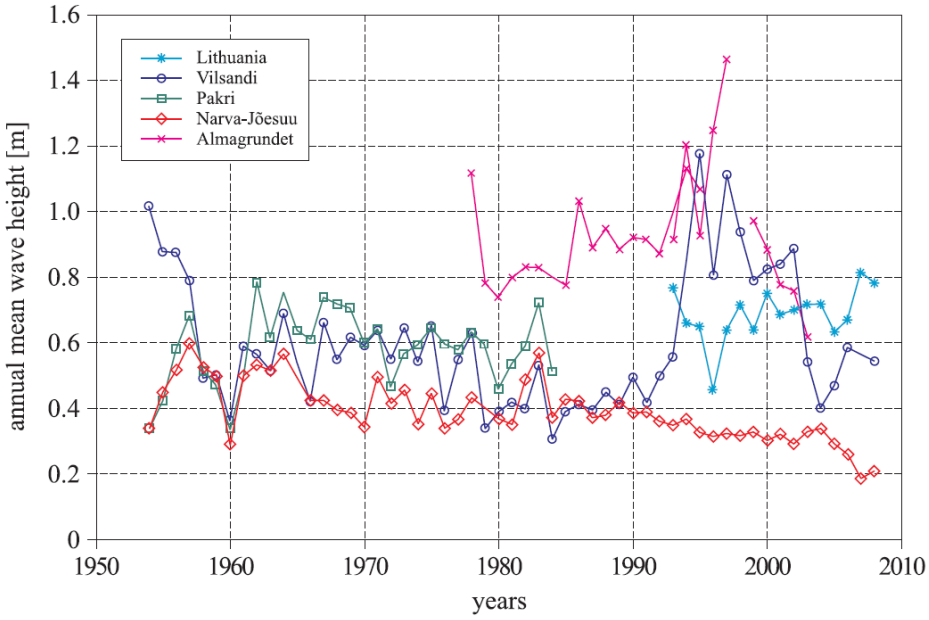

Figure 98. Long-term variations in wave heights at Vilsandi, Pakri, Narva-Jõesuu and Almagrundet and the average over Lithuanian sites.

The short-term interannual variations in the temporal course of the annual mean wave heights calculated from climatologically corrected data sets of visual observations are almost identical to those in Figure 98. The climatological correction of observed wave data leads to a substantial increase in the correlation between simulated and observed annual mean wave heights, in particular, for years of coherent observed and simulated interannual changes. The case of the Gulf of Finland: no changes in averages, large variations in extremes. The gulf is the second largest sub-basin of the Baltic Sea, extending from the Baltic Proper to the mouth of the River Neva (Figure 99). It is an example of an elongated water body (length about 400 km, width from 48 to 135 km) oriented obliquely with respect to predominant wind directions.

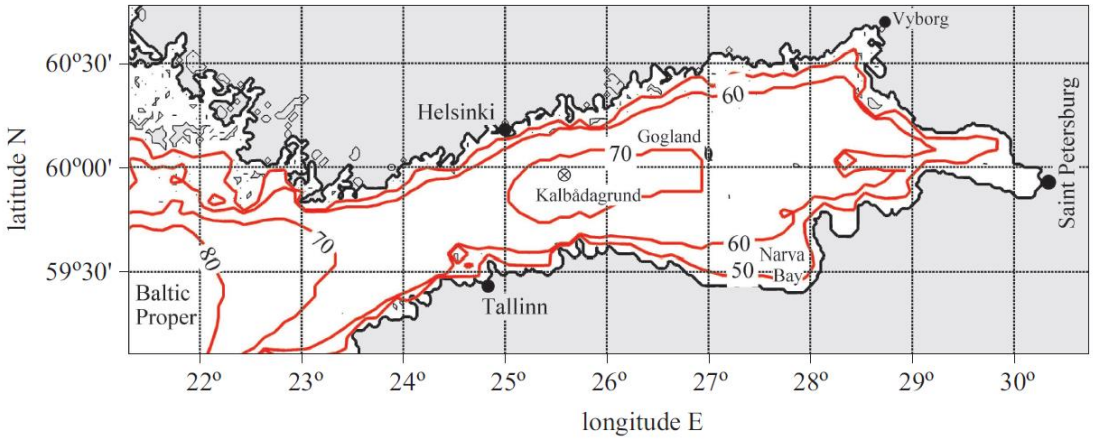

Figure 99. Spatial distribution of the long-term average of the modelled significant wave height [cm] in the Gulf of Finland (adapted from Soomere et al. 2010).

Both long-term average and maximum wave heights in the gulf are about half those in the Baltic Proper, whereas the wave periods in typical conditions are almost the same as in the Baltic Proper.

Discussion and conclusions:

A key message from these results is that the extension of spatial patterns of wave climate changes is substantially different for phenomena at different scales. While interannual variations in wave heights are correlated well over distances > 500 km during about a half-century, the decadal variations embrace much smaller areas and are of a different nature at distances exceeding 200–300 km. The spatial pattern of changes to the average and extreme wave heights signifies that open sea areas as small as about 100×200 km may host changes of a completely different nature. An amazing design feature of the existing wave observation and measurement network in the Baltic Sea is that virtually all the information comes from areas where average and extreme wave heights have hardly changed. Although the relevant spatial distribution of changes is currently based exclusively on numerical hindcast, a number of matches of the simulation results and observed and measured data at selected locations suggests that the major features of the spatial patterns discussed reflect real changes to the sea state statistics. The reason for the changes described may be connected with the gradual changes to the directional structure of predominant winds in the areas adjacent to the Gulf of Finland: namely, during the last 40 years, there has been a significant increase in the frequency of south-westerly winds and a decrease in southerly and easterly winds all over Estonia. Such a change may be responsible for a large part of the increase in the maximum wave heights in the downwind part of the Gulf of Finland, as it leads to a systematic increase in the fetch length typical of the northern part of the basin.

19.3 Equations of motion

19.3.1 Quick Strip Theory Calculations in Ship Design

This paper describes a strip theory-based calculation method for ship design purposes, which delivers information on ship motions and added resistance within a very short computation time.

For ship design purposes information on seakeeping is required. Model experiments are expensive, time consuming and not practical. Numerical methods like strip theories can be used instead for seakeeping analysis.

Computational method described in this paper uses database which contains all required information on two-dimensional potential hydrodynamic coefficients in the sway, heave, and roll mode for a very wide range of mono-hull cross-sections. For the determination of these two-dimensional coefficients of ship-like cross-sections, these sections are conformally mapped to the unit circle by the so-called two parameter Lewis transformation. Method two parameters are represented by half the breadth to draught ratio and the area coefficient of the cross-section.

The hydrodynamic potential coefficients of cross sections of any monohull ship can be found by an interpolation in this database. According to the strip theory, the total hydrodynamic coefficients for the ship can be found easily by integrating the sectional values over the ship length.

Using this computational method ship motion calculations have been carried for container ship, crude oil tanker, trawler, and other transformed container ships.

In all sea states a good agreement has been found. Some small deviations in high seas are caused by using a Lewis hull form instead of the actual hull form, when calculating the sectional Froude-Krylov loads and equivalent orbital accelerations.

Based on method validations, it is expected that this simple calculation method can be used safely for conventional mono-hull ships. However, a few restrictions must be made:

- high-speed vessels, full-bodied ships, bulbous bows give less accurate results.
- because of using a linear theory large motions in extreme sea conditions are less accurate.
- shape of the cross-section is defined with two parameters, different shapes can have same parameters.
- static and dynamical swell-up is not accounted for.
- method of estimating the viscous roll damping is not suitable for all ship shapes.
- method is used for an infinite water depth; shallow water depth effects are not included.

For project ship Ondo design case computational method based on strip theory could be used to calculate ship motions and added resistance. This has, in fact, been done in test carried out in NAPA seakeeping manager.

19.3.2 Identification of the nonlinear ship rolling motion equation using the measured response at sea

A new robust method for the identification of the parameters has been described in the equation of rolling motion of a ship using only its measured response at sea. The random decrement equations as well as the auto- and cross-correlation equations are derived for a ship performing rolling motion in random beam waves. The linear and nonlinear parameters in the equation of motion are identified using a combination of the random decrement technique, auto- and cross-correlation functions, a linear regression algorithm, and a neural networks technique. The combination of the classical parametric identification techniques and a

neural networks technique provides robust results and does not require a large amount of computational time. The stability of a ship in realistic sea is mainly dependent on its rolling motion, which is the most critical factor in defining ship survivability. In fact, most available approaches for the assessment of ships' survivability in a seaway are based on the study of rolling motion.

Two approaches are used in this assessment: a static approach (quasi-static) and a dynamic one. The former is based on the minimum value that the metacentric height, GM, should have and the shape of the static stability curve (GZ–h). This approach is still being applied in the assessment of ship's stability criterion. The latter approach is based on the analysis of the stability of the equation of the rolling motion. This involves constructing a model for a ship rolling in a realistic sea. The linear restoring parameters can be easily obtained from ship hydrostatics; however, the damping parameters are not. Therefore, the main objective of this paper is to develop a reliable and robust method that can be used in the identification of the parameters involved in the equation describing the roll motion of a ship in a random sea using only its measured random response. The identification method is based on the derivation of the random decrement equations and the auto-correlation functions for the rolling motion.

Random decrement equations:

The random decrement technique is an averaging technique that has been used successfully in the on-line failure detection and damping identification of linear structures. A forced second order differential equation is a reasonable model for a ship performing rolling motion in random seas. The main parameters of this model are the virtual moment of inertia, the damping moment, the restoring moment, and the exciting moment. This equation can be normalized with respect to the virtual moment of inertia. The equation describing the rolling motion of a ship excited by random beam waves can be written as

$$\ddot{\Phi} + N(\dot{\Phi}) + D(\Phi) = K(t) \tag{1}$$

Where Φ is the roll angle, N(Φ) and D(Φ) are the nonlinear damping and restoring moments per unit virtual moment of inertia of the ship, and K(t) is the wave exciting moment per unit virtual moment of inertia of the ship. A dot over the variable denotes the differentiation with respect to time. Using the following change of variables:

$$y_1 = \Phi \tag{3}$$
$$y_2 = \dot{\Phi}$$

Eq. (1) can be easily replaced by two first order differential equations as shown in Eq. (4)

$$\dot{Y} = F(Y) + E(t) \tag{4}$$

where:

$$\dot{Y} = [y_1 \ y_2]^{\mathrm{T}}$$
$$F(Y) = [y_2 - N(y_2) - D(y_1)]^{\mathrm{T}}$$
$$E(t) = [0 \ K(t)]^{\mathrm{T}} \tag{5}$$

Assuming that the process Y(t) is a Markov process, the Fokker–Planck equation can be used to describe the conditional probability density function for the random process:

$$\frac{\partial P}{\partial t} = -\frac{\partial}{\partial y_1}(y_2 P) + \frac{\partial}{\partial y_2}([N(y_2) + D(y_1)]P) + \frac{1}{2}\frac{\partial^2}{\partial y_2^2}(\Psi_2 P) \tag{6}$$

Where Φ_2 is the variance of the exciting function *K(t)* and can be calculated if *K(t)* is measurable:

$$\Psi_2 = E[K(t) \ K(t)] \tag{7}$$

Where E […] denotes the expected value. The solution of Eq. (5) subject to the initial condition

$$P(Y, t|Y_{\mathrm{o}}) = \delta(y_1 - y_{1\mathrm{o}})\delta(y_2 - y_{2\mathrm{o}}) \tag{8}$$

Yields the conditional probability density function which describes the Markov process Y(t) completely. Where y_{io}, i=1, 2 are the initial conditions for the roll displacement and the roll rate, respectively. Multiplying Eq. (5) by the variables $y_1(t)$ and $y_2(t)$, respectively, and integrating the whole equations over the range of the two variables, the propagation of the expected values of $y_1(t)$ and $y_2(t)$ can be obtained as:

$$\dot{\mu}_1 = \mu_2$$
$$\dot{\mu}_2 = -E[N(y_2) + D(y_1)] \tag{9}$$

$$\mu_1 = \int\int y_1 P(Y, t) \ \mathrm{d}y_1 \ \mathrm{d}y_2$$
$$\mu_2 = \int\int y_2 P(Y, t) \ \mathrm{d}y_1 \ \mathrm{d}y_2 \tag{10}$$

The evaluation of the averages on the right-hand side of Eq. (9) poses a problem since the probability density function P(Y, t), for the Markov process Y(t), is yet to be determined. Replacing these averages by their Taylor series expansion about μ_1 and μ_2 solves this problem. The damping moment, $N(y_2)$, can be expressed as the sum of two terms: a linear term in the roll rate and a nonlinear term.

$$N(y_2) = 2\zeta\omega_\phi[1 + \varepsilon_1 y_2^2]y_2$$
$$D(y_1) = \omega_\phi^2[1 + \varepsilon_2 y_1^2]y_1 \tag{11}$$

Where ζ_1, ε_1 and ε_2 are the nondimensional linear damping coefficient, the nonlinear damping coefficient, and the nonlinear restoring moment coefficient, respectively, ε_φ is the linear natural frequency. Using Eqs. (10) and (11), the nonlinear damping and restoring moments in Eq. (4) can be written in the following form:

$$N(y_2) + D(y_1) = 2\zeta\omega_\phi y_2 + \omega_\phi^2 y_1 + F(y_1, y_2) \tag{13}$$

$$F(y_1, y_2) = 2\zeta\omega_\phi \varepsilon_1 y_2^3 + \omega_\phi^2 \varepsilon_2 y_1^3 \tag{14}$$

$$E[N(y_2) + D(y_1)] = 2\zeta\omega_\phi \mu_2 + \omega_\phi^2 \mu_1 + \bar{F}(y_1, y_2) \tag{15}$$

$$\bar{F}(y_1, y_2) = 2\zeta\omega_\phi \varepsilon_1 E[y_2^3] + \omega_\phi^2 \varepsilon_2 E[y_1^3] \tag{16}$$

Eq. (16) represents the lamped nonlinear terms of the damping and restoring moments. Eqs. (6) and (7) are combined as:

$$\ddot{\mu}_1 + 2\zeta\omega_\phi \dot{\mu}_1 + \omega_\phi^2 \mu_1 + \bar{F}(y_1, y_2) = 0 \tag{17}$$

It is obvious that the approximate equation describing the expected value of the roll response, μ_1 satisfies the differential equation, which describes the free rolling motion of a ship. The linear terms and the nonlinear function, F (1, 2), in Eq. (17) are identified in the following two sections, respectively.

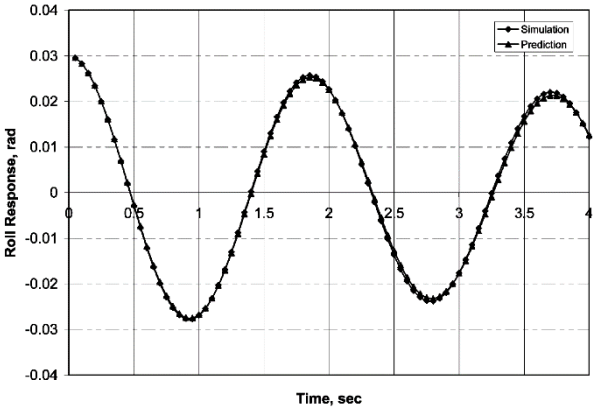

Figure 100. Comparison between the simulated and the predicted free response (light damping).

The results for the lightly damped motion case are shown in Figure 100. This figure shows a comparison between the generated free roll response and the predicted one. Figure 101 show similar results for the heavy damping motions. The agreement between the generated and the predicted free roll response for the light damping case is excellent; however, and for the heavy damping motions, it is good.

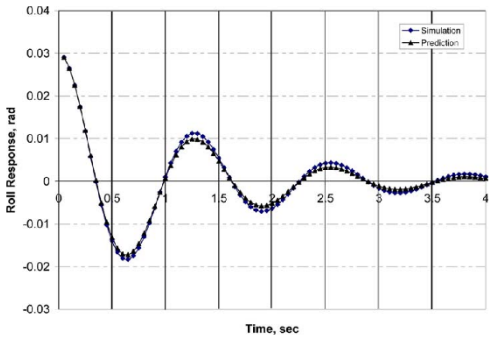

Figure 101. Comparison between the simulated and the predicted free response (heavy damping).

Experimental data have been obtained by testing a Series 60 Model in the towing tank of Memorial University. Table 8 shows the main particulars of the model. JONSWAP wave spectrum with different significant wave heights and different modal frequencies was used as an exciting moment in the tank. Three main runs were used to validate the proposed method with each being carried out twice. For the first two runs JONSWAP spectra were taken with constant wave modal frequency of 0.5 Hz and with two significant wave heights of 4 and 6 cm, respectively. In addition, calm water experiments have been carried out to measure the free roll motion response (A0005) for the model. This has been conducted by giving the model an initial angle of heel. After the model is initially inclined, it is then released, and the free rolling response is measured. The random and free roll motion responses are measured using the available data acquisition system at the wave tank.

Table 8. Hydrostatic particulars for Series 60 Model (without appendages) block coefficient 0.60, and scale= 1:40.

Length between perpendiculars	3.0480 m
Length on water line	3.0920 m
Waterline beam at midships	0.4065 m
Draught at midships	0.1625 m
Draught at maximum section	0.1625 m
Maximum draught	0.1625 m
Draught above the keel	0.1625 m
Maximum section forward of midships	0.0380 m
Area of midships section	0.1295 m^2
Longitudinal center of buoyancy	+0.0455 m
Vertical center of buoyancy above datum (KB)	0.0870 m
Wetted surface area	1.5924 m^2
Volume of displacement	0.1206 m^3
Displacement in fresh water	120.45 kg
Longitudinal center of floatation (LCF)	+0.1155 m
Area of waterline plane	0.8768 m^2
Transverse metacentric radius (BM)	0.0767 m

Conclusions

It has been shown from the experimental results that the effect of varying a significant wave height on the agreement between the random decrement, auto-correlation, and free response signatures is not significant. However, varying the wave modal frequency may cause a considerable effect on that agreement. In addition, the proposed method highlights that the estimated nonlinear parameters of damping and restoring moments in the rolling equation are no longer to be closed to the actual ones. The accuracy of the proposed method

has been tested using numerical generated data and has been validated using experimental data. The proposed method is shown as an accurate method in the identification of the parameters involved in the equation describing the rolling motion of a ship in a realistic sea using only the measured response at sea.

Approximate theoretical basis for estimating the free nonlinear roll response of a ship from its steady state response in random waves has been investigated. It has been proven that the free response for the nonlinear rolling motion can be obtained using the proposed method as well as from either the propagation of the expected value of the rolling motion response in a random sea, or from the calculation of the auto-correlation function of the steady state random rolling response. In all cases the measurement of the wave excitation is not required. The linear and nonlinear damping and restoring moments parameters predicted using the proposed method seem to be more accurate since a good agreement between the predicted free response and the measured one is excellent. The error in the damped natural frequency of rolling motion predicted using the proposed method is less than 1%.

The procedure shown in this article, could be applied to the analysis of seakeeping for Ondo. For instance, instead of making a simplified analysis as presented in 10 for the equations of motion, the analysis could be extended to take into account non-linearities in the equations of motion. This would mean that the simple harmonic functions would not be considered and the equations of motion that we would deal with would be of much higher difficulty. For a more thorough analysis, some insights from this article could be used to develop Ondo's behaviour in waves further into detail.

19.3.3 A Non-Linear Mathematical Model of Higher Order for Strong Parametric Resonance of the Roll Motion of Ships in Waves

Non-linear equations of ship motions in waves describing the couplings between heaves. roll and pitch are investigated. A third order mathematical model is introduced aimed at describing strong parametric excitation associated with cyclic changes in the ship restoring characteristics. A derivative model is employed to describe the coupled restoring actions up to third order. Non-linear coupling coefficients are derived in terms of hull form characteristics. Experimental results corresponding to excessive motions of a transom stern fishing vessel in head seas are compared to numerical simulations obtained from the derived third order non-linear mathematical model. It is shown that this enhanced model gives good results and a better comparison with the experiments than a second order model.

Much of such attention has been devoted to the configuration of longitudinal regular waves, either with or without speed, bow or stern waves. Roll motion has usually been modelled as an uncoupled Mathieu type equation.

Equations of motion:

Two right-handed coordinate systems are employed to describe the motions. An inertial reference frame (C, x, y, z) is assumed to be fixed at the mean ship motion, defined by the ship speed U. Regular waves are assumed to travel forming an angle X with ship course. Another reference frame (O, x, y, z) is fixed at the xy ship having the plane coinciding, for the ship at rest, with the undisturbed sea surface, z -axis passing through the vertical that contains the centre of gravity. The two systems coincide when excitations are absent. This is shown in Figure 102.

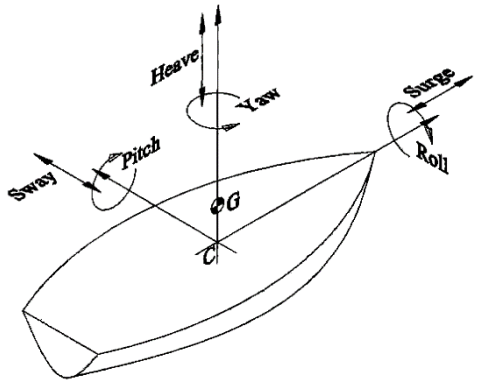

Figure 102. Coordinate axis and definition of motions.

Non-linear equations of motion considering the three restoring degrees of freedom may be expressed in matrix form using a displacement vector:

$$\vec{s}(t) = [\, z(t) \;\; \phi(t) \;\; \theta(t) \,]^T \tag{1}$$

defining the heave translational mode together with the roll and pitch angular modes.

$$(\tilde{M} + \tilde{A})\ddot{\vec{s}} + \tilde{B}(\dot{\phi})\dot{\vec{s}} + \vec{C}_{res}(z, \phi, \theta, \zeta) = \vec{C}_{exc}(\zeta, \dot{\zeta}, \ddot{\zeta}) = \vec{Q}_w(\chi, A_w, \omega_e, t) \tag{2}$$

Hull inertia M is a diagonal 3x3 matrix. Its elements are: m, the ship mass, J_{xx}, J_{yy} the mass moments of inertia in the roll and pitch modes, respectively, taken with reference to centre O. Elements in matrix A represent hydrodynamic generalized added masses. Elements in matrix A represent hydrodynamic generalized added masses. Damping terms B_Φ may incorporate non-linear terms in the roll equation and describe hydrodynamic reactions dependent on ship velocities. The hydrodynamic inertia and damping matrices are expressed respectively, as:

$$\tilde{A} = \begin{bmatrix} Z_{\ddot{z}} & 0 & Z_{\ddot{\theta}} \\ 0 & K_{\ddot{\phi}} & 0 \\ M_{\ddot{z}} & 0 & M_{\ddot{\theta}} \end{bmatrix} \quad ; \quad \tilde{B} = \begin{bmatrix} Z_{\dot{z}} & 0 & Z_{\dot{\theta}} \\ 0 & K_{\dot{\phi}}(\dot{\phi}) & 0 \\ M_{\dot{z}} & 0 & M_{\dot{\theta}} \end{bmatrix} \tag{3}$$

Vector $C_{max}(z, \phi, \zeta, \theta)$ describes non-linear restoring forces and moments dependent on the relative motions between ship hull and wave elevation ζ (t). Wave elevation, according to the Airy linear theory, is defined as:

$$\zeta(x, y, t; \chi) = A_w Cos[kxCos(\chi) + kySen(\chi) - \omega_e t] \tag{4}$$

In longitudinal waves, head seas, the equation of wave surface elevation is:

$$\zeta(x, t) = A_w Cos[kx + \omega_e t] \tag{5}$$

On the right-hand side of equation (2), generalized vector Q_w represents wave external excitation, usually referred to in the literature as the Froude-Krilov plus diffraction wave force terms, dependent on wave heading χ. encounter frequency ω, wave amplitude A_w and time t:

$$\vec{Q}_W(t) = \begin{bmatrix} Z_W(t) \\ K_W(t) \\ M_W(t) \end{bmatrix} \tag{6}$$

$$\begin{aligned} Z_w(t) &= Z_{w0} Cos(\omega_e t + \alpha_{w3}) \\ K_w(t) &= 0 \\ M_w(t) &= M_{w0} Cos(\omega_e t + \alpha_{w5}) \end{aligned} \tag{7}$$

where Z_{wo}, and M_{wo} are the amplitudes of force and moment in the heave and pitch modes, respectively; and $\alpha_{\omega 3}$, and $\alpha_{\omega 5}$, are the corresponding phase differences with respect to wave passage.

Heave and pitch motions:

In head seas, the heave and pitch motions are very important in favouring the occurrence of roll parametric amplification. For small wave amplitudes, these motions are typically linear. Yet, for larger waves, these motions may lose this character, and asymmetries may be noticed and become remarkable. Figure 103 shows simulations of the heave and pitch motions for the considered ship in head seas, F_n = 0.11, wave amplitude A_w = 0.5m. Results from the third order model are plotted against the linear response. It is observed that both third order heave and pitch motions are comparable to the linear displacements. In Figure 104 the same curves are given for the same speed and encounter frequency, but for a higher wave, Aw = 1.0 m. Now, some asymmetries are observed in the responses of both modes, making it dear that the heave and pitch motions are not linear anymore. This result points out to the fact that the exchange of energy between the vertical modes and the roll motion, which is an essential aspect of the dynamics of parametric resonance in head seas, must be described as a set of coupled equations, if all the complexities of excessive motions are to be taken into consideration.

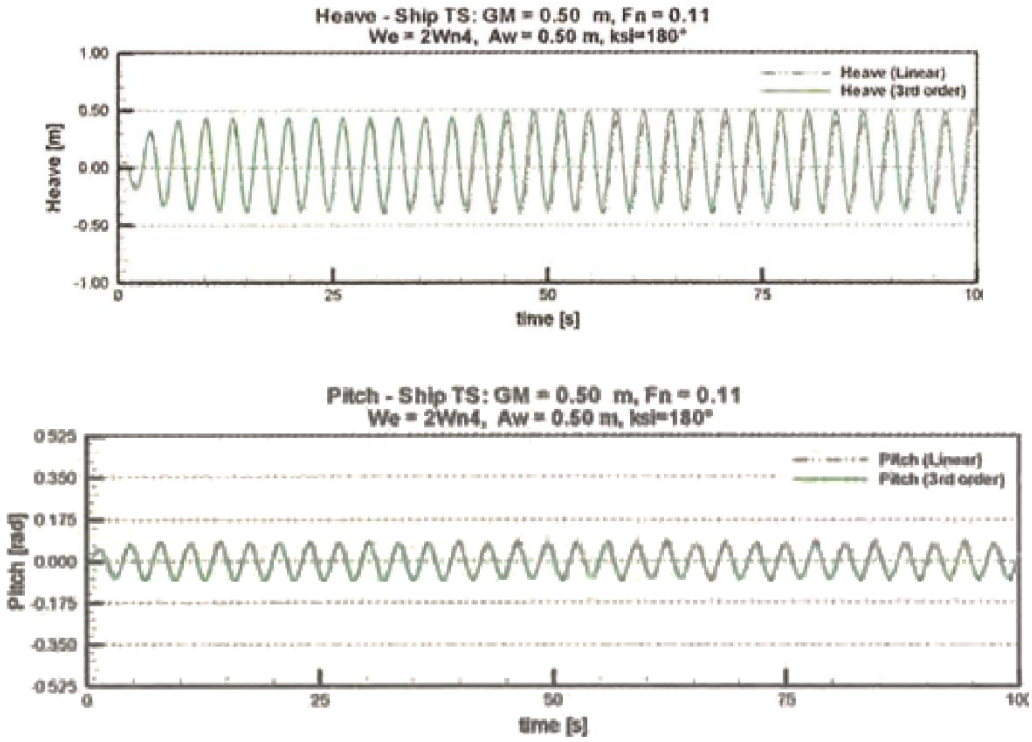

Figure 103. Linear and non-linear responses in heave and pitch.

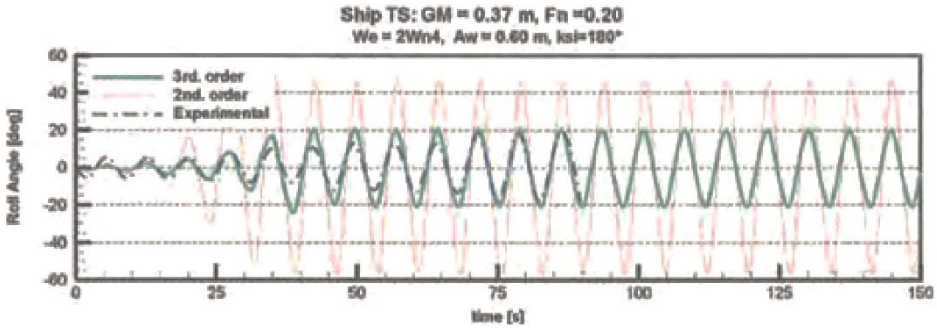

Figure 104. Experimental, Linear and non-linear responses of roll motion.

Discussion and conclusions

A detailed mathematical model was introduced, in which the heave, roll and pitch motions and wave passage effects were described with terms up to the third order. Analytical derivation of all the coupling coefficients due to heave, roll and pitch, and wave passage has been developed. The derivation is structured such that all coupling coefficients are expressed in terms of hull-wave characteristics. This may be recognized as relevant from the point of view of understanding the non-linear responses. It is shown that, depending on the level of excitation, the heave and pitch motions may display asymmetries. The appearance of these non-linear effects is indicative of the importance of taking the ship motions in a coupled way, whenever strong

parametric excitation may occur. Roll amplifications for low metacentre height tended to be strong. In these cases, the 3rd order numerical simulations based on the proposed model give quite good comparisons with the experimental results. In the tested conditions with high metacentre height the roll amplification is not excessive. Second and third order models do not give very distinct responses.

Just as in the previous article, in this one a model considering non-linearities is looked at. This is once again showing an improvement that could be done to the analysis made in section 10 by not making some implications explained in section 9, such as linearity, superposition of motions and uncoupling of equations of motion. This article showed the importance of considering the equations of motion in a coupled form so this would be an improvement to be done when doing a more in-depth analysis.

19.4 Motions and loads

19.4.1 A comprehensive study on ship motion and load responses in short-crested irregular waves

Wave-induced ship motion and load responses are usually investigated on the assumption that the incident waves are long-crested. The realistic sea waves are however short-crested irregular waves. Real practice reveals that the ship motion and load responses induced by short-crested waves are different from those induced by long-crested waves. This paper aims to conduct a comprehensive study on ship motions and loads in different wave-fields. For this purpose, comparative studies by small-scale model towing tank test and large-scale model sea trial are conducted to experimentally identify the difference between ship motions and loads in long-crested and short-crested irregular waves. Moreover, the influences of directional spreading function of short-crested waves on ship motions and loads are analysed by numerical seakeeping calculation. The results and conclusions obtained from this study are of great significance for the further extrapolation and estimation of ship motions and loads in short-crested waves based on long-crested wave response results.

To date, majority of the current numerical and experimental seakeeping investigations are focus on ship motion and load responses in two-dimensional (2D) long-crested waves. As a matter of fact, the realistic ocean waves are however three-dimensional (3D) short-crested waves and they are associated with nonlinearity, randomicity and directional spreading characteristics. Therefore, accurate prediction of ship motion and load responses induced by short-crested waves is of great significance for full-scale ship design, assessment and operational guidance.

Design of two experimental models

To allow the comparative experimental investigations, two segmented models were constructed by material of Fiberglass Reinforced Plastic (FRP) at different scales of 1/50 and 1/25 according to the prototype. The

small-scale model and large-scale model were tested in 2D laboratory tank waves and in 3D real sea waves, respectively. For the comparative benchmarking investigations, model setup and sensor arrangement of the two models are designed to be the same while with different scales. A comparative overview of the two testing models is shown in below.

Figure 105. Model overview.

A 72,000 ton class ship is adopted for comparative investigation, which includes 1/50 small-scale model tank test, 1/25 large-scale. For the measurement of wave loads and hydro-elastic responses, the models are designed to be cut into seven parts of segments at the 2nd, 4th, 6th, 8th, 10th and 12th stations. Stations from 13th to 20th at the stern area are used for housing the self-propelled mechanism, which mainly includes motors, shafts, gearboxes and propellers. Steel backbone beams, which are fixed at the height of model's vertical bending neutral axis, are used to connect the segments. Wave-induced global VBM and Vertical Shearing Force (VSF) at these cut sections are measured by strain gauges mounted on the backbone surface. The VBM is measured by full-bridge circuit formed by four strain gauges, and the VSF is obtained by differencing the adjacent VBMs. Accelerometers are mounted on deck of bow, middle and stern areas to measure the vertical acceleration. The large-scale model's overall arrangement is shown below.

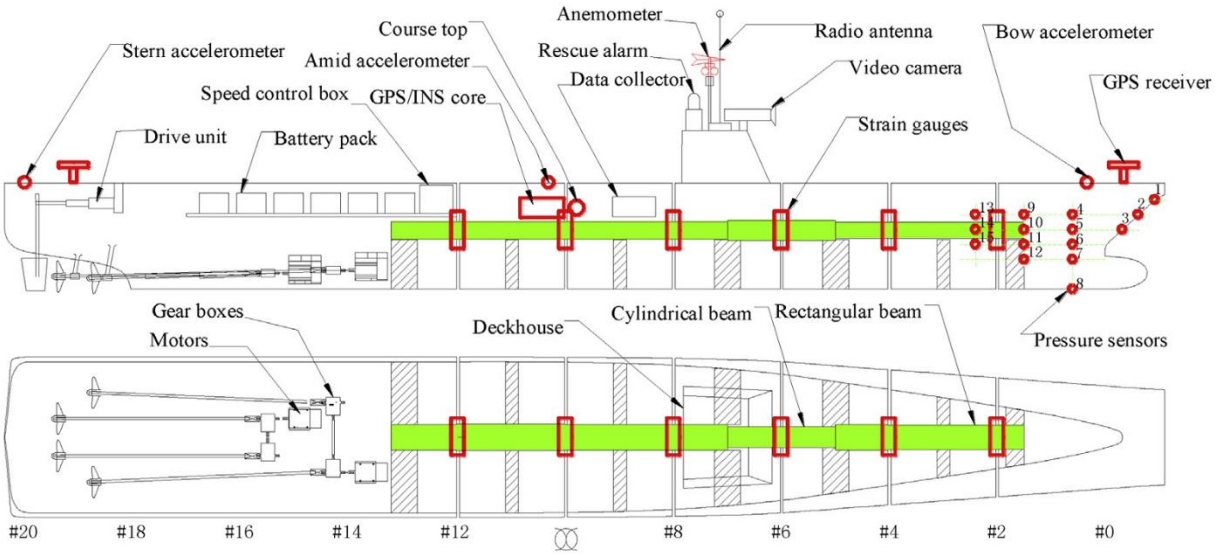

Figure 106. Large-scale segmented model arrangement.

The experimental site was selected at about 5 km away from the beach to prevent wave shoaling, reflection and diffraction effects. The experiments should be conducted at high-tide time to prevent swell waves. The sea trial measurement is conducted in different sea conditions, at different forward speeds and headings. During the experiment, the forward speed and heading angle of the large-scale model are controlled by crew on board an auxiliary yacht via radio signal. The heading angle of large-scale model is kept by an autopilot system. Meanwhile, a wave buoy is used to measure the experimental sea wave-field. A comparative view of the experimental environments and testing facilities for the two models is shown in Figure below.

(a) Small model tank test (b) Large model sea trial

Figure 107. Comparison of experimental conditions and facilities.

Given that the incident wave-fields of tank waves and sea-waves are quite different, the ship responses obtained by different models should be evaluated and compared in an improved way. Therefore, the large-scale model's vertical motion and load responses are assumed to be induced by the dominant component waves. The responses of ship induced by unit wave height for different wave conditions has been shown in the following table.

Table 9. Ship vertical responses induced by unit wave height.

Item	Extreme sea state			Design sea state		
	2D wave	3D wave	3D dominant wave	2D wave	3D wave	3D dominant wave
Pitch (°)	0.28	0.26	0.32	0.34	0.30	0.38
Heave (m)	0.36	0.38	0.47	0.40	0.44	0.56
Acceleration (m/s^2)	0.18	0.20	0.25	0.42	0.42	0.52
VBM (MN·m)	159.33	130.78	163.87	186.59	135.05	169.14
VSF (MN)	2.00	1.53	1.92	2.22	1.81	2.27

The ship motion and load responses in short-crested waves are predicted under the extreme sea state ($H_{1/3}$=15 m, T_{02}=14.5 s and U=5 knots) and design sea state ($H_{1/3}$=9m, T_{02}=12.5 s and U=18 knots). The directional wave spectrum can be expressed by the product of overall wave spectrum and directional function:

$$S_{\zeta\zeta}(\omega,\theta) = S_{\zeta}(\omega)D(\omega,\theta)$$

The hull surface governing grid is established based on the hull line information. Then the hull wetted grid, which is used for hydrodynamic calculation, is generated by means of cubic spline curve method using the

surface governing grid. The influence of mesh number on numerical simulation results is analysed in order to achieve a compromise between the calculation efficiency and accuracy. For this propose, five kinds of hull grid scheme are involved for comparative investigation. The ship responses for head waves at two typical speeds (i.e. 5 knots and 18 knots) are selected for calculation. The calculated RAOs of pitch, heave, VBM amidships and VSF at quarter ship length from FP for different mesh schemes are shown in below.

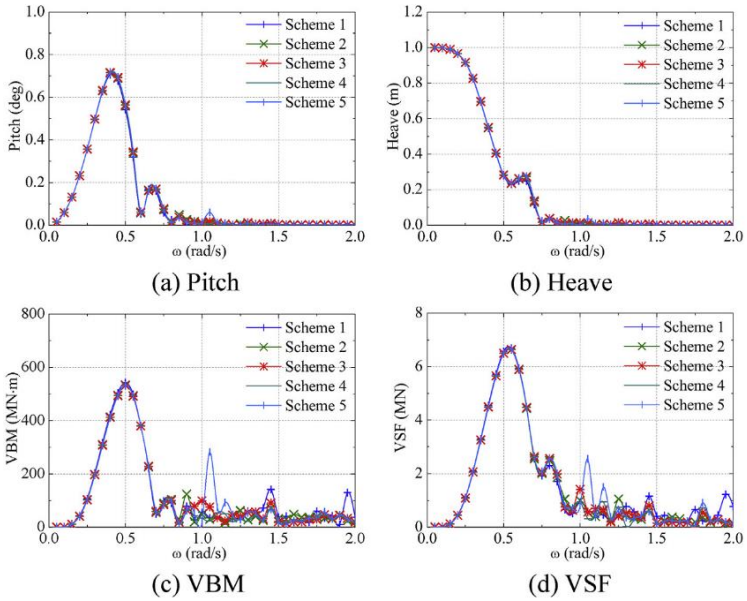

Figure 108. Comparison of calculation results at 5 knots by different meshes.

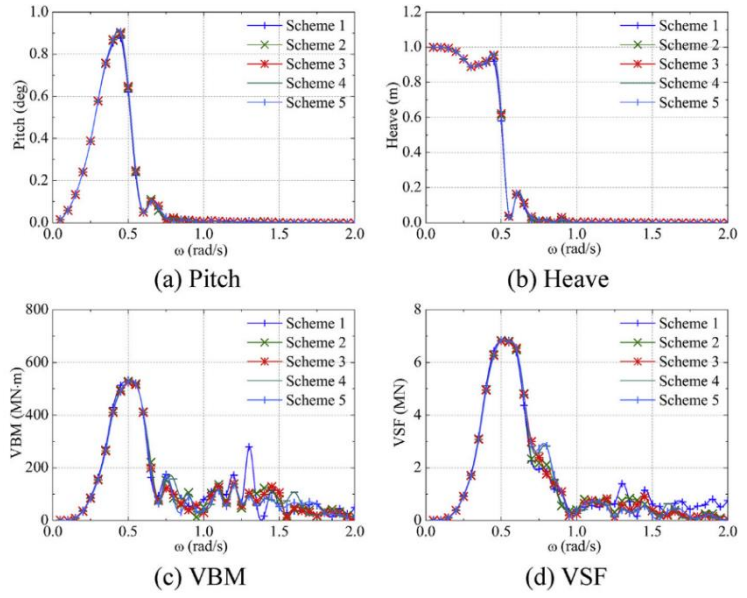

Figure 109. Comparison of calculation results at 18 knots by different meshes.

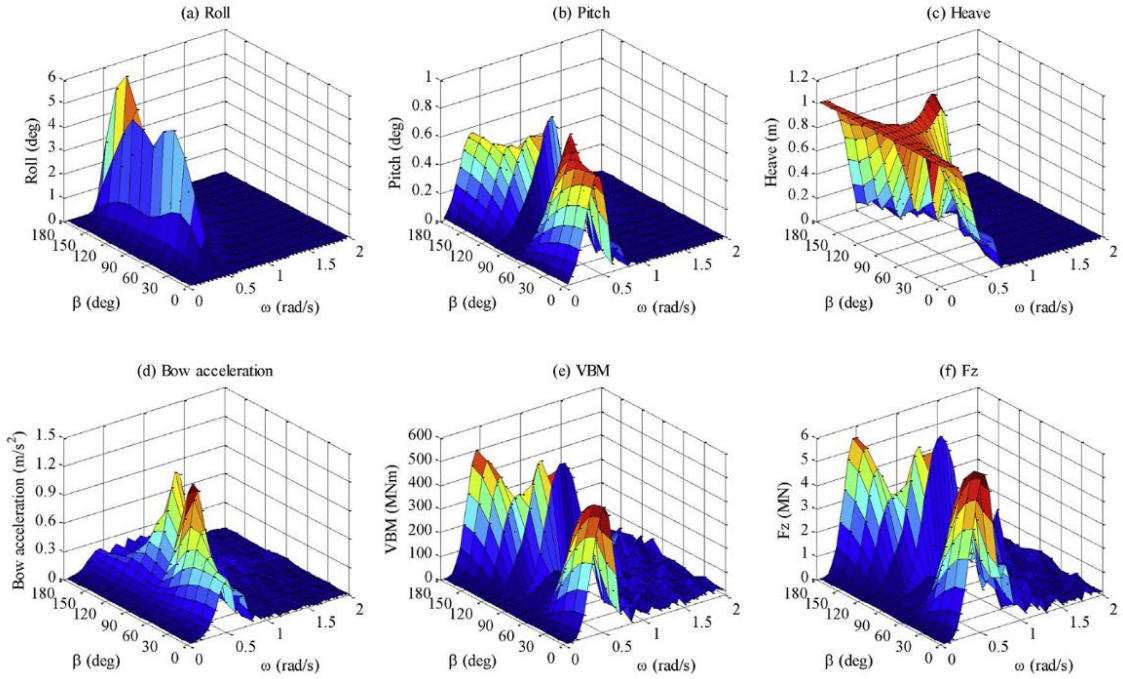

Figure 110. The motion and load RAOs for ship at forward speed 5 knots.

Discussion and conclusions

In this paper, a series of seakeeping investigations, including small-scale model tank test, large-scale model sea trial and numerical calculation, were conducted on a ship to benchmark the motion and load responses in short-crested irregular waves. Based on the work carried out in this study, the following conclusions can be drawn: (1) The comparison between the small- and large-scale model tests shows that the 2D long-crested waves over-estimate ship pitch and sectional load responses in head wave conditions compared with 3D short-crested waves; the pitch and sectional load responses of ship in 2D waves are however closer to those induced by the dominant sea waves. (2) The adopted direction spectral analysis method combined with 3D hydro-elasticity theory is capable and applicable for the estimation of ship motion and load responses in short-crested waves. Good agreement between the results by experimental measurement and theoretical calculation is also achieved. (3) The vertical motion (i.e. pitch and heave) and acceleration are not very sensitive to the varying of the directional function. The long-crested wave condition over-estimates hull sectional VBM and VSF compared with short-crested wave condition for head and following wave conditions. Moreover, the influence of directional function on ship responses differs from different wave heading conditions. The concluded co-efficient list provides useful reference for the further rapid estimation of ship motion and load responses in short-crested waves based on the long-crested wave response estimations.

In terms of relation between this article and our results obtained using the NAPA seakeeping manager, we can conclude that what we obtained seem reasonable as their appearance in terms of RAOs for the degrees

of freedom studied can somehow relate to the ones presented in Figures 39 and 40 (curves of similar shape). However, the results in the article cannot help us relate to whether the numerical results are correct. But information on other types of models are given and how these can be further implemented in Ondo's design. In addition, the importance of model tests in seakeeping is shouted out. As discussed in the lectures of the course, we cannot rely in only one source of results as this is a very wrong principle. In fact, several sources must be used, such as different softwares in combination with model tests and possibly full-scale testing if sister or similar ships have already been built and are at use at the stage that a ship is being designed. Our initiative of moving forward with two different seakeeping computations was a good step towards following this principle. BV HydroStar will be further improved during the following weeks so that at some point in time it will be possible to make reasonable comparison and verification of results coming from both analyses. For instance, by using the same input spectrum and sea state conditions it would be interesting to see how and if results differ.

19.5 Added resistance and manoeuvring

19.5.1 Practical Ship Hydrodynamics, Ship manoeuvring 151, Bertram, Volker, 2000

19.5.1.1 Seakeeping design criteria

Seakeeping of ships is investigated with respect to the following issues:

- Maximum speed in a seaway: 'involuntary' speed reduction due to added resistance in waves and 'voluntary' speed reduction to avoid excessive motions, loads etc.
- Route optimization (routing) to minimize, e.g., transport time, fuel consumption, or total cost.
- Structural design of the ship with respect to loads in seaways.
- Habitation comfort and safety of people on board: motion sickness, danger of accidental falls, man overboard.
- Ship safety: capsizing, large roll motions and accelerations, slamming, wave impact on superstructures or deck cargo, propeller racing resulting in excessive rpm for the engine.
- Operational limits for ships (e.g., for offshore supply vessels or helicopters landing on ships).

Tools to predict ship seakeeping are:

- Model tests.
- Full-scale measurements on ships at sea.

- Computations in the frequency domain: determination of the ship reactions to harmonic waves of different wave lengths and wave directions.
- Computations in the time domain (simulation in time): computation of the forces on the ship for given motions at one point in time; based on that information the computation of the motions at a following point in time etc.
- Computations in the statistical domain: computation of statistically significant seakeeping values in natural (irregular) seaways, e.g. average frequency (occurrence per time) of events such as exceeding certain limits for motions or loads in a given seaway or ocean region.

This procedure assumes (respectively requires) that the reaction of one wave on the ship is not changed by the simultaneous occurrence of another wave. This assumption is valid for small wave heights for almost all ship reactions with the exception of the added resistance. This procedure is often applied also for seaways with large waves. However, in these cases it can only give rough estimates requiring proper corrections. One consequence of the assumed independence of the individual wave reactions is that all reactions of the ship are proportional to wave height. This is called linearization with respect to wave height. The computations become considerably more expensive if this simplification is not made. Non-linear computations are usually necessary for the treatment of extreme motions (e.g. for capsizing investigations); here simulation in the time domain is the proper tool. However, for the determination of maximum loads it often suffices to apply corrections to initially linearly computed loads. The time-averaged added resistance is in good approximation proportional to the square of the wave height. Here the effect of harmonic waves of different lengths and direction can be superimposed as for the linear ship reactions.

Experimental approaches (model and full scale)

Seakeeping model tests usually employ self-propelled models in narrow towing tanks or broad, rectangular seakeeping basins. The models are sometimes completely free being kept on course by a rudder operated in remote control or by an autopilot. In other cases, some degrees of freedom are suppressed (e.g. by wires). If internal forces and moments are to be determined, the model is divided into a number of sections. The individual watertight sections are coupled to each other by gauges. These gauges consist of two rigid frames connected by rather stiff flat springs with strain gauges. Model motions are determined either directly by or by measuring the accelerations and integrating them twice in time. Waves and relative motions of ships and waves are measured using two parallel wires penetrating the water surface. The change in the voltage between the wires is then correlated to the depth of submergence in water. The accuracy of ultrasonic devices is slightly worse. The model position in the tank can be determined from the angles between ship and two or more cameras at the tank side. Either lights or reflectors on the ship give the necessary clear signal. The waves are usually created by flaps driven by hydraulical cylinders. The flaps are inclined around a

horizontal axis lying at the height of the tank bottom or even lower. Traditionally, these flaps were controlled mechanically by shaft mechanisms which created a (nearly) sinusoidal motion. Modern wavemakers are computer controlled following a prescribed time function. Sinusoidal flap motion creates harmonic waves. The superposition of many sinusoidal waves of different frequency creates irregular waves similar to natural wind seas.

In towing tanks, waves are generated usually by one flap at one tank end spanning the complete tank width. The other tank end has a 'beach' to absorb the waves (ideally completely) so that no reflected waves influence the measurements and the water comes to rest after a test as soon as possible. If several, independently controlled flaps are used over the tank width waves with propagation direction oblique to the tank longitudinal axis can be generated. These waves will then be reflected at the side walls of the tank. This is unproblematic if a superposition of many waves of different direction ('short-crested sea') is created as long as the distribution of the wave energy over the propagation direction is symmetrical to the tank longitudinal axis. In natural wind seas the energy distribution is similarly distributed around the average wind direction.

Rectangular wide seakeeping basins have typically a large number of wave-making flaps at two adjacent sides. An appropriate phase shift in the flap motions can then create oblique wave propagation. The other two sides of such a basin are then equipped with 'beaches' to absorb waves. Seakeeping model tests are usually only performed for strongly non-linear seakeeping problems which are difficult to compute. Examples are roll motion and capsizing, slamming and water on deck. Linear seakeeping problems are only measured for research purposes to supply validation data for computational methods. In these cases many different frequencies can be measured at the same time. The measured data can then be decomposed (filtered) to obtain the reactions to the individual wave frequencies.

Seakeeping tests are expensive due to the long waiting periods between tests until the water has come to rest again. The waiting periods are especially long in conventional towing tanks. Also, the scope of the experiments is usually large as many parameters need to be varied, e.g. wave length, wave height, angle of encounter, ship speed, draught and trim, metacentric height etc. Tests keep Froude similarity just as in resistance and propulsion tests. Gravity and inertia forces then correspond directly between model and full-scale ship. However, scale effects (errors due to the model scale) occur for forces which are due to viscosity, surface tension, compressibility of the water, or model elasticity. These effects are important, e.g., for slamming pressure, water on deck, or sway, roll and yaw motions of catamarans. However, in total, scale effects play a lesser role for seakeeping tests than for resistance and propulsion tests or manoeuvring tests. Wind-induced seaways can be approximated by the superposition of regular waves of small wave height (elementary waves, Airy waves). Each elementary wave has a sinusoidal profile with an infinite number of

wave troughs and wave crests (Figure 111). The wave troughs and crests are perpendicular to the direction of wave propagation. Such elementary waves are an important building block for all computational methods for linear seakeeping problems. Steep regular waves can be computed by, e.g., Stokes' theory or panel methods. However, the superposition principle no longer applies to these waves.

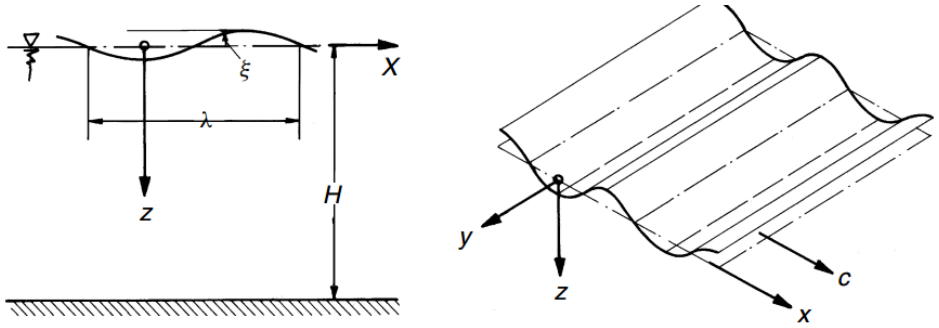

Figure 111. Elementary waves.

The elementary wave was so far described in an earth-fixed coordinate system. In a reference system moving with ship speed Vin the direction of the ship axis xs under an angle of encounter (Figure 112), the wave seems to change its frequency. The (circular) frequency experienced by the ship is denoted encounter frequency:

$$\omega_e = |\omega - kV\cos\mu| = \left|\omega - \frac{\omega^2 V}{g}\cos\mu\right|$$

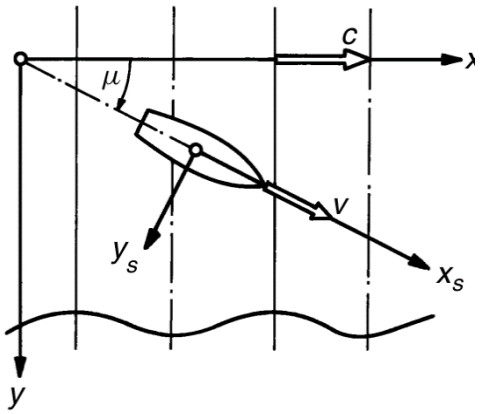

Figure 112. Definition of angle of encounter.

Figure 3 illustrates this phenomenon. For course against the sea $(\mu > 90^\circ)$ > the encounter frequency is higher than the incident wave frequency ω. For course with the sea $(\mu < 90^\circ)$ the encounter frequency is usually lower than the incident wave frequency ω. An exception are short following seas which are passed by the ship.

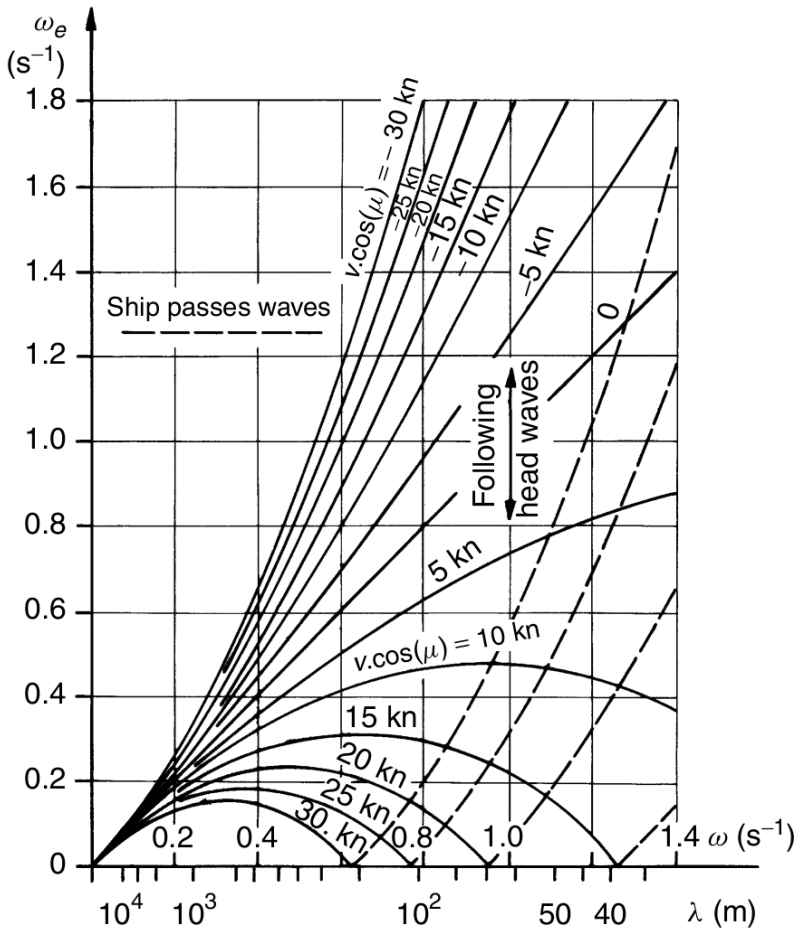

Figure 113. Relation between wave frequency, wave length and encounter frequency.

19.5.1.2 Added resistance

Interaction between ship and propeller

Any propulsion system interacts with the ship hull. The flow field is changed by the (usually upstream located) hull. The propulsion system changes, in turn, the flow field at the ship hull. However, traditionally naval architects have considered propeller and ship separately and introduced special efficiencies and factors to account for the effects of interaction. While this decomposition is seen by many as an important aid in structuring the complex problems of ship hydrodynamics, it also hinders a system approach in design and can confuse as much as it can help. Since it is still the backbone of our experimental procedures and ingrained in generations of naval architects, the most important concepts and quantities are covered here. The hope is, however, that CFD will in future allow a more comprehensive optimization of the ship interacting with the propeller as a whole system.

Decomposition of resistance

As the resistance of a full-scale ship cannot be measured directly, our knowl-edge about the resistance of ships comes from model tests. The measured calm-water resistance is usually decomposed into various components, although all these components usually interact and most of them cannot be measured individually. The concept of resistance decomposition helps in designing the hull form as the designer can focus on how to influence individual resistance components. Larsson and Baba (1996) give a comprehensive overview of modern methods of resistance decomposition (Figure 114).

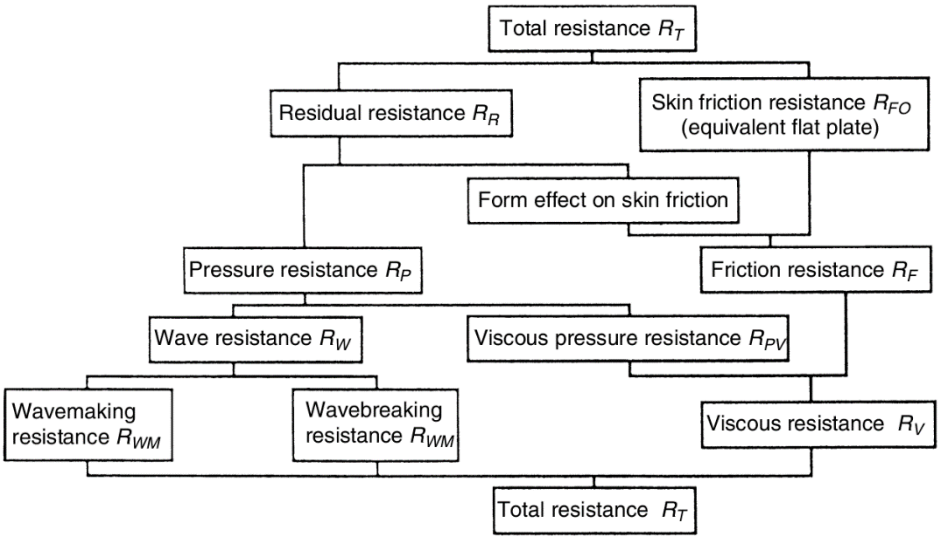

Figure 114. Resistance decomposition.

Towing tanks and experimental set-up

Despite the ever-increasing importance of numerical methods for ship hydrodynamics, model tests in towing tanks are still seen as an essential part in the design of a ship to predict (or validate) the power requirements in calm water which form a fundamental part of each contract between shipowner and shipyard. We owe the modern methodology of predicting a ship's resistance to William Froude, who presented his approach in 1874 to the predecessor of the RINA in England. His hypothesis was that the ship resistance is divisible into frictional and wave making resistance, with the wave making resistance following his 'law of comparison' (Froude similarity). This ingenious concept allowed Froude to show, for the first time, how the resistance of a full-scale ship may be determined by testing scale models. His success motivated building the first model basin in 1879 in Torquay, England. Soon further model basins followed in Europe and the USA. Tests are usually performed in towing tanks, where the water is still, and the model is towed by a carriage. (Alternatively, tests can also be performed in circulating tanks, where the model is still, and the water moves.) The carriage in a towing tank keeps its speed with high precision.

Resistance test:

Resistance tests determine the resistance of the ship without propeller (and often also without other appendages; sometimes resistance tests are performed for both the 'naked' hull and the hull with appendages). Propulsion tests are performed with an operating propeller and other relevant appendages. A problem is that the forces on appendages are largely driven by viscosity effects with small to negligible gravity effects. As Reynolds similarity is violated, the forces cannot be scaled easily to full scale. For ships with large and unusual appendages, the margins of errors in prediction are thus much larger than for usual hulls where experience helps in making appropriate corrections. The model is towed by weights and wires (Figure 115). The main towing force comes from the main weight G1. The weight G2 is used for fine tuning:

$$R_T = G_1 \pm G_2 \sin\alpha$$

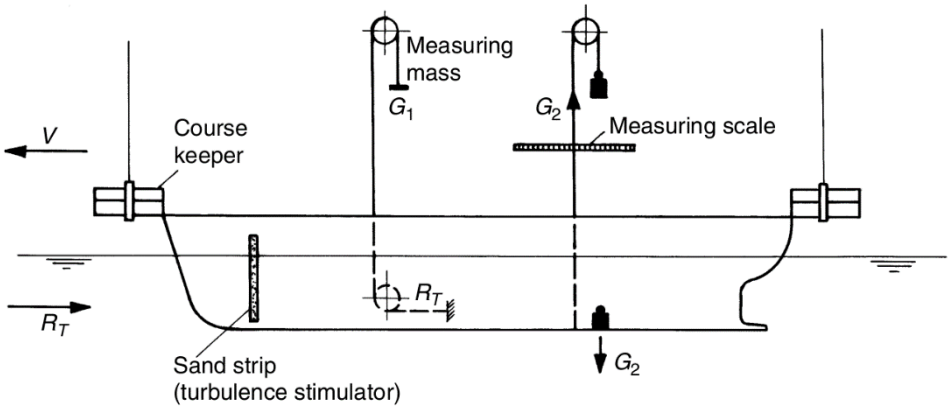

Figure 115. Experimental set-up for resistance test.

19.5.1.3 Manoeuvring

- course keeping (this concerns only the direction of the ship's longitudinal axis);
- course changing;
- track keeping (important in restricted waters);
- speed changing (especially stopping.

The sustained turning ability appears to be the least important, since it describes the ship behaviour only for a time long after initiating a manoeuvre. The stopping ability is of interest only for slow speeds. For avoiding obstacles at high ship speed, it is far more effective to change course than to stop. (Course changes require less distance than stopping manoeuvres for full speed. Understanding ship manoeuvring and the related numerical and experimental tools is important for the designer for the choice of manoeuvring equipment of a ship. Items of the manoeuvring equipment may be:

- Rudders
- fixed fins (e.g., above the rudder; skeg)

- jet thrusters
- propellers (including fixed pitch, controllable pitch, slewable, and cycloidal
- adjustable ducts for propellers, steering nozzles
- waterjets

For scaling these forces and moments from model to full scale, or for estimating them from results in similar ships, X, Y, K, and N are made non-dimensional in one of the following ways:

$$\begin{Bmatrix} X' \\ Y' \\ K' \\ N' \end{Bmatrix} = \frac{1}{q \cdot L^2} \begin{Bmatrix} X \\ Y \\ K/L \\ N/L \end{Bmatrix} \quad \text{or} \quad \begin{Bmatrix} C_X \\ C_Y \\ C_K \\ C_N \end{Bmatrix} = \frac{1}{q \cdot L \cdot T} \begin{Bmatrix} X \\ Y \\ K/L \\ N/L \end{Bmatrix}$$

With $q = \rho \cdot u^2/2$, ρ water density. Note that here we use the instantaneous longitudinal speed u as reference speed. Alternatively, the ship speed at the begin of the manoeuvre may be used as reference speed. L is the length between perpendiculars. The term 'forces' will from now on include both forces and moments unless otherwise stated. The motion velocities and accelerations are made non-dimensional also by suitable powers of u and L:

$$v' = v/u; \quad r' = r \cdot L/u; \quad \dot{u}' = \dot{u} \cdot L/u^2; \quad \dot{v}' = \dot{v} \cdot L/u^2; \quad \dot{r}' = \dot{r} \cdot L^2/u^2$$

CFD may be used to determine some of the coefficients but is not yet established to predict all necessary coefficients. Therefore, the body forces are usually determined in model experiments, either with free-running or captured models.

Physical explanation and force estimation

In the following, forces due to non-zero rudder angles are not considered. If the rudder at the midship position is treated as part of the ship's body, only the difference between rudder forces at the actual rudder angle υ and those at υ=0° have to be added to the body forces treated here. The gap between ship stern and rudder may be disregarded in this case. Propeller forces and hull resistance in straightforward motion are neglected here. We use a coordinate system with origin fixed at the midship section on the ship's centre plane at the height of the centre of gravity (Figure 116).

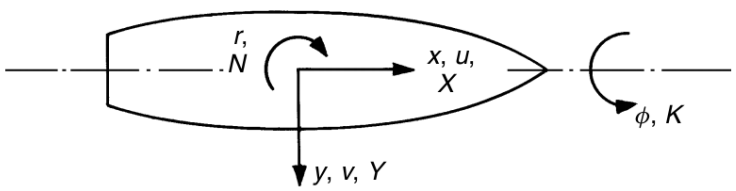

Figure 116. Coordinates x, y; direction of velocities u, v, r, forces X, Y, and moments K, N.

The x-axis points forward, y to starboard, z vertically downward. Thus, the system participates in the motions u, v, and r of the ship, but does not follow the ship's heeling motion. This simplifies the integration in time of the ship's position from the velocities u, v, r and eliminates several terms in the force formulae.

Hydrodynamic body forces can be imagined resulting from the change of momentum of the water near to the ship. Most important in manoeuvring is the transverse force acting upon the hull per unit length (e.g., metre) in the x-direction. According to the slender-body theory, this force is equal to the time rate of change of the transverse momentum of the water in a 'strip' between two transverse planes spaced one unit length. In such a 'strip' the water near to the ship's side mostly follows the transverse motion of the respective ship section, whereas water farther from the hull is less influenced by transverse ship motions. The total effect of this water motion on the transverse force is the same as if a certain 'added mass' per length m' moved exactly like the ship section in transverse direction.

Manoeuvring tests for full-scale ships in sea trial

The main manoeuvring characteristics as listed in the introduction to manoeuvring are quantified in sea trials with the full-scale ship. Usually, the design speed is chosen as initial speed in the manoeuvre. Trial conditions should feature deep water (water depth>2.5 ship draft), little wind (less than Beau-fort 4) and 'calm' water to ensure comparability to other ships. Trim influences the initial turning ability and yaw stability more than draft. For comparison with other ships, the results are made non-dimensional with ship length and ship length travel time (L/V). The spiral test results in a curve as shown in Figure 117. The spiral test is used to evaluate the turning ability and the yaw stability of the ship. For yaw unstable ships, there may be three possible rates of turn for one given rudder angle as shown in Figure 117. The one in the middle (dotted line) represents an instable state which can only be found by the indirect method. In the direct method, the rate of turn 'switches' at the vertical sections of the curve suddenly to the other part of the curve if the rudder angle is changed. This is indicated by the dotted arrows in Figure 117

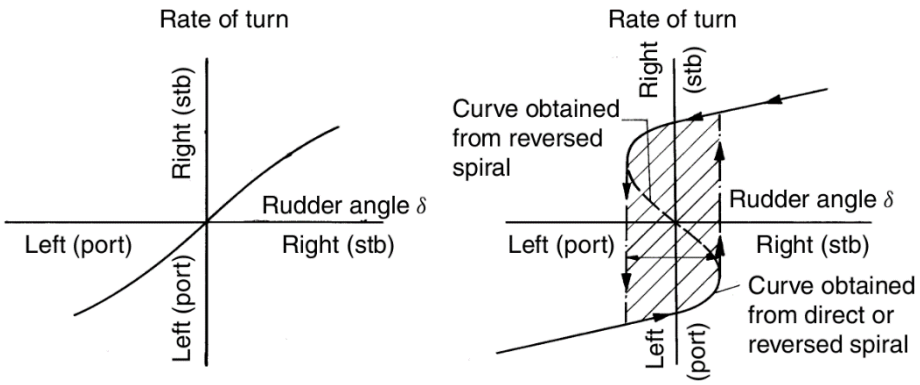

Figure 117. Results of spiral tests for yaw stable and yaw unstable ship.

With the ship on an initial straight course, the rudder is put hard to one side until the ship has reached a constant rate of change of heading. The rudder angle is then decreased in steps and again held until a steady condition is reached. This process is repeated until the rudder has covered the whole range to the maximum rudder angle on the other side. The rate of turn is noted for each rudder angle. The test should be performed at least for yaw unstable ships going both from port to starboard and from starboard to port.

19.5.2 Manoevring test for a self-running ship model in various water depth conditions. Sustainable development and innovations in marine technologies.

In the recent years there is a growing interest in the topic of unmanned navigation, with the ultimate goal of design a sophisticated and intelligent ship-ping system to make the maritime trade safer and more efficient. During the operation of merchant ships, one of the most critical phases is the navigation in restricted waters, i.e. ports and channels, where most of marine causalities occurs. Therefore, the development of a decision support system, able to assist the ship master during this phase is fundamental. In order to develop an automatic system to perform complicated manoeuvres in restricted waters, it is crucial to have an accurate mathematical model.

The model tests were performed following the ITTC recommended procedures. In total a set of 48 runs were executed, considering zig-zag and turning manoeuvres, and various model speeds and rudder deflection angles. The experiments were conducted in a covered tank located at National Laboratory of Civil Engineering (LNEC), Lisbon, Portugal, during the month of December 2018. The self-running model is a scaled model of 2.5 m equipped with several motion sensors, inertial measurement unit, propulsion DC motors and WI-FI communication.

The motions of marine vehicles in 6 DOF are conveniently defined in two coordinate frames. The moving coordinate frame X0 Y0 Z0 is attached to the vehicle and is called the body-fixed reference frame. The origin “0” of the body-fixed frame is usually chosen to coincide with the centre of gravity (CG) when CG is in the principal plane of symmetry or at any other convenient point if this is not the case, i.e, the mid perpendicular could be also used, in order to have a fixed reference. For marine vehicles, the body axes X0, Y0 and Z0 coincide with the principal axes of inertia, and are usually defined as:

X0— longitudinal axis (directed from aft to fore);

Y0— transverse axis (directed to starboard);

Z0— normal axis (directed from top to bottom).

The motion of the body-fixed frame is described relative to an inertial reference frame. For marine vehicles it is usually assumed that the accelerations of a point on the surface of the Earth can be neglected. Indeed, this is a good approximation since the motion of the Earth hardly affects low speed marine vehicles. As a result of this, an earth-fixed reference frame XYZ can be considered to be inertial. This suggests that the position and orientation of the vehicle should be described relative to the inertial reference frame while the linear and angular velocities of the vehicle should be expressed in the body-fixed coordinate system. The different quantities are defined according to the SNAME (1950) notation, as indicated in Table 10.

ITTC zig-zag tests The zig-zag manoeuvre is obtained by reversing the rudder alternately by δ degrees to either side at a deviation φ from the initial course. After a steady approach the rudder is put over to right (first execute). When the heading is φ degrees off the initial course, the rudder is reversed to the same angle to left (second execute). This process continues until a total of 5 rudder executes have been completed. A typical zig-zag manoeuvring test is given in Figure 118.

Table 10. Notation used for marine vehicles.

DOF	Motion/rotation	τ	v	η
1	In x-direction (surge)	X	u	x
2	In y-direction (Sway)	Y	v	y
3	In z-direction (heave)	Z	w	z
4	About x-axis (roll)	K	p	ϕ
5	About y-axis (pitch)	M	q	θ
6	About z-axis (yaw)	N	r	ψ

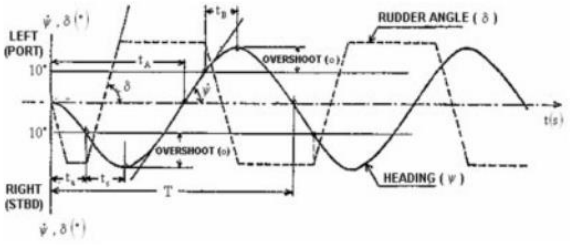

Figure 118. Zig-zag manoeuvre parameters (ITTC).

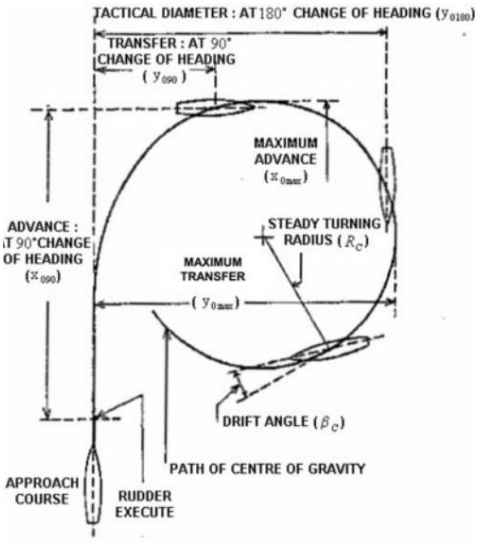

Figure 119. Turning circle definitions (ITTC).

Scaling effects in model tests

Hydrodynamic model tests are usually performed according to Froude's scaling law. This ensures that the correct relationship is kept between inertial and gravitational forces when the full-scale vessel is scaled down to the model dimensions and is therefore appropriate for model tests. Thus, Froude's law requires the Froude Number, Fn, to be the same at model and full scales:

$$F_n = \frac{U}{\sqrt{gL}} = F_{n,model} \tag{1}$$

Where L and U are the length and velocity of the ship, respectively. Notice that, Fn leads to a non-correct functioning point of the propeller due to the higher CT in model scale. Geometrical scaling is usually used throughout, in order to ensure that correct Froude Number scaling is applied to all physical quantities of the ship. This means that all lengths involved in a particular model.

Table 11.Froude scaling of various physical quantities.

Quantity	Typical Units	Scaling factor
Length	m	k
Time	s	$k^{1/2}$
Frequency	1/s	$k^{-1/2}$
Velocity	m/s	$k^{1/2}$
Acceleration	m/s^2	1
Volume	m^3	k^3
Water density	Kg/m^3	r
Mass	Kg	rk^3
Force	N	rk^3
Moment	N.m	rk^4

Table 11 shows how Froude's scaling law is applied in hydrodynamic model testing to various commonly used physical quantities. K is the scaling factor applied to lengths, and r is the ratio between salt water density and freshwater density. Scaling laws for other quantities may be found by combining relevant mass, length and time dimensions in the appropriate way. The vessel model considered is this study is presented in the following Figures.

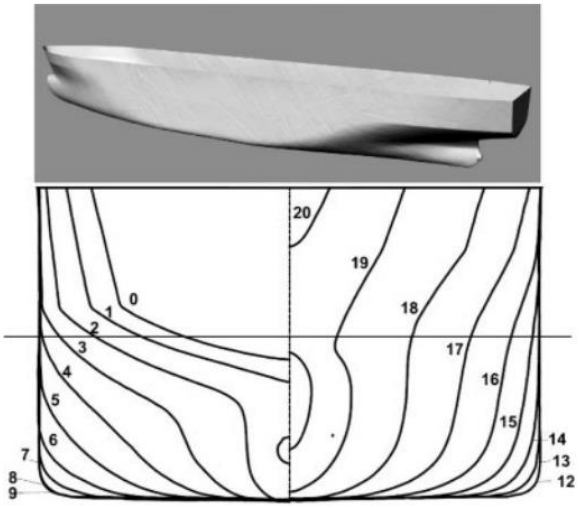

Figure 120. Ship body plan and a 3D view of ship hull.

Figure 121. Self-running ship model during test.

In order to have significant information of the manoeuvres with the self-running model in deep, intermediate and shallow water. Two different manoeuvres, zig-zag and turning tests were carried out and table 4 presents the detailed plan of tests. The speeds considered for the tests were V1 Ship speed equal to 40% Vmax and V2 corresponding to 60% Vmax.

Table 12. Test plan.

Type		No. water depths	No. ship speeds	No. tests
zig-zag tests	10°–10°	4	2	8
	20°–20°	4	2	8
	35°–35°	4	2	8
turning test	±10°	4	2	8
	±20°	4	2	8
	±35°	4	2	8
Total				**48**

Table 12 presents the recorded signals during the tests, all the sensors work properly with exception of the accelerometers (CXL02TG3 3-axis accelerometer), which is non-sensitive at low accelerations. The yaw angle is measured using an optical gyrocompass with a high precision, the yaw rate is recorded using a tilt sensor with range, the commanded rudder angle is calculated from the internal PWM generator of a National Instrument board, the roll and pitch angles are also recorded using a Inertial measurement unit.

This section presents the plots and data tables from the manoeuvring tests for zig-zag and turning trials. For each manoeuvre the corresponding time series of ship heading angle, rudder command and measured yaw rate are plotted. The tables present the mean values of principal characteristics, i.e. time to 2nd execute, yaw overshoot and total period for zig-zag and tactical diameter for the turning test. Table 14 presents the log of the experiments, where is possible to see that most tests were carried successfully except for some cases in shallow water, where the tactical diameter exceeds the tank dimensions.

Table 13. Signals recorded during tests.

Parameter	Unit	Equipment	Range	Estimated uncertainty
Heading angle	degrees	OCTANS – Gyrocompass	[0, 360]	<0.01
Yaw rate	deg./s	CRS03 – Tilt sensor	±100	<±1
Roll and pitch angles	degrees	Inertial measurement unit	±180, ±90	<0.01
Shaft RPM	rpm	NI 9505 – Bridge	[0, 1000]	–
Ruder angle	degrees	NI 9239 – PWM generator	[−40 , 40]	0.1
3 DOF Accelerations	m/s^2	CXL02TG3 3-axis accelerometer	±2g	–

Table 14. Logs of the trials.

Ship manoeuvre	Data characteristics
zig-zag 30° /30°	Good data for all the water depths and ship speeds.
zig-zag 20° /20°	Good data, except for in shallow water case
zig-zag 10° /10°	Good data except for shallow water
turning 30°	Good data
turning 20°	Good data except for shallow water and low speed.
turning 10°	Good data except for shallow water.

The Figure 122 and Figure 123 presents the plots of the zig-zag manoeuvres. In this chart in red is plotted the rudder angle command, in blue the ship yaw angle and in yellow the measured yaw rate. In general, a good agreement with the expected ones is observable except for some asymmetries, these asymmetries could be because, a bad distribution of weighs in the model, or the rudder angle command to the portside is higher due to nonlinearity in the PWM signals generated to control the DC motor.

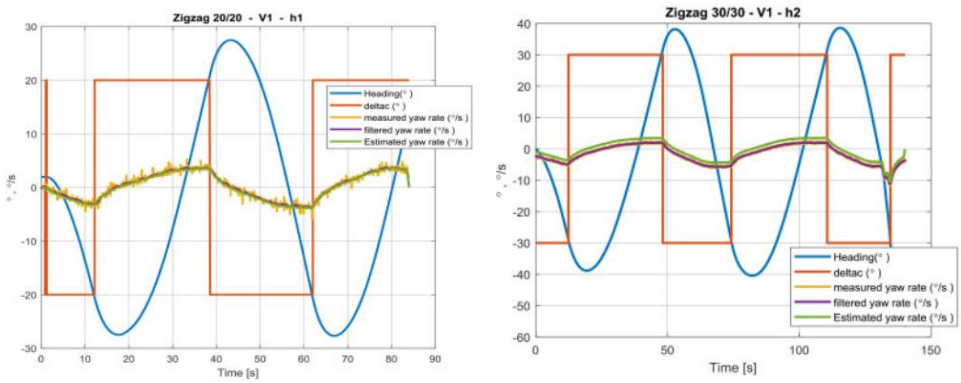

Figure 122. Zig-zag test for speed V1 and water depth h1, h2.

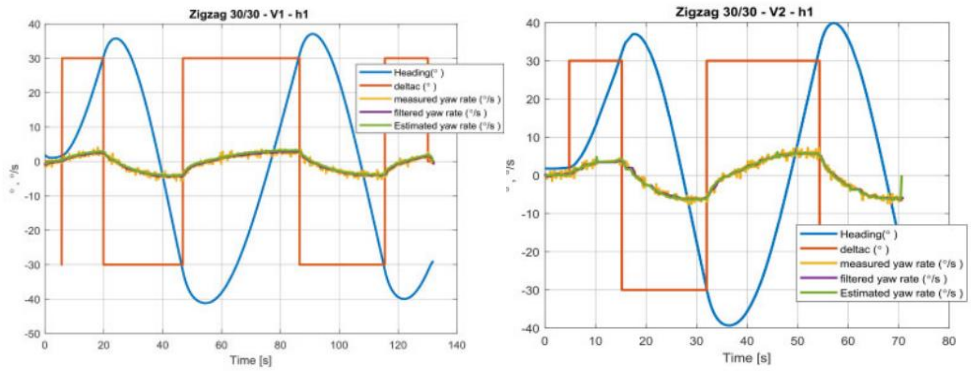

Figure 123. Zig-zag manoeuvres results for different speeds V1, V2 and water depth h1.

Figure 124 presents time series of heading angle, rudder angle, yaw rate and estimated trajectory of turning manoeuvre 10◦ for speed V2* and deep water, h1. The plot shows a good performance of the system during the test execution. Figure 125 shows the plots for turning manoeuvre 30 o with speed V2 in intermediate water depth. The plots show a good agreement with the theoretically expected, except for small deviation of the vessel, it is possible due to small wind during the tests and small waves due to wall reflection in test execution. It is important mentioned that a considerable time (10 min) was the space between test, but due to waves reflection, always small waves were observed.

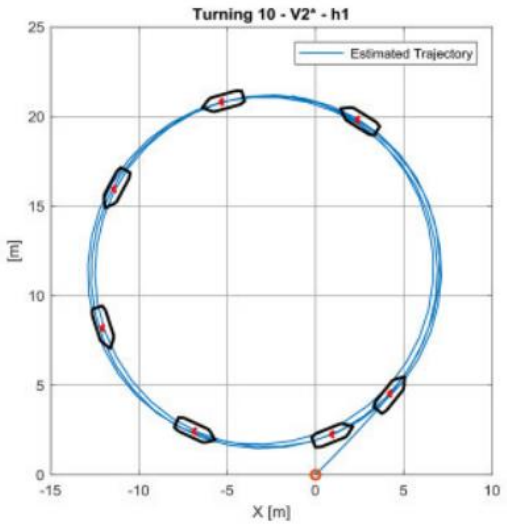

Figure 124. Turning manoeuvre for water depth h1 and speed V2.

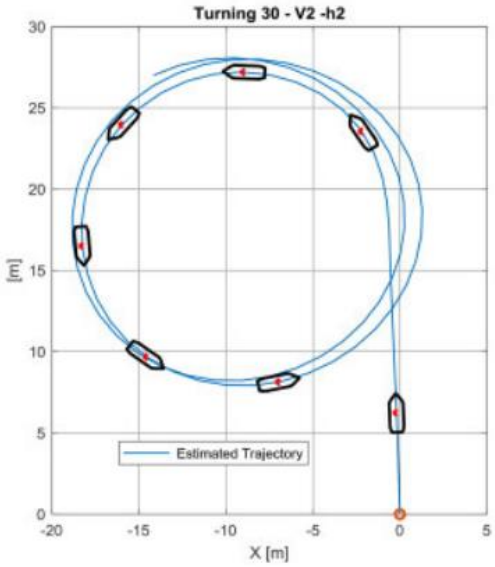

Figure 125. Turnings manoeuvre for water depth h2 and speed V2.

Conclusions

The experimental results are presented of manoeuvring tests for a self-running ship model in a still water tank, considering various water depths, ship speeds and rudder angles. A total of 48 runs for 4 water depths, 2 model speeds and 3 rudder angles are plotted and analysed. From the plots the negative influence of the shallow water in the manoeuvrability capabilities of the ship model is observed. Additional accelerometers were installed to record lateral accelerations. However due to the slow motions of the model, the measurements were around zero. Thus, it is highly recommended use sensitive accelerometers for manoeuvring tests with small models, 2-3 m length. The zig-zag manoeuvres results are in a good agreement with the expected results, except, for a couple of runs where, a small drift to one side of the model was detected, possibly because of the reflected waves in the tank. The turning manoeuvres presents a good agreement with the expected theoretical models and in the case of shallow water, the tactical diameters are higher than in deep or intermediate waters.

20 References

Park, J. H., & Choi, J. E., & Chun, H. H. (2015). Hull-Form Optimization of KSUEZMAX to Enhance Resistance Performance. Int. J. Nav. Archit. Ocean Eng.

Jiang, Y., & Yeung, R. W. (2017). Bilge-Keel Influence on Free Decay of Roll Motion of a Realistic Hull. Journal of Offshore Mechanics and Arctic Engineering.

Matusiak, J. E., & Rautaheimo, P. P. (2017). Feasibility Study on Thrust Produced by Stabilizing Fins in Waves. International Ocean and Polar Engineering Conference.

Hasselman. Measurements of wind-wave growth and swell decay during the Joint Sea Wave project (JONSWAP). 1973.

Holthuijsen. Waves in Oceanic and Coastal Waters. Cambridge University Press. Cambridge. 2007.

Class Guideline. DNVGL-CG-0130. Wave Loads. Edition January 2018.

Recommended Practice. DNV-RP-C205. Environmental Conditions and Environmental Loads. April 2014.

Tarmo Soomer, Andrus R¨a¨amet, Spatial patterns of the wave climate in the Baltic Proper and the Gulf of Finland, OCEANOLOGIA, Elsevier, 53, 2011. pp. 335–371.

Alessandro Toffoli and Elzbieta M. Bitner-Gregersen, Types of Ocean Surface Waves, Wave Classification, Encyclopedia of Maritime and Offshore Engineering, 2017 John Wiley & Sons, Ltd.

Historical Ocean Weather Data Statistics Freely Available. November 28, 2016. MetOcean Solutions. https://app.metoceanview.com/hindcast/. Last accessed: 28/03/2021.

SEAKEEPING: Ship behavior in rough weather. A R J M Lloyd (1998).

Ten Lectures on Ship Dynamics (1st Edition). Hirdaris, Spyros. Aalto University (2021).

Principles of Ship Buoyancy and Stability. Ruponen, Pekka. Aalto University (2020).

Quick Strip Theory Calculations in Ship Design, J.M.J. Journée, Delft University of Technology, 1992.

Identification of the nonlinear ship rolling motion equation using the measured response at sea, Elsevier, Ocean Engineering 31 (2004) 2139– 2156.

A Non-Linear Mathematical Model of Higher Order for Strong Parametric Resonance of the Roll Motion of Ships in Waves, Springer, Marine Systems & Ocean Technology volume 1, pages 69–81(2005).

Principles of Ship Buoyancy and Stability. Ruponen, Pekka. Aalto University (2020).

Practical Ship Hydrodynamics. Chapter 4 “Seakeeping”. Volker Bertram.

A comprehensive study on ship motion and load responses in short-crested irregular waves. Elsevier. International Journal of Naval Architecture and Ocean Engineering. Volume 11, Issue 1. January 2019. Pages 364-379.

Practical Ship Hydrodynamics, Ship maneuvering 151, Bertram, Volker, 2000

Maneuvering test for a self-running ship model in various water depth conditions. Sustainable Development and Innovations in Marine Technologies, Taylor & Francis Group, London, 2020, 40951-7

“Dynamics of Marine Vehicles” by R. Bhattacharyya. John Wiley & Sons, New York, 1978. p. 137 – 170.

“Motion Sickness Incidence: Exploratory Studies of…”, by M. E. McCauley et al. Human Factors Research Inc., Technical report, 1976.

On the prediction of the added resistance of large ships in representative seaways. Shukui Liu and Apostolos Papanikolaou. Ship Design Laboratory, National Technical University of Athens, Athens, Greece. 2016.

Added resistance of ships in waves. H. Söding and V. Shigunov. Ship Technology Research – Schiffstechnik. University of Duisburg-Essen. 2015